A RECONFIGURABLE AND WEARABLE WIRELESS SENSOR SYSTEM AND ITS CASE STUDY IN THE TRAINING OF HAMMER THROWERS

YE WANG
Master of Science, University of Lethbridge, 2015

A thesis submitted
in partial fulfilment of the requirements for the degree of

DOCTOR OF PHILOSOPHY

in

THEORETICAL AND COMPUTATIONAL SCIENCE

Department of Mathematics and Computer Science
University of Lethbridge
LETHBRIDGE, ALBERTA, CANADA

A RECONFIGURABLE AND WEARABLE WIRELESS SENSOR SYSTEM AND ITS CASE STUDY IN THE TRAINING OF HAMMER THROWERS

YE WANG

Date of Defence: August 15, 2020

Dr. H. Li	Associate Professor	Ph.D.
Dr. G. Shan	Professor	Ph.D.
Thesis Co-Supervisors		
Dr. R. Benkoczi	Professor	Ph.D.
Thesis Examination Committee Member		
Dr. W. Osborn	Associate Professor	Ph.D.
Thesis Examination Committee Member		
Dr. J. Zhang	Associate Professor	Ph.D.
Internal External Examiner		
Department of Mathematics & Computer Science		
Faculty of Arts and Science		
Dr. J. Han	Associate Professor	Ph.D.
External Examiner		
University of Alberta		
Edmonton, Alberta		
Dr. Y. Chali	Professor	Ph.D.
Chair, Thesis Examination Committee		

DEDICATION

To my parents, teachers, and friends who lead me the way to my destiny, I am truly grateful for all your support and love.

ABSTRACT

Wearable sensors have been popularly used in many applications with the development of computer science and engineering. However, wearables for biomechanical feedback in motor learning and training are still rare. Therefore, this thesis focuses on developing an efficient and cost-effective wireless sensor system through a case study on the hammer throw. The results have shown that the proposed reconfigurable and wearable system can implement real-time biomechanical feedback in the hammer-throw training. Furthermore, the experimental results suggest that various throw-control patterns could be identified by using one tension-sensor and two inertial measurement units (i.e., more superior practicality than 3D motion capture), indicating that the low-cost wearable system has potential to substitute the expensive 3D motion capture technology. The proposed system can be easily modified and applied to many other applications, including but not limited to healthcare, rehabilitation, and smart homes, etc.

CONTRIBUTIONS OF AUTHORS

Some portions of the texts in Section 1.1 in Chapter 1, Section 3.1.4, Section 3.2 and Section 3.3 in Chapter 3, Section 4.2.2 in Chapter 4, and Section 5.1 in Chapter 5 have already been published as part of separate co-authored materials in other open access journal papers [19] [23] [24] [45] mentioned in Preface. Any content included this thesis from those articles was drafted by me. I have received permission to include this work in my thesis from other co-authors.

For the article (1), I designed and programmed the sensor system and tested the performance. Dr. Bingjun Wan helped the field tests and analyzed and interpreted the data. Dr. Hua Li and Dr. Gongbing Shan proposed the architecture and improved the design. Dr. Gongbing Shan secured the research funding. All authors participated in the manuscript writing. All authors read and approved the final manuscript.

For the article (2), I designed, prototyped, programmed the wearable system, and tested its performance. Dr. Bingjun Wan, Xiang Zhang and Dr. Gongbing Shan analyzed and interpreted the data. Dr. Gongbing Shan and Dr. Hua Li proposed the architecture and improved the design. Dr. Hua Li, Dr. Gongbing Shan and I prepared the draft. All authors contributed to the revisions and proof reading of the article.

For the article (3), Xiang Zhang, Dr. Gongbing Shan, Dr. Bingjun Wan, Dr. Hua Li and I performed the literature search and design. Xiang Zhang, Dr. Gongbing Shan and I prepared the draft. Xiang Zhang, Dr. Gongbing Shan, Dr. Bingjun Wan, Dr. Hua Li and I contributed to the revisions and proof reading.

For the article (4), Dr. Bingjun Wan, Yuanyuan Gao, Xiang Zhang and Dr. Gongbing Shan designed the study. Dr. Bingjun Wan, Yuanyuan Gao, Xiang Zhang and I performed the data collection. Dr. Hua Li and I provided the technical support. Dr. Bingjun Wan, Yuanyuan Gao, Xiang Zhang and Dr. Gongbing Shan analyzed and interpreted the data. Dr. Bingjun Wan, Yuanyuan Gao and Dr. Gongbing Shan prepared the draft. All authors contributed to the revisions and proof reading of the article.

PREFACE

Four journal papers have been published based on the work in the thesis:

(1) Y. Wang, B. Wan, H. Li, G. Shan, "A wireless sensor system for a biofeedback training of hammer throwers," *SpringerPlus*, vol. 5, *(1)*, pp. 1-14, 2016.

(2) Y. Wang, H. Li, B. Wan, X. Zhang, and G. Shan, "Obtaining Vital Distances Using Wearable Inertial Measurement Unit for Real-Time, Biomechanical Feedback Training in Hammer-Throw," *Applied Sciences,* vol. 8, *(12),* p. 2470, 2018.

(3) X. Zhang, G. Shan, Y. Wang, B. Wan, and H. Li, "Wearables, Biomechanical Feedback, and Human Motor-Skills' Learning & Optimization," *Applied Sciences,* vol. 9, *(2),* p. 226, 2019.

(4) B. Wan, Y. Gao, Y. Wang, X. Zhang, H. Li, and G. Shan, "Hammer Throw: A Pilot Study for a Novel Digital-Route for Diagnosing and Improving Its Throw Quality," *Applied Sciences*, vol. 10, *(6)*, p. 1922, 2020.

My research work of M.Sc. study (article 1) and Ph.D. study (article 2) in computer science has laid the technology foundation which enables me to collaborate with kinesiologists and coaches to explore the practical values (article 3 and 4) of the technology development in this Ph.D. study. I am thankful to Dr. Li and Dr. Shan who initiated the cross-disciplinary collaboration. Such a collaboration has led me to finish this interdisciplinary Ph.D. thesis.

ACKNOWLEDGEMENTS

I take this opportunity to express my sincere gratitude to my supervisors Dr. Hua Li and Dr. Gongbing Shan. I appreciate so much for their insightful guidance and helpful comments and their support with this thesis. Their careful and strict attitudes to the research will keep educating me and leading the way in my life.

Furthermore, I appreciate my committee members, Dr. Robert Benkoczi and Dr. Wendy Osborn, for their helpful suggestions and encouragement during our committee meetings. I appreciate them so much for spending time on reviewing this thesis carefully and giving me invaluable comments and feedback.

I also appreciate my internal and external examiners, Dr. John Zhang and Dr. Jie Han, for their encouragement and careful review of this thesis. I appreciate them so much for their invaluable comments and feedback to help me improve this thesis and my research study.

This research project has been supported by funding from the National Science and Engineering Research Council of Canada (NSERC).

A special thank is also extended to Mr. Heinz Fischer for his help with the hardware configuration and troubleshooting for the wearable prototype.

A special thank is also extended to Mr. Vincent Weiler for his help with the redesign of the circuits for the wearable prototype.

TABLE OF CONTENTS

Dedication iii

Abstract iv

Contributions of Authors v

Preface vii

Acknowledgements viii

List of Tables xii

List of Figures xiii

List of Abbreviations xv

Chapter 1: Introduction 1

1.1 Motivation 2

1.2 Outline 5

1.3 Contributions 8

1.4 Thesis Overview 9

Chapter 2: Framework of Prototyping 12

2.1 The Current Reliable Method of Biomechanical Feedback Training 14

2.2 Practicality of the Wearable System 14

2.3 Design of the Wearable System 15

2.3.1 Selection of the Sensors 16

2.3.2 Selection of the Wireless Communication Method 16

2.4 Programming of Data Collection 17

2.5 System Calibration 17

2.6 Return to Biomechanical Parameters 17

Chapter 3: Background 19
3.1 Overview of Wearables 20
3.1.1 Wireless Sensor Networks and Internet of Things 20
3.1.2 Classification of Wearables 22
3.1.3 Inertial Measurement Unit 23
3.1.4 Status of Wearables' Development in Biomechanical Feedback Training 24
3.2 Overview of Biofeedback 26
3.2.1 Biofeedback and Its Types 27
3.2.2 Milestones of Biofeedback Training in Human Motor-skill Learning and Training 27
3.2.3 Unique Aspects of Biomechanical Feedback 30
3.2.4 Principle of 3D Motion Analysis 32
3.3 Discussion on Developing Wearables for Biomechanical Feedback 33
3.3.1 Biomechanical Steps 34
3.3.2 Challenges and Obstacles 35
3.3.3 AI for Motor Control Quantification 37
3.3.4 Real-time Biomechanical Feedback Training in the Hammer Throw 40
3.4 Summary 42
Chapter 4: The Proposed Real-time Biomechanical Feedback System 43
4.1 XBee Configuration 47
4.2 Sensor Node 50
4.2.1 Hardware 50
4.2.2 Calibrations 61

4.2.3 Arduino Programming 69
4.3 Receiver Node 70
4.3.1 Graphical User Interface 72
4.3.2 Madgwick's Implementation of Mahony's AHRS Algorithm 74
4.4 Deep Learning Models 78
4.5 Summary 84
Chapter 5: Experiments and Results 86
5.1 Experiments and Results of the Hardware 86
5.2 Experiments and Results of the Deep Learning Models 94
5.3 Summary 98
Chapter 6: Conclusions and Future Work 99
6.1 Conclusions 99
6.2 Future Work 101
References 104
Appendix 1: Research Consent Form 118

LIST OF TABLES

Table 1: The Results of Literature Search in All Databases of Web of Science on 11 October 2018 25

Table 2: The Article Types of Real-time Biomechanical Feedback Training Found in Web of Science 26

LIST OF FIGURES

Figure 1: The 3D motion capture system's setup and a sample of the 3D data 4

Figure 2: Four types of the sensor nodes 6

Figure 3: Figure 3: A general modus operandi/framework for developing wearable devices to realize real-time biomechanical feedback training in human motor learning (Note: MoCap – motion capture) 13

Figure 4: Previous system architecture 21

Figure 5: The flowchart of the proposed system 45

Figure 6: Updated system architecture 47

Figure 7: An example of the XCTU configuration interface 48

Figure 8: One view of the customized box and its lid 52

Figure 9: Another view of the customized box and its lid 53

Figure 10: The board inside the 3D printed box 55

Figure 11: PCB design 58

Figure 12: Logic diagram of the major electronic components on the PCB 59

Figure 13: Calibration jumper pins 60

Figure 14: Calibration for the load cell 63

Figure 15: IMU testing device 65

Figure 16: Receiver node 71

Figure 17: A field test 72

Figure 18: MATLAB GUI receiving, processing and displaying data 73

Figure 19: A sample of the raw data from the VICON system 79

Figure 20: A sample of the processed data from the VICON system 80

Figure 21: A sample of the training dataset for the simple model 82

Figure 22: A sample of the testing dataset for the simple model 83

Figure 23: Drifting error 87

Figure 24: Three times of up-and-down movements by using the IMU testing device with Madgwick's filter 88

Figure 25: A synchronized test's data obtained from 3d motion capture (VICON data, top, sampling rate 200 Hz) and the IMU testing device without re-calibration (IMU data, bottom, sampling rate 50 Hz) 90

Figure 26: A renewed synchronized test's data obtained from 3D motion capture (VICON data, top, sampling rate 200 Hz) and the IMU testing device after calibration (IMU data, bottom, sampling rate 50 Hz) 91

Figure 27: The upper and lower limbs' coordination (i.e., motor control pattern) revealed by the vertical distances of hip and wrist as well as the wire-tension during a hammer throw by a college-level athlete 92

Figure 28: The wearable prototype 93

Figure 29: An example of training the deep learning model for 1000 epochs 95

Figure 30: An example of the plot of the simple model's predictions 96

Figure 31: An example of the plot of the complicated model's predictions 96

LIST OF ABBREVIATIONS

3D	Three Dimensional
MoCap	Motion Capture
RF	Radio Frequency
PCB	Printed Circuit Board
IMU	Inertial Measurement Unit
IDE	Integrated Development Environment
AHRS	Attitude and Heading Reference System
GUI	Graphical User Interface
AI	Artificial Intelligence
WSN	Wireless Sensor Network
IoT	Internet of Things
GSM	Global System for Mobile
EEG	Electroencephalogram
mm	Millimeters
cm	Centimeters
m	Meters
PAN	Personal Area Network
V	Volts
SA	Slave Address
I2C	Inter-Integrated Circuit
MOSFET	Metal-Oxide-Semiconductor Field-Effect Transistor
OPAMP	Operational Amplifier
lb	Pounds
ADC	Analog to Digital Converter
GRN	Green
YLW	Yellow
GND	Ground
CAL	Calibration

kg	Kilograms
DoF	Degree of Freedom
FTDI	Future Technology Devices International
USB	Universal Serial Bus
DTR	Data Terminal Ready
RXI	Receiving Asynchronous Input
TXO	Transmitting Asynchronous Output
CTS	Clear to Send
g	Gravity of Earth
LSB	Least Significant Bit
dps	Degree per Second
Hz	Hertz
MARG	Magnetic, Angular Rate, and Gravity
acc	Accelerometer
gyr	Gyroscope
ReLU	Rectified Linear Unit
MSE	Mean Squared Error
MAE	Mean Absolute Error
WPAN	Wireless Personal Area Network
WLAN	Wireless Local Area Network
API	Application Programming Interface
LWRA	Left Wrist Thumb Side
LWRB	Left Wrist Pinkie Side
LASI	Left Anterior Superior Iliac Spin
RASI	Right Anterior Superior Iliac Spin

CHAPTER 1: INTRODUCTION

In the era of information technology, Computer Science applications have been increasingly spread and extended in various fields thanks to the explosive advances of computer technologies since last century. As a consequence, wireless sensor applications can be found in every corner of the world now, such as in sport activities, art performances, healthcare practices, occupational training, and many other human physical behaviours [1] – [7]. The variety of wearable sensors allows people to collect different kinds of data related to various human physical behaviours. However, among so many choices, how would people be able to make full use of these scientific tools? Research in theoretical and computational science will help to find the answer. This research works towards this goal. It requires computer-related skills, knowledge of motion analysis and knowledge of applying the interdisciplinary understanding to human motor learning practice. By designing and developing a reconfigurable and wearable wireless sensor system for the training of the hammer throwers, this thesis has demonstrated a case study of the combination of theory and practice. Along with the artificial intelligence (AI) technology applied, it has been confirmed that various throw-control patterns could be identified by using a wearable system with one load cell and two inertial measurement units (IMUs). In terms of the practicality, the features of the wearables (e.g., portable, easy-to-use, etc.) make this system more superior than the 3D motion capture system which currently is still the most reliable and widely used method in biomechanical study. However, wearable applications would not just be limited to the hammer throw. People with imagination and creativity can be inspired by this thesis to adapt this idea to other areas, such as healthcare,

rehabilitation, etc. In other words, the wearables' application prospects are wider and brighter.

In summary, this thesis will concentrate on elaborating on a wearable system that can provide real-time biomechanical feedback in the training of the hammer throw. In the first chapter, this thesis will be presented by starting from introducing the research motivation. Then, there will be an outline of introducing all the methods used in this thesis for realizing the research goal. Next, a summary of the main contributions of this thesis will be presented. Finally, an overview of this thesis will be provided.

1.1 MOTIVATION

Optimization of any sport skill requires re-organization of the limb coordination responsible for governing the movement performance [8]. This type of motor learning can be enhanced through a number of methods that are utilized in research and application settings alike. In general, verbal feedback of coaches in real-time is commonly used as a preliminary means of instilling motor learning, such as in [8] and [9]. Due to the rapidity and complexity of some sports skills as well as invisibility of some parameters (e.g., force), the real-time feedback from coaches is often a subjective guess based on experience. For increasing the reliability of feedback in training, biomechanical means can be used to supplement the verbal instructions [10] – [13]. The hammer throw is such a sport that needs a combination of a coach's experience and biomechanical feedback in elite sports training to facilitate motor learning and optimize outcomes.

Men's hammer throw has been part of Olympics track-and-field competitions since 1900, but unlike other events, it has not seen a new world record since 1986 [14].

This standstill may be caused by the lack of scientifically based training. While extensive three-dimensional (3D) motion analysis technologies do supply highly trustworthy information for human motor skill quantification [15] – [18], due to their drawbacks, the analysis and feedback has traditionally occurred offline after completion of a given testing session (i.e., it is post-measurement feedback, rather than real-time feedback) [18] – [21]. The drawbacks of a 3D motion capture system include [22]:

(1) Lab-based,
(2) Complicated operation,
(3) High cost (over 300,000 US dollars),
(4) Long calibration and setup procedures,
(5) Time-consuming course on data collection, processing and analysis,
(6) Movement constraints induced by dozens of motion capture markers attached on a subject's body.

These drawbacks have hindered the use of 3D motion capture systems in sports training and practice.

Motivated by developing a practical method, I have participated in a research project that initiated a development of a real-time biomechanical feedback device for the hammer-throw training. In this project, I have begun the development of the wire-tension measurement in the hammer throw [19]. As one of principal investigators in the cross-disciplinary team, I was heavily involved in a pilot study for a development of wearable-sensor device in the hammer throw [23]. The investigation using 3D motion capture technology, as shown in Figure 1, found that the timely displacements of the hip and wrist

may be used to reveal the upper and lower limbs' coordination when analyzing the hammer throw. Figure 1 shows (a) the set-up of the data collection and (b) one sample of the 3D data. The pilot study has indicated that the timely change of the vertical displacements of the hip and wrist are closely related to the turning speed, the ratio of one-leg/two-leg support (power generation), and the hammer's velocity change during the skill performance. Therefore, obtaining the dynamic distance data of these two anatomical landmarks would be vital for real-time biomechanical feedback training. In addition, it is also critical to use a machine learning algorithm, such as regression, to verify the feature that the pilot study has found.

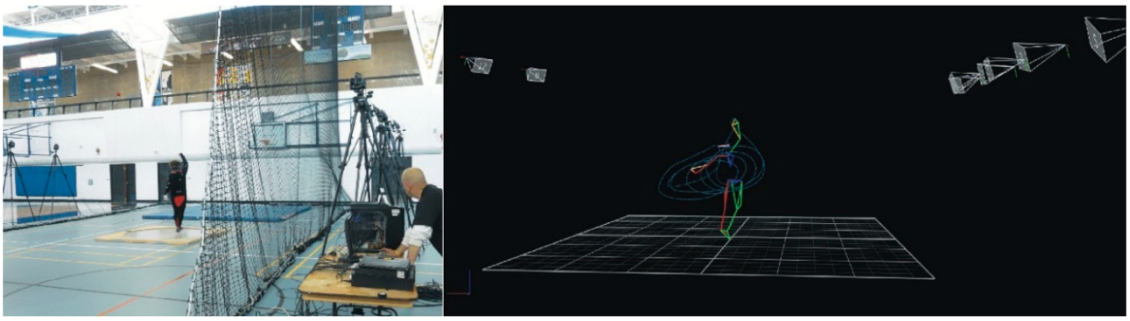

(a) (b)

Figure 1: The 3D motion capture system's setup and a sample of the 3D data [24]

Further, integrating the results [23] with my previous wire-tension study in the hammer throw [19], one would logically find that a combination of the wire-tension measurement and the dynamic vertical displacements of the hip and wrist could have great potential to be used instead of the 3D motion capture technology in the skill analysis of the hammer throw. Therefore, developing such a wearable system for tracking hip and wrist movements and gathering the wire-tension measurements along with the help of

machine learning could realize the real-time biomechanical feedback system in the hammer-throw training.

1.2 OUTLINE

This research is a cross-disciplinary work which requires various methods in different areas to realize the goal – establishing a real-time biomechanical feedback system. In general, a wearable/wireless sensor system is required to be developed, that can be separated into two basic elements: (1) the sensor node that is used for data collection and (2) the receiver node that is used for data processing. Therefore, the thesis will be introduced mainly from the following two aspects: the sensor node and the receiver node.

Before introducing the details about the sensor node and the receiver node, as it is a wireless sensor system, a specific protocol in telecommunications has to be followed to make the two nodes communicate remotely with each other. Four types of the sensor nodes were proposed for different applications where users can configure the system architecture by their own requirements, as shown in Figure 2. The first type was selected in this case study, i.e., the XBee modules which are more convenient and user-friendly in the initial research stage were used. XCTU [25] is used to configure the XBee modules. A section about configuring the XBee modules will be presented initially.

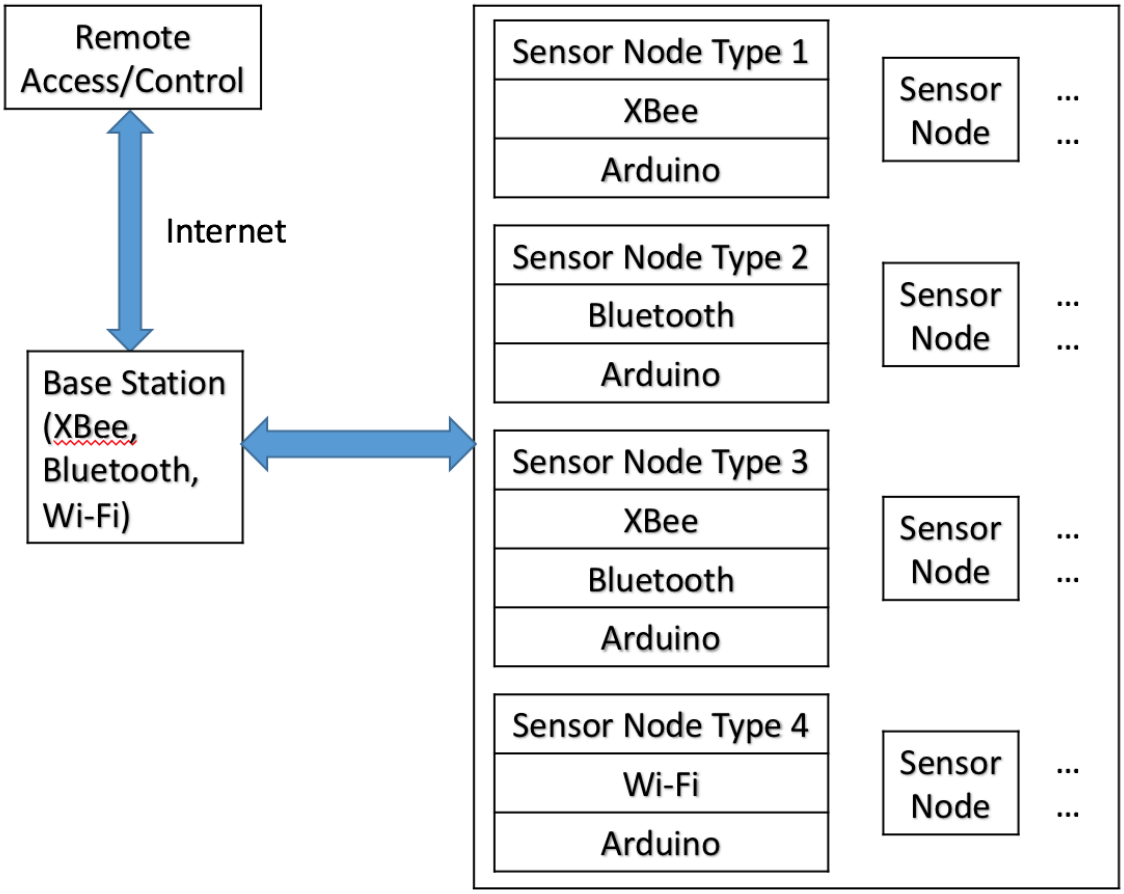

Figure 2: Four types of the sensor nodes

The XBee module [26] is a kind of ZigBee, based on IEEE 802.15.4 standard [27] which was designed for low-data-rate, low-power, and low-complexity short-range radio frequency (RF) transmissions. In an ideal condition, its maximum range can reach 90 meters. XBee modules support mesh network that every node in the network can have capability of routing. Even if one node is down, the other nodes can still work. So, XBee modules can be used to construct a very strong and flexible wireless sensor network. In addition, it has high-level security. As a result of these features, XBee modules have been widely used in many research studies [28] – [30].

Bluetooth has been developed and updated for many different versions since 1998. After the 4.0 version, the traditional Bluetooth was treated differently from Bluetooth Low Energy (BLE). In recent years, BLE are more popular and commonly used in wireless sensor applications, such as [31] – [34]. So, the Bluetooth in the proposed wireless communication method refers to BLE. The power and cost consumption of BLE are reduced compared to the classic Bluetooth, and the range of BLE is usually within 100 meters. It uses 2.4 GHz radio frequencies and adopts the protocol of the classic Bluetooth that is IEEE 802.15.1 standard [35] which was designed for wireless personal area network (WPAN). It also has high-level security. However, the size of a data packet is limited by using BLE. In addition, the maximum number of devices in a network is limited as well. The third node type is proposed to combine the XBee and Bluetooth to try to provide both of their advantages so that the users can select one wireless communication method depending on their own requirements.

Wi-Fi is a group of wireless network protocols that are based on IEEE 802.11 standards [36] which were designed for wireless local area networks (WLANs). Wi-Fi has also become very popular in recent years. This wireless communication method has the advantages of the convenience of deployment and the fast data transmission speed. However, its energy cost and security are potential issues.

Next, the sensor node will be introduced beginning with its hardware. In terms of the hardware, a wearable prototype for collecting vital data has been developed. The size of the wearable device is miniatured by designing a printed circuit board (PCB). In addition, Autodesk Inventor 2014 [37] is used to design a customized 3D printed box along with its lid to protect and hold the board and the sensors. There are three sensors

used in the wearable device: two inertial measurement units (IMUs) [38] and one load cell [39]. These sensors need to be calibrated and tested before assembly. So, there will be a section to describe how to calibrate and test the sensors and the problems that occurred during the calibration work in detail. Last but not least, as an Arduino board [40] is used as the microcontroller, the program implemented in the Arduino IDE (Integrated Development Environment) [41] will also be introduced.

For the receiver node, the graphical user interface (GUI) implemented in MATLAB will be presented first. It is the key to make the system display real-time feedback intuitively. Next, an applied algorithm – Madgwick's implementation of MahonyAHRS algorithm [42] will be introduced. It is also implemented in MATLAB for calculating reliable vertical displacements obtained by the IMUs.

In addition, two existing deep learning models based on Keras API (application programming interface) [43] have been built in Python to verify the feature that the timely change of vertical hip and wrist displacements could reveal the upper and lower limbs' coordination in the hammer throw. It is also a goal to find out whether a complicated model or a simple model should be used in a biomechanical study by comparing the two models' predicting results.

1.3 CONTRIBUTIONS

By designing and developing a reconfigurable and wearable wireless sensor system, this research work mainly contributes to the initiation and realization of real-time biomechanical feedback training in the hammer-throw practice as the following points:

(1) Establishing a general modus operandi (i.e. a general framework) for developing wearables of real-time biomechanical feedback applied in human motor skills' learning and training;

(2) Improving the effectiveness of the wearable device designed for the training of the hammer throw by adding two IMUs and miniaturizing the device with the help of PCB design;

(3) Demonstrating that the wearable device that uses a load cell and two IMUs has potential to substitute the 3D motion capture cameras (such as the VICON high-speed multi-camera system [44]);

(4) Providing a method of transferring the biomechanical feedback training from a post-measurement one to a real-time one;

(5) Providing a method of simplifying the scientific quantification from operating a complicated 3D motion capture system to an easy-to-use wearable device;

(6) Inspiring people in the wearable application field to not only monitor key parameters but also diagnose any issue that occurs from the monitoring.

1.4 THESIS OVERVIEW

A general idea of the cross-disciplinary research has been provided in this chapter. The remainder of the thesis will be organized as follows.

In Chapter 2, a brief summary of my years' experience in studying, developing and prototyping biomechanical wearables will be provided. The most relevant contribution of my Ph.D. study is an establishment of the general modus operandi/framework for developing wearable devices to realize real-time biomechanical feedback training in human motor learning. The elaboration of the framework would help

future researchers and developers with better understanding the more detailed contents of the thesis, because this cross-disciplinary research area is relatively rare. Hopefully, the established framework would promote more future studies and developments in this relatively underdeveloped application area of computer science and wearable technology.

In Chapter 3, the research background will be elaborated through a literature review on the wearables and biofeedback training. The description will focus on the current successes of the development in this area as well as the existing limitations faced by the wearable technology in human motor learning. The chapter shows that the development of a real-time biomechanical feedback training tool is challenging, but it is a growing trend of applying the scientific means in learning of various human motor skills. The chapter also presents differences between the biomechanical feedback training and the other biofeedback trainings to explain why it is more difficult to develop a real-time biomechanical feedback training tool than the other types of tools. Although there are many challenges, the advantages of wearables combined with artificial intelligence (AI) technology will provide an excellent platform with great potential and make a huge and positive impact in this field.

In Chapter 4, the research methodologies used in developing the real-time biomechanical feedback system for training of the hammer throw will be elaborated. The system consists of two basic elements: the sensor node and the receiver node. XBee is used as the wireless communication method between the sensor node and the receiver node. So, it is significant to introduce the XBee configuration at the beginning. Then for the sensor node, the wearable device will be introduced from its hardware development to its software development including the calibration procedures. On the receiver node side,

the GUI and the applied algorithm will be discussed in detail. The last part of this chapter will be a discussion of the deep learning models.

In Chapter 5, detailed discussions on the experiments and their results will be presented. The discussions will cover contents from a hardware perspective to a software perspective (i.e., the experiments and the results of an IMU testing device, the wearable prototype, and the deep learning models).

In the last chapter (Chapter 6), conclusions of the thesis will be made and the research potential in the future work will be discussed.

CHAPTER 2: FRAMEWORK OF PROTOTYPING

Since this interdisciplinary research work belongs to an underdeveloped field that only few people work in the same or similar direction, an elaboration of idea-development will be provided in this chapter as an overview or summary of my years' research experiences so that readers could follow the detailed contents of the thesis easily and might be clearer for thorough understanding.

Nowadays, wearable devices that supply real-time biofeedback related to our body during physical activities are common. They have changed the ways of our exercise and improved our physical health. However, the real-time biomechanical wearables for human motor learning is rare [45]. There is even no general modus operandi for its development. The most important contribution of my years' Ph.D. study is to establish a general modus operandi for developing biomechanical wearables (Figure 3).

Figure 3 shows that, in essence, the development of biomechanical wearables is to apply the knowledge of computer science and sensing technology (black font in Figure 3) into human motor learning & training (green font in Figure 3). Obviously, there is a gap between the two sides, i.e. a connecting piece is missing (red font in Figure 3). For well-developed areas, researchers have already established modus operandi to find the missing piece for practitioners/users. Unfortunately, such a modus operandi did not exist for the development of biomechanical wearables. My years' study has created the modus operandi to find the missing piece for researchers and practitioners. The method begins with 3D motion capture/biomechanical quantification (green), followed by how to simplify the 3D motion capture to wearables (red), design of wearable systems (black), programming (black), quantification of dominant variables (green), and ends up with

transitions from the wearables' data to biomechanical variables (black). If the transition is successful, the prototyping is finished (red); otherwise, one should go back for a revision (e.g. adding more sensors) until reaching the accuracy required. Although the framework is developed for the training of hammer throw, the methodology/the modus operandi could be extended into various human motor skills. The following sections are description of steps involved.

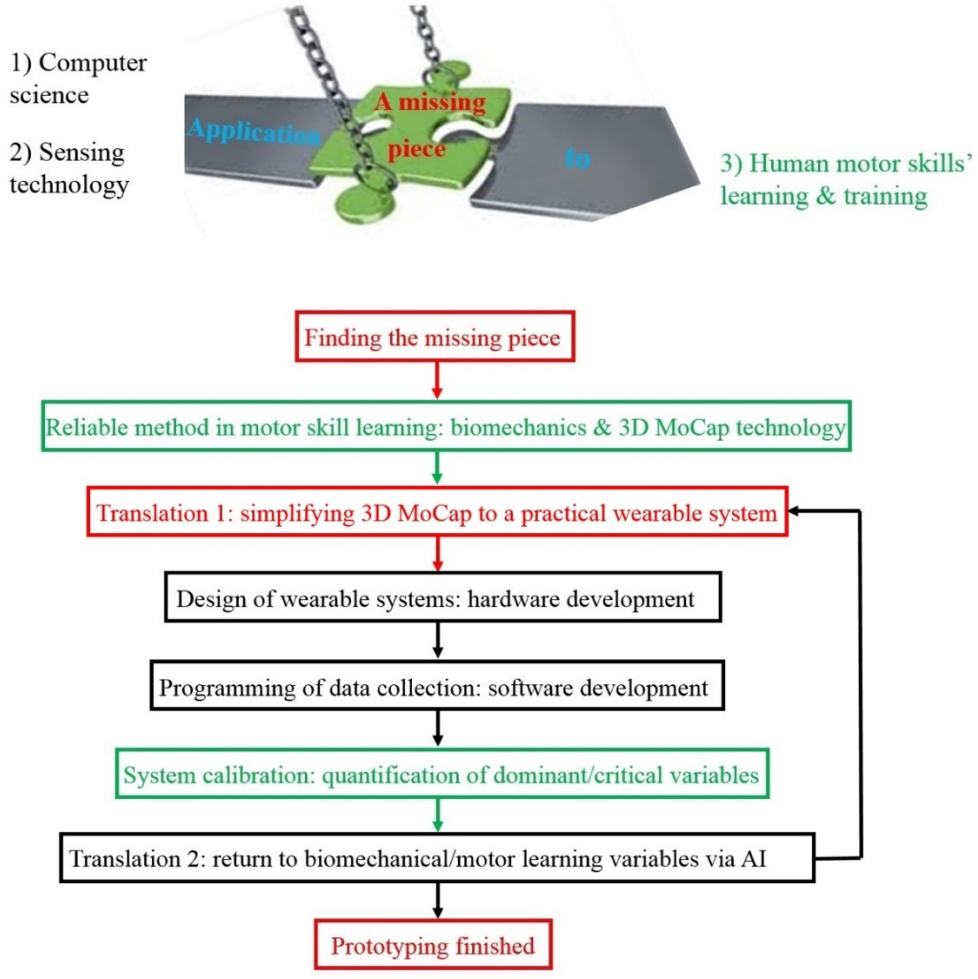

Figure 3: A general modus operandi/framework for developing wearable devices to realize real-time biomechanical feedback training in human motor learning (Note: MoCap – motion capture)

2.1 THE CURRENT RELIABLE METHOD OF BIOMECHANICAL FEEDBACK TRAINING

In order to apply the knowledge of computer science and sensing technology into human motor skills' learning & training, it is important to know the current reliable methods as well as their mechanisms; and then, one could consider various novel means for improving human motor learning.

In human motor learning, one of the scientific training methods is through biomechanical feedback training. The common factor used in biomechanical feedback training is the limb coordination, which can be revealed by the changes of joints' angles overtime. Therefore, obtaining this vital information would be an irrevocable goal of the biomechanical feedback training no matter what kind of feedback tools are used.

Currently, the most reliable biomechanical feedback training is 3D motion analysis. In this case study, the VICON system, which is one of the most reliable 3D motion capture and analysis systems, was used for 3D motion analysis in order to quantify joints' coordination during hammer throw. The VICON multi-camera system can provide the trajectories of ~40 markers (almost weightless) attached to joints and segments of a subject for quantifying the limb coordination during any complex human movements. The principle of 3D motion analysis will be introduced in Chapter 3. So, for more details, please see Section 3.2.4 and Section 3.3.1 in Chapter 3.

2.2 PRACTICALITY OF THE WEARABLE SYSTEM

In contrast to 3D motion capture systems, wearable systems use sensors to collect vital information instead of cameras and markers. For example, the IMUs are a kind of

sensors for getting an object's orientation. By applying some data fusion algorithm of motion tracking, the trajectories can be gained by using IMUs. If using the same number of IMUs as the number of markers applied in 3D motion capture system and putting the IMUs on the same positions where the markers are located, then the wearable system would be able to fully replace the 3D motion capture technology. However, it is impossible to attach too many IMU sensors on a human body because of the size and weight of the current IMU technology. The weight will cause skin vibration during movements (i.e. inaccurate measurement) and many weights on skins also add movement constraints, resulting changes in human motor control. Therefore, in terms of practicality, the most important and challenging issue is how to minimize the number of the sensors applied in a wearable system.

The basic principle is to capture the main characteristics of a motor skill by applying as less sensors as possible (i.e. simplification). Ideally, single wearable device would be the best solution if it could provide the main biomechanical information needed for skill learning. This is why the iWatch is so popular for physiological feedback. In this study, the characteristics of the hammer-throw movement were extracted through a pilot study [23]. The number of sensors identified for developing the wearable system has been determined to be three. For more details of quantification and identification of the sensor number, please see Section 3.3.4 in Chapter 3.

2.3 DESIGN OF THE WEARABLE SYSTEM

After the determination of sensors required, one can start to design a wearable system based on the determined main characteristics of the movement. For a wearable

system, there are mainly two factors to be considered that are the selection of the sensors and the selection of the wireless communication method.

2.3.1 SELECTION OF THE SENSORS

Depending on the dominant parameters extracted from the characteristics of the movement, appropriate sensors should be selected for building the wearable system. In this hammer-throw case study, tension and two distance data are the dominant parameters. For obtaining the tension data, the only option is to use a tension sensor also called load cell. For obtaining distance data, there are several options, such as optical distance sensor, ultrasonic distance sensor, and IMUs. The first two types of sensors are more direct and easier to be used for data collection. However, they have limitations due to their one-dimensional feature. Therefore, IMUs were finally selected and used in the wearable system in the case study. For more details, please see Section 3.1.1 and Section 3.1.3 in Chapter 3.

2.3.3 SELECTION OF THE WIRELESS COMMUNICATION METHOD

A wearable system usually uses a wireless communication method. Some different types of wireless communication methods have been introduced in Section 1.2 in Chapter 1. XBee was selected in the case study because of its advantages in the prototyping stage. One reason why the proposed wearable system uses only two XBee modules for point to point wireless communication is that one sensor device attached to an athlete's waist would not cause too much influence on his/her movement by reducing the number of Arduino microcontrollers. Therefore, the tension sensor and an external IMU have to be connected to the device by cables. It is possible to change the wireless communication method in the future. For more discussion on this, please see Section 6.2 in Chapter 6.

2.4 PROGRAMMING OF DATA COLLECTION

Once the sensors and the wireless communication method are selected, one can start the software development for data collection. In this case study, Arduino IDE and MATLAB are used in developing the software part of the wearable system. For more details, please see Section 4.2.3 and Section 4.3 in Chapter 4.

2.5 SYSTEM CALIBRATION

The next step is to do the system calibration after the hardware and software development of the wearable system. The calibration procedure is very important because accurate and meaningful data are required instead of a whole bunch of raw data. For more details, please see Section 4.2.2 in Chapter 4.

2.6 RETURN TO BIOMECHANICAL PARAMETERS

After calibration, the last but not least procedure is to return the collected data to the biomechanical parameters. As mentioned in Section 2.1, a new approach should not change the original structure of human motor skill learning. One should note that, due to reduction of sensors applied, the wearable system can only provide data revealing the main movement characteristics. Coaches and practitioners could not link the feedback data to joints' coordination. A "translator" is needed to interpret the data back to the biomechanical parameters (i.e., limb coordination). The "translator" is AI technology. It is the key to re-establishing the joint angles (i.e., revealing limb coordination) by using the sensor-collected data.

In the hammer-throw case study, I have proved the potential of deep learning models as a good "translator". Due to the limited data volume, the deep learning models

are still in an initial stage for a validation purpose. For more details, please see Section 4.4 in Chapter 4 and Section 6.1 in Chapter 6.

In summary, prototyping biomechanical wearable system is essentially to apply the knowledge of computer science and sensing technology into human motor learning and training. The key point is to find the missing piece to bridge the gap between the two sides. For finding the missing piece, two “translations” are vital. One is to identify the minimal sensors required (simplification) and the other one is to transfer the wearables’ data back to biomechanical data.

CHAPTER 3: BACKGROUND

This research study belongs to the area of applied sciences. For the specific study case in the hammer throw, it involves the application of wireless sensor networks (WSN), the hardware and software development of a wearable prototype, the application of AI technology, and the 3D motion capture and analysis in biomechanical study. Many researchers have contributed to WSN related applications in different fields [46], [47], such as health monitoring [48], [49], human activity monitoring, sport, and so on. Wearable prototype elements such as inertial measurement units (IMUs) are commonly used in human movement analysis and its applications [50], [51]. Deep learning models of AI technology have also become a popular tool in various applications [52]. 3D motion capture technology is currently the most reliable way of obtaining biomechanical feedback [11] and [53] – [55].

Among all these technologies used in this thesis, wearables and biomechanical feedback training are the two key methods. Therefore, in this chapter, an overview of wearables will be presented firstly by introducing some basic knowledge of wireless sensor networks (WSN) and the Internet of things (IoT) that are playing significant roles in this era of information, the classification of wearables, and the development of wearables in biomechanical feedback training. Next, an overview of biofeedback will be presented by introducing biofeedback and its types, showing its milestones in human motor-skill learning and training. Lastly, developing wearables for biomechanical feedback will be discussed.

3.1 OVERVIEW OF WEARABLES

Wearable sensors have gained great interest in biofeedback training, owing to their tremendous promise for a plethora of applications. They supply real-time non-invasive monitoring of physical-activity parameters as indicators of a trainee's physical progress. Yet, the absence of a reliable method of applying wearables in biomechanical feedback training has greatly hindered wearable applications in the area of human motor skill learning, training, and optimization. In this section, WSN and IoT will be introduced first because the rapid growth of wearables is based on these two concepts. Next, the classification of wearables and the current status of wearables' development in biomechanical feedback training will be discussed.

3.1.1 WIRELESS SENSOR NETWORKS AND INTERNET OF THINGS

WSNs can be described as the networks consisting of two or more nodes that can transmit information collected by various sensors remotely by following some specific wireless communication protocol. For example, Figure 4 illustrates the system architecture in my previous research [19], which consists of two nodes where one node can collect data for transmission which can be called the sensor node, and the other node receives this data which can be called the receiver node. The XBee modules were used as the wireless communication method.

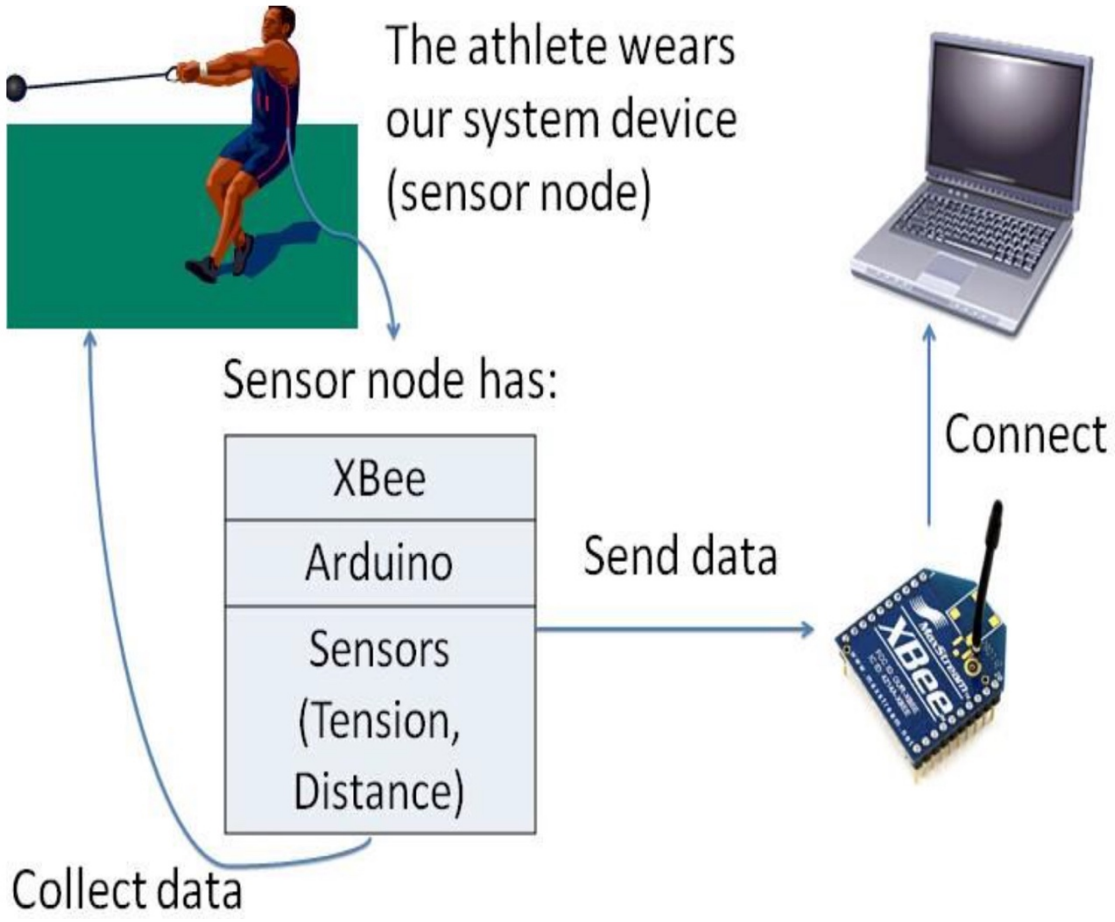

Figure 4: Previous system architecture [19]

Wireless sensors are typically more convenient than wired sensors. As discussed in [56], compared to wired networks, low-power and low-cost wireless sensors are used to reduce the capital expenditure and operational expenditure without losing any quality of service from an industrial perspective. The previous wireless sensor device [19], also called the sensor node in Figure 4, used a tension sensor and an infrared distance sensor because these sensors are the most straightforward way of collecting the required data that can reveal the critical parameters. These two sensors are both one-dimensional. The tension sensor was proved to collect the wire-tension measurements successfully. However, the distance sensor was proved to be ineffective after performing some field

tests. Because the distance sensor uses infrared to measure distance, it is required to keep vertically towards the ground for collecting reliable data. However, during the hammer-throw movement, the device will swing as the athlete rotates his/her body. Therefore, it is hardly to use a one-dimensional sensor (i.e., optical distance sensor, ultrasonic distance, etc.) to collect accurate distance data in this specific situation. IMUs are commonly used in human motion tracking. They can provide not only the one-dimensional distance data but also the 3D location of an object. So, IMUs are quite popular in many different areas [57] – [59]. However, every coin has two sides. IMUs are more difficult to be applied. More details about IMUs will be introduced in Section 3.1.3 and in Chapter 4.

IoT is a relatively newer and wider concept compared with WSN. WSN can be treated as a subset of IoT because only the wireless sensor applications belong to WSN while IoT can have both wireless and wired sensors as long as they can transmit data to the Internet [60]. Also, WSN applications may not transmit data to the Internet directly, like the wearable device illustrated in Figure 3. For example, if the wearable device was able to send the collected data to a server through a Wi-Fi module within a Wi-Fi environment or a GSM (Global System for Mobile) module within any mobile coverage area, then it would become an IoT application. No matter if it is a WSN application or an IoT application, wearable devices can be very useful in many different fields.

3.1.2 CLASSIFICATION OF WEARABLES

Wearables or wearable devices simply refer to those wireless devices that can be worn by people or attached to human bodies. A wearable device usually contains a microcontroller and different types of sensors to collect data remotely from the wearer or the environment for monitoring or data processing purposes. As mentioned in [61], the

authors classified existing commercial wearables into three categories: (1) Accessories, (2) E-Textiles, and (3) E-Patches by surveying over 100 products. The most popular category are accessories, including wrist-worns, head-mounted devices, and other accessories like smart jewellery, straps, etc. The wearable device in this research can be classified into the smart straps as it is supposed to be tied on an athlete's waist with a belt. They also stated that smart straps usually are used to monitor human physiological signals and biomechanics.

In another review [62], wearable sensors can be classified into two categories that are flexible and non-flexible by the materials of the sensors. The wearable device in this research belongs to the latter one which is rigid and made of brittle materials. The flexible wearable sensors are made of malleable materials that can be reshaped to some extent without changing the sensors' properties. As mentioned in [62], wearable sensors have been applied in many different areas, such as, medical, security, communication, etc. Although wearables have already been developed so broadly, there is still a great potential need for wearables used in sports.

3.1.3 INERTIAL MEASUREMENT UNIT

Usually, an inertial measurement unit (IMU) consists of an accelerometer, a gyroscope and a magnetometer. The accelerometer can collect acceleration data in three directions (X, Y and Z axes) in a 3D coordinate system. The gyroscope can collect rotation speed in three directions and the magnetometer can collect magnetic field intensity in three directions as well. Therefore, this type of IMU is a 9 degrees of freedom (DoF) IMU. Some IMUs are 6DoF that only have an accelerometer and a gyroscope.

Suppose an object is in an absolutely still condition on Earth, then there will only be the Gravity on it. When the object is tilted, the acceleration that the accelerometer detects will be the projection of the Gravity on the object's own coordinate system. So, by using some mathematical formulas, the roll (around X axis) and pitch (around Y axis) angles can be calculated out. However, the yaw (around Z axis) angle cannot be obtained with the acceleration data because the Gravity is orthogonal to the horizontal plane. One way to get calculate the yaw angle is to use the magnetometer. There are also some mathematical formulas for calculating out the yaw angle with the magnetic field intensity.

In reality, nothing can stay in an absolutely still condition. There are always some noisy signals leading to the errors that occur in the calculations from using the accelerometer's and the magnetometer's data. These two sensors are inaccurate due to the hardware limitation. That is why the gyroscope plays a very important role for an IMU. The gyroscope can collect the instant rotation speed that can be integrated with time to calculate out the angles directly. However, the fact that the time period cannot be sliced infinitely can lead to a drifting error when integrating the rotation speed with time. Therefore, an IMU data fusion algorithm or filter is required, which will be introduced in Chapter 4.

3.1.4 STATUS OF WEARABLES' DEVELOPMENT IN BIOMECHANICAL FEEDBACK TRAINING

Wearables in sports are only few years old; however, they have expanded radically, from the real-time monitoring of players' signs of exhaustion or injury while on the field to including perceptual and psychological aspects of professional team sports to enhance performance [63] – [65]. Wearable technology is leading a revolution in sport

[63], [65], [66]. Various sensors are now fitted into sports equipment, wristbands, and/or clothing to determine athletic performance, like speed, acceleration, power, distance, heart, and metabolic conditions during training. All the crucial data is sent to the coach and training team instantly, allowing for them to perform an individualized training for increasing athletic competence.

Nevertheless, real-time biomechanical feedback training currently does not look so optimistic. A search using keywords in the authority database – Web of Science – revealed the following scenario: when the keyword "biofeedback training" was applied, 5588 articles were found. However, when the keyword was changed to "biomechanical feedback training", the article numbers dramatically dropped to 569. Even more theatrically, when two additional keywords "real-time" and "sport" were added for a search, the number decreased to 23. A scarcity of articles occurred when the keyword "sport" was substituted by "dancing" (i.e., only one article was found in Table 1). These results would suggest that, when comparing to other biofeedback applications, the real-time biomechanical feedback applications lag far behind.

Table 1

The Results of Literature Search in All Databases of Web of Science on 11 October 2018 [45]

Biofeedback Training	Biomechanical Feedback Training	Biomechanical Feedback Training & Real-time & Sport	Biomechanical Feedback Training & Real-time & Dancing
5588	569	23	1

A close look at the published papers revealed that real-time biomechanical feedback training in motor learning is still an infant science. For example, only two applied studies attempt to reveal its potentials in human motor learning/training in Table 2. When considering the booming popularity of wearables in sports as well as in health-related applications, the number of biomechanical inquiries appears to be disproportionately low. The rarity of this occurrence could be a product of both the fact that there is a lack of a general biomechanical model for feedback motor learning and that researchers are still searching for methodological breakthroughs to link biomechanical quantification and human motor learning in real-time.

Table 2

The Article Types of Real-time Biomechanical Feedback Training Found in Web of Science [45]

	Motor Learning/Training	Method/Development	Injury Prevention/Rehabilitation	Review Articles	Patents	Total
Sport	2	10	7	2	2	23
Dancing	0	1	0	0	0	1

3.2 OVERVIEW OF BIOFEEDBACK

Effective human motor-skill learning/training benefits nearly every one of us, as it can help develop interests in more physical activities and lead to more active lifestyles [67]. The main aims of research related to human motor-skill learning are to improve learning techniques (education), to accelerate skill acquisition (learning), and to maintain motor function (training). All the three aspects rely on feedback mechanisms for their efficiency and effectiveness [9]. Given the complexity of human sensory-motor

behaviours, informed learning and training hold a great potential to improve efficiency, particularly in the acquisition of cognitive and psychomotor skills for highly complicated performance activities [18] and [68] – [71]. The two key components in human motor skill learning and training are practice and biofeedback [72]. Previous studies have shown that, when properly understood and applied, biofeedback training is an excellent tool for enhancing practice and performance of human motor skills [73] – [79]. In this section, biofeedback and its types will be introduced first. Then the milestones of biofeedback training in human motor-skill learning and training will be presented. Next, the unique aspects of biomechanical feedback will be discussed.

3.2.1 BIOFEEDBACK AND ITS TYPES

Biofeedback is usually gained by connecting the human body to electrical sensors that receive information (feedback) about the human body (bio). It is a technique that one can use to learn to control one's body functions or physical performance [80]. Generally, there are four types of biofeedback: physiological (e.g., heart rate and blood pressure), neurological (e.g., electroencephalogram (EEG)/brainwave), biochemical (e.g., electrolytes and metabolites in sweat or saliva), and biomechanical (e.g., joint angles and applied force) [81], [82]. In human motor learning, biofeedback training familiarizes us with the activity in our various body systems, so it is a useful educational and/or training tool for mastering and/or maintaining human motor skills [83].

3.2.2 MILESTONES OF BIOFEEDBACK TRAINING IN HUMAN MOTOR-SKILL LEARNING AND TRAINING

Learning and training of human motor skills has a history of over thousands of years [18], [72], experiencing some key periods, such as apprenticeship, class education,

individualized instruction, and integrated performance support. However, the appearance of (bio)feedback in systematic motor skill training did not occur until the early 1950s [84], [85]. After World War II, individualized instruction was first developed in industry for training human physical skills (i.e., human motor skills) efficiently and reducing expense while still obtaining high instructional value for various professionals. The training method broke the learning into small steps with an activity afterward to check comprehension. This reinforcement learning behaviour opened the door for biofeedback intervention in motor learning and practicing new motor skills.

This early form of feedback learning in essence requires immediate feedback (i.e., real-time feedback) given after each skill practice. The training can be knowledge-based (trainer), or more objectively, technology-based. The advantages of feedback learning are: (1) it allows for a learner to practice at his or her own pace and to find mistakes and correct them and (2) it reduces learning time, produces a low error rate, and improves learning efficiency through immediate feedback [18], [72]. A successful example of feedback learning is a computer-based training developed and used primarily in the military [85]. The benefits of such training are more opportunities for realistic training and feedback; and, increased availability and accessibility of training in operational units.

From a scientific point of view, human motor-skill development is a biological process. Therefore, the influential feedback should be those related to the changes to the biological parameters of the human motor system. In essence, feedback in human motor-skill training is primarily biofeedback. Biofeedback as a research major was first reported in the 1960s, supplying single-parameter feedback in real-time training [81]. Until the end of the last century, biofeedback had been able to supply multiple parameters, such as body

temperature, heart rate, respiratory rate, muscle activity, impact, joint angle, and others during training [86] – [88]. Due to the limitation of sensing technology at that time, the application was commonly lab-based, and participants were equipped with wires. As such, the applications were mainly in areas of less human mobility or less human movement complexity, such as in senior health care, physiotherapy, and rehabilitation [81] and [89] – [93].

Over the past decade, wearables are becoming the trend in sports training. Technological developments have led to the production of inexpensive, non-invasive, miniature sensors, which are ideal for obtaining sports performance measures during training or competition. The miniature sensing devices are worn on the wrist, clothes, and/or shoes. They supply real-time biofeedback for sports analyses. The sensing technology has turned towards creating devices with new form factors that augment sports activities.

The overwhelming impression of wearables' success in sport is mainly in monitoring physical condition and preventing injuries. For sport-related injuries, soft-tissue injury remains the most common type among athletes. The injury is often caused by fatigue, overtraining, or dehydration [94] – [96]. Wearable sensors are now able to collect data related to these risk physical conditions from athletes' physical conditions, muscle activities, and sweat [82] and [63] – [65]. The real-time biofeedback helps coaches to alternate their training or competition strategies for decreasing this injury in trainings and competitions [63], [65], [94].

Existing evidence demonstrates that wearables have successfully supplied real-time information related to athletes' speed, acceleration, power, distance (i.e., locomotion/physical characteristics), heart rate, muscle activities (i.e., physiological feedback), and electrolytes and metabolites (i.e., biochemical feedback). Although, these parameters are useful in analyzing the general physical condition of an athlete, they do not provide information that is related to the limbs' control of human motor skills. The biomechanical feedback is still missing. Without this vital information, the motor learning of complicated skills (e.g., artistic performance, gymnastics/acrobatics skills, and many others) is largely formed of art based on the trainers' subjective experiences of "what works" [68], [69], [97]. While this can be effective for some learners, large and widespread biological diversity unfortunately limits the generalizability of a single individual's experiences [68], [69], [98], [99]. Even small variations in bone length, muscle, and tendon attachments, for example, can disrupt this traditional form of knowledge transfer. Therefore, scientifically described training targets and routes need to be established to improve motor-skill learning. In other words, biomechanical feedback tools are required for measuring and quantifying characteristics of effective limb coordination (i.e., motor control).

3.2.3 UNIQUE ASPECTS OF BIOMECHANICAL FEEDBACK

Physiological, neurological, and biochemical feedback present information related to one's physiological variation, muscle tension, physical condition, and thought processes. Such information is conserved across human motor skills, i.e., across different movement forms. Therefore, feedback devices monitoring these parameters can be universally applied to all activities [100], [101].

In contrast to physiological, neurological, and biochemical feedback, biomechanical feedback mainly provides information that is related to the limbs' control of human motor skills, which directly accelerates motor skill learning and optimization, but must be tailored to the activity being examined [16] and [102] – [104]. In other words, biomechanical feedback is a more useful tool but complicated for its development.

Several studies in the past decades confirmed the importance of real-time biomechanical feedback, showing up to 100% improvement with its applications [105] – [108]. However, the development of biomechanical feedback is still in its infancy. While the real-time biofeedback of the first three types (i.e., physiological, neurological, and biochemical feedback) has been well developed for the past decades and is now a routine application (successfully transferred from lab-based to training and/or competition environments), the studies and applications of the biomechanical one are still rare. After reviewing 666 publications between 1960's and 2010's, Tate and his colleagues found that there were only seven studies using real-time biomechanical feedback for physical training in a laboratory environment [81]. Additionally, the current state has not shown a considerable change, especially in sports performances (Table 1 and Table 2). The rarity could be caused by the numerous obstacles that must be overcome during the development of the real-time biomechanical feedback tools. The primary one is that biomechanical feedback must always be tailored to an activity (i.e., non-generalizable), requiring different design parameters for different motor skills. Thus, to develop a biomechanical feedback device, one must first obtain a thorough understanding of the selected motor skill in order to select the useful parameters for monitoring. Furthermore, the devices must not interfere with the motor skill being executed. This technical limitation alone has proved

to be a major hindrance to the development of biomechanical feedback devices in motor learning and training.

3.2.4 PRINCIPLE OF 3D MOTION ANALYSIS

In a 3D motion analysis, a 3D motion capture system needs to be used to measure a full-body movement by using ~40 reflective markers. VICON is a commonly used 3D motion capture system. With respect to a full-body modeling in the VICON system, the collected kinematic data can supply primary information, such as each marker's position, the positional changes, the velocities, and the accelerations.

In this case study, each subject needs to wear a black garment made of stretchable material, which can cover the upper and lower body of each subject. Affixed to the garment were 39 reflective markers, each with a diameter of 9 mm. Markers on the upper body were placed on the acromion process, lateral epicondyle of the humerus, styloid process of the ulna and radius, third metacarpophalangeal joint, as well as on the upper and lower arm (the four markers on the upper and lower leg were only used to determine segmental rotations. As they were not involved in segmental translations, no specific anatomical position is needed for these four markers), sternal notch, xiphoid process, C7, T10, and left back. Four markers were also placed on the head—one on the left and right temples each and two on the posterior portion of the parietal bone. Markers on the lower body were placed on the anterior superior iliac crest, posterior superior iliac crest, lateral condyle of the tibia, lateral malleolus of the fibula, calcaneal tuberosity, and the head of hallucis, as well as on the upper and lower leg (again, no specific anatomical position is needed for these four markers). Raw kinematic data was processed using a five-point (1-3-5-3-1 function) smoothing filter. From these 39 markers, a full-body biomechanical

model with 15 segments can be built to reveal undisclosed aspects of the motor control [10], [13], [15], [109] – [111].

The model worked as follows: from motion capture, anatomical positions could be established, which then allowed the construction of a 15-segment full-body model. Using the fundamental precepts of physics, simple positional data were translated into the movement of the multi-segment model. In such individualized biomechanical modeling, the anthropometric characteristics of the body were established using anthropometric regression equations found in statistical studies [98], [112]. The 15 segments were the head and neck, upper trunk, lower trunk, two upper arms, two lower arms, two hands, two thighs, two shanks, and each foot. In addition, three markers were attached on the handle. Furthermore, reflective tape was glued to the shot to determine hammer release speed.

3.3 DISCUSSION ON DEVELOPING WEARABLES FOR BIOMECHANICAL FEEDBACK

For human motor-skill learning, people are always looking for ways to speed up training, ways to make it more economical, efficient, and effective, and ways to minimize injuries. Real-time biomechanical feedback training could be the best solution that people are looking for, because the technology would have the potential for: (1) moving scientific monitoring from a lab-based environment to the field, (2) simplifying a scientific quantification from using a complicated motion capture system to easily-applied wearables, and (3) transferring the vital biomechanical feedback quickly to prevent the movement errors from happening, while still finding individual compensation and optimization. However, biomechanical wearables still require much more research before they can become impactful tools in the real world. Developing real-time biomechanical

feedback training tools needs to search ways (e.g. individualization) to supply information, which should consider the motor-control diversity, the anthropometric variation, and the physical compensation/optimization. In this section, the biomechanical steps required in developing wearables for biomechanical feedback will be presented first. Then, the challenges and obstacles in its development will be discussed. Finally, how to use AI technology to make a breakthrough in the research will be explained.

3.3.1 BIOMECHANICAL STEPS

A successful motor learning outcome can be supported by useful and timely biomechanical feedback to the athlete targeting performance defects. Systematic, objective, and reliable performance monitoring and evaluation, performed by means of quantitative analyses of biomechanical variables, can reinforce biomechanical feedback training in sports practice [69], [97], [102]. Therefore, the approaches of quantifying a motor skill with high spatial and temporal accuracy (i.e., the limb coordination) would be the key to developing wearables for biomechanical feedback training.

Currently, the most reliable biomechanical feedback method is 3D motion capture, which identifies and tracks markers that are attached to a human subject's joints and body parts to obtain 3D skeleton information [11], [53], [54]. The spatiotemporal human representation based on 3D motion capture data is currently the most trustworthy approach in motor skill quantification [10], [12], [13], [23], [109], [110]. This method, however, mainly supplies post-measurement feedback (i.e., not real-time) due to its drawbacks: multiple cameras placed in a room, long calibration and setup procedures, a time consuming course on data collection, processing, analysis, and interpretation, and the high cost of the equipment [20], [21], [113].

For practitioners, real-time feedback is more useful. Yet, due to the drawbacks of 3D motion analysis technology and the diversity of human motor skills in sport, research on biomechanical feedback training has to undergo:

(1) selection of a specific motor skill,

(2) 3D motion analysis of the skill,

(3) verification of post-measurement feedback in practice, and

(4) development of a feedback device for monitoring the critical/vital parameter(s) (e.g., coordination among certain segments or joints) for the given motor skill.

These steps are, at present, required for developing a reliable wearable device that is capable of supplying real-time biomechanical feedback [87].

3.3.2 CHALLENGES AND OBSTACLES

Current sensing development has shown its potential to mitigate problematic constraints of biofeedback devices on human movement and has demonstrated its great promise to expand the capabilities of biofeedback to motor-skill learning [63]. The successes in health and physiotherapy [19] [86], [89], [114] suggest that biomechanical wearables will become a reality in human motor learning and training in sport. However, the transition from the simple motor-skill trainings to the complicated ones would face several challenges.

It is no doubt that the greatest challenge for developing biomechanical wearables is the practicality. Any device attached to a human body will supply certain constraints for his/her movement and alternate the movement control in a way that may not reach the goal of training. Currently, the reliable 3D motion capture technology requires around 40

markers for motor skills' quantification and characterization [11], [13], [15]. Even the non-ideal test condition cannot be substituted by simply replacing the ~40 markers (sphere shape of 9 mm in diameter and almost weightless) with wearables, because the weight and volume of current wearables (e.g., IMUs) can cause unknown experimental artifacts (i.e. the experiment itself that biases the measurements). Therefore, how to apply as few wearables as possible for accurately rebuilding sports motor skills would be the primary focus for the development of wearables in human motor-skill learning.

The second challenge is the identification of motor control patterns. Motor control patterns exhibit the characteristic wherein either gross or fine motor control appears to be dominant. In most sports, it is reasonable to conceive that the majority of activities (e.g., running, jumping and throwing) mainly rely upon large muscles (i.e., gross motor control), where smaller muscles function in significant stabilizing roles. Fewer activities, like shooting, rely mainly on smaller muscle group coordination (i.e., fine motor control) where gross motor control supplies foundational support or is nearly rested [16], [53].

The third challenge is the expert-knowledge needed (i.e., compensatory strategies depending on an individual anthropometry and physical condition) for complicated motor-skill learning. Motor control in sport is acknowledged to be an activity requiring complex behaviour and long-time motor control development [13], [71], [102]. Athletes take significant amounts of training and practice for individualized development, i.e., motor-skill optimization based on their body structures and physical uniqueness. During their years of training, the desirability of acquiring skills efficiently and effectively while simultaneously avoiding injury would seem self-evident. Therefore, athletes at various levels are continually searching for opportunities to improve their motor skills and gain

advantages or perfection in their competitions. Study on developing individualized compensatory joint coordination is still feeble.

3.3.3 AI FOR MOTOR CONTROL QUANTIFICATION

AI systems are performance driven – one focus is on the predictive accuracy, based on known characteristics learned from the previous data/training samples [115], [116]. In the past decades, AI techniques have experienced a resurgence following concurrent advances in computing power, large amount of data (big data), and theoretical understanding. AI techniques have become a powerful tool for helping to solve many challenging problems in human motor-skill evaluations and analyses [117] – [121].

The idea of AI prediction is to find a way to learn general features in order to make sense of new data [115], [116]. This description highlights the central role of data for establishing implicit knowledge. The amount of data must be sufficiently large to provide many training examples from which a large set of parameters can be extracted.

In summary, machine leaning is one of the methods of realizing AI while deep learning is a subfield of machine learning [122]. The conventional machine learning methods can be classified as supervised learning and unsupervised learning. Most recently, semi-supervised learning, reinforcement learning and deep learning, etc. were proposed. Although there are so many different machine learning methods, they still use those classic statistical methods, such as Support Vector Machine, Naive Bayes, Neural Networks, Decision Trees, K-means Clustering, etc.

Among AI technologies, deep learning is considered a powerful tool that percolates through to all application areas of machine learning, such as image

identification, speech recognition, natural language processing, and, indeed, biofeedback support [123] – [125]. Usually, deep learning requires large amounts of data to train a network. Convolutional neural network (CNN) and Recurrent Neural Network (RNN) are most commonly used deep networks [122]. In the proposed wearable system, two Sequential models were built based on Keras API. The Sequential models use an RNN to process the inputs. RNNs consisting of input layers, hidden layers and output layers are rather powerful and dynamic systems. In general, if a model has at least two hidden layers, then it can be treated as a deep learning model. A hidden layer in a neural network is located between the inputs and the outputs [126]. In each layer, the inputs or the outputs from the previous layer will be calculated through an activation function, and the outcomes from the calculation will be the next layer's inputs or the final outputs. The activation function can determine the outputs of a deep learning model, its accuracy and the computational efficiency [127].

When training a neural network, optimization algorithms, also called optimizers, are used to reduce the losses which indicate the error. Because the goal of training a neural network model is to minimize the error, the loss functions can tell people "how good" the model is at making predictions for a given set of parameters. One can set and adjust the learning rate which is a tuning parameter in an optimizer to determine the step size at each iteration (i.e., epoch) for minimizing the losses. Bigger learning rates will never reach the global minima and will wander around it. In contrast, smaller learning rates can be easily trapped in a local minima, and its training time will be longer [128]. Metrics are used for evaluating learning models.

The success of deep learning networks encourages their implementation in further applications for the enhancement of human physical activities [129], [130]. Most recently (September 2018), Nature Neuroscience published the latest developments in the area of markerless and video-based motion tracking, indicating that the power of deep learning will enable motion tracking to human-like accuracy [131]. This study confirms that motion capture or quantification of limb coordination will move from an expensive and difficult task restricted to the laboratory to an effortless daily routine for researchers and practitioners.

From a motor learning point of view, wearables would have much higher potential than video shooting in future practice. This is not only because of the fast advance in miniaturizing wearables, but also due to two inherited drawbacks of the video-shooting approach. Reliable biomechanical feedback should be obtained from accurate quantification of human movement in the field, with some sports requiring large space. Even with a multiple-camera setting, unexpected environmental factors (e.g., interactions among athletes) will create data-gaps. Further, it is true that massive movement data (e.g., from YouTube, Flickr) already exists for training of deep learning models. However, those video datasets are uncalibrated and have very little information on the hardware and conditions used to capture particular videos, which can bias the deep learning recognition algorithms [132]. Currently, the availability of reliable motion capture data for developing deep learning models is significantly limited.

3.3.4 REAL-TIME BIOMECHANICAL FEEDBACK TRAINING IN THE HAMMER THROW

The hammer throw has a long-standing history in track and field, but unlike some other sports events, men's hammer throw has not seen a new world record since 1986 [14]. This sport involves complex human motor skills, such as quick body spins, dynamic balancing, explosive power generation, and so on [23]. One of the possible reasons for this stagnation could be the lack of real-time biomechanical feedback training. Due to the fast speed of the body movement and the invisibility of all the forces generated during the movement, it is very difficult for the coaches to give reliable feedback; and therefore, they have to mainly guess what works best for the athletes based on their experience in the hammer-throw training sessions [23].

Developing a wearable device that can be used in the hammer-throw training will be able to provide coaches with scientifically based feedback. Wearable wire-tension measurement has garnered great interest in biofeedback training of the hammer throw [19] and [133]. They supply real-time, in-field/non-lab-based monitoring of tension/force generation as indicators of a trainee's performance progress. It seems that the hammer throw could be numerically analyzed in practice and the details of the motor control could be immediately available for coaches. However, the absence of a reliable method of linking the wire-tension data to the motor control of the throw has greatly hindered its application in practice. In order to bridge the gap, a synchronized measurement of 3D motion capture (kinematics of the throw/motor control) and wire-tension (kinetics of the throw) was applied to find the missing piece that could link the two types of data.

In the pilot study [23], one national-level athlete (body weight: 115 kg, body height: 178 cm, personal performance: 66.7 m) and one college-level athlete (body weight: 111 kg, body height: 176 cm, personal performance: 49.5 m) was tested, analyzed, and compared in order to find the link. No restrictions were placed on the subjects before and during the trials in an effort to preserve their normal motor control style. The university human-subject committee scrutinized and approved the test as to meet the criteria of ethical conduct for research involving human subjects. The subjects were informed on the testing procedures and voluntarily participated in the data collection. A twelve-camera VICON motion capture system (Oxford Metrics Ltd., Oxford, England) was set up on fully extended tripods around an indoor hammer pit with a safety set in front of the cameras. Six cameras were placed in a row parallel with the safety net on each side of the hammer throw pit. Capture occurred at a rate of 200 frames/second. Calibration residuals were determined in accordance with VICON's guidelines and yielded an accuracy within 1 mm. After warm-up, the national-level athlete performed five trials and the college-level athlete performed six trials. The trial (judged by the fastest release speed) of each subject was selected, analyzed, and compared. The experimental results have found the two key parameters – vertical wrist and hip displacements that need to be collected by a wearable device.

Meanwhile, deep learning predictions based on the IMUs' data have shown great potential in developing real-time biomechanical feedback training for an efficient human motor-skill learning and optimization. Deep learning models can help to validate that the data of displacements of the hip and wrist, which can be collected by a wearable device,

could reveal the upper and lower limbs' coordination so that the proposed system can provide real-time biomechanical feedback along with the tension data.

3.4 SUMMARY

In this chapter, the background of wearables and biofeedback have been reviewed. Also, a discussion on developing wearables for biomechanical feedback has been provided. The key skills of developing a wearable system that can provide real-time biomechanical feedback are 3D motion analysis, and computer science related skills, such as hardware and software development of a wearable device, AI modeling, etc.

Therefore, the next chapter will focus on the system following with the background in this chapter. Although this research aims to develop a real-time biomechanical feedback training just in hammer throw, it could be a practitioner's desire that, like physiological, neurological and biochemical wearables, a biomechanical wearable device could also be universally applied to all motor skills for their learning and training in any sport (i.e., not only limited to the hammer throw).

CHAPTER 4: THE PROPOSED REAL-TIME BIOMECHANICAL FEEDBACK SYSTEM

In a traditional hammer-throw training session, a coach helps athletes to improve their performance just by watching their throwing movements. However, the men's hammer-throw world record has not been broken for over three decades. The lack of scientifically based training may be one of the reasons for this stagnation. A scientific training method requires quantification of some fundamental features that can reveal key factors influencing athletes' scores after a throwing movement. Although 3D motion capture systems can provide highly trustworthy biomechanical feedback, it is not in real-time. In addition, a wearable device can help to reduce the negative effects (such as movement constraints, complicated operation, long procedure, etc.) of the motion capture markers attached to the athletes. It also helps to avoid carrying the whole camera system which usually consists of multiple high-speed cameras along with their corresponding heavy camera stands and the system machine to the training field. Thus, developing a wearable system for the elite training of the hammer throw is necessary. The proposed real-time biomechanical feedback system can be used to facilitate motor learning and optimize motor skills for the hammer-throw athletes. However, the quantification of one vital feature found by the pilot study [23], that the timely change of the vertical wrist and hip displacements can reveal the upper and lower limbs' coordination, requires AI technology for validation.

Figure 5 illustrates the flowchart of the proposed wearable system consisting of three basic elements: sensor node, receiver node and deep learning models. The sensor node, which is the wearable device, is used to collect data for transmission. A customized

PCB (printed circuit board) has been designed to miniaturize the wearable device, and a 3D printed box along with its lid has been designed for housing the PCB and other related components. The receiver node has an XBee module connected to a laptop through USB for data transmission. A MATLAB program has been implemented to receive, process and display the collected data in real-time. The two nodes can communicate with each other remotely through XBee modules. Two deep learning models have been built to validate the predictions for the change of the following key joints' angles: the left and right hip angles, the left and right knee angles, the left and right ankle angles, the left and right shoulder angles, the left and right elbow angles, the left and right wrist angles, and the thorax angle. Developing such a wearable system could replace the VICON motion capture system which can only provide post-processed biomechanical feedback. However, the motion capture technology is still the most reliable for obtaining 3D data. Therefore, the VICON system helps with the calibration of IMUs (inertial measurement units) and provides the training and testing datasets for the deep learning models.

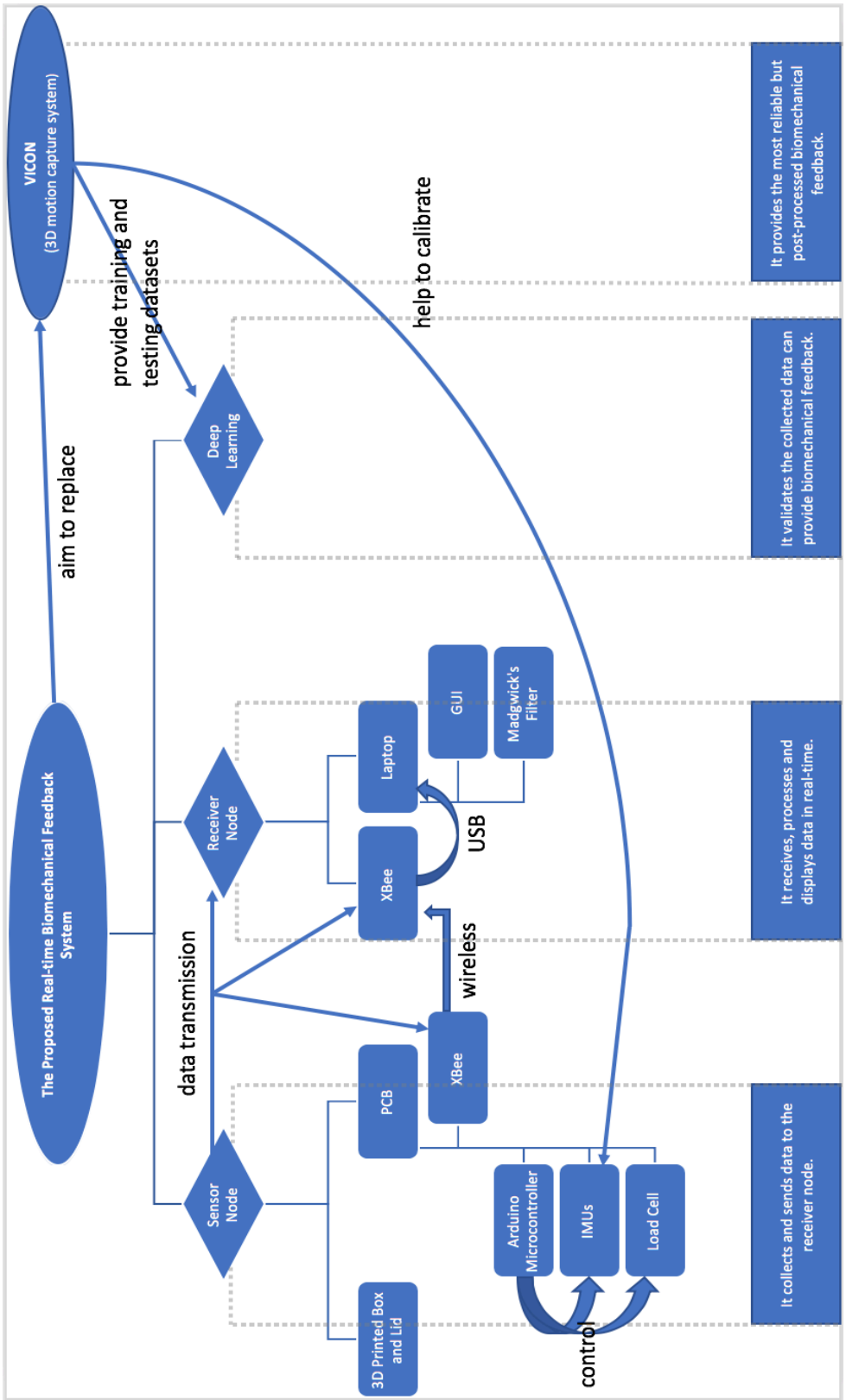

Figure 5: The flowchart of the proposed system

As discussed in 3.1.1 in Chapter 3, two issues were found from the previous design [19]. One is that the distance sensor could not work as expected. The other one is that the size of the device was still a little bit large due to the big size of the Arduino Mega board which was used as the microcontroller. Therefore, the new system was proposed to improve its efficiency by replacing the distance sensor and the microcontroller with the help of PCB design. Figure 6 illustrates the updated system architecture. The previous distance sensor and microcontroller have all been replaced with new components. So, the new sensor node consists of an XBee module [26], an Arduino Pro Mini board [40], and the sensors including two IMUs [38] and a load cell [39]. One IMU is on board and the other one is attached to the wrist of an athlete by an Ethernet cable (approximately 170 cm in length). The load cell is embedded in the narrow end of a hammer-throw handle which is also attached by an Ethernet cable (approximately 325 cm in length). One reason of using Ethernet cables here is that there are various coloured wires inside the Ethernet cable which makes it convenient to connect the sensors to the PCB. The Arduino board is responsible for controlling all the sensors to collect the required data from a field test and sending the data through the XBee module to the receiver node. The receiver node has another XBee module connected to a laptop to receive and process the data. A GUI on the receiver node side, designed in MATLAB, is used to display real-time feedback. There is also a MATLAB program for saving and processing the raw data.

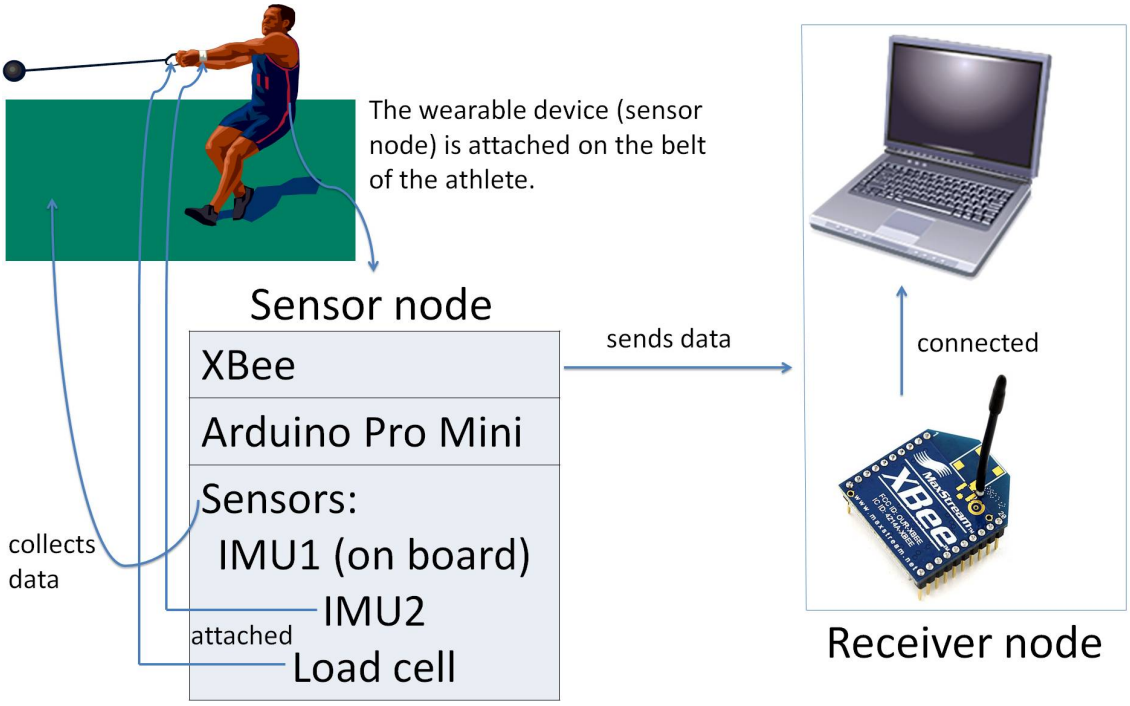

Figure 6: Updated system architecture

In this chapter, the configuration of the XBee [26] modules which is the wireless communication channel in the system will be described in detail with the XCTU [25] software. Then, the sensor node and the receiver node will be introduced respectively. Lastly, the deep learning models will be discussed.

4.1 XBEE CONFIGURATION

The two XBee [26] modules are the key to wireless communication in the system. I configured the two XBee modules with XCTU [25], which is a free software application to configure and test the XBee RF (Radio Frequency) modules through a graphical interface, to pair them with each other, which allows the sensor node to send data to the

receiver node. One example of the XCTU configuration interface is shown in the Figure 7.

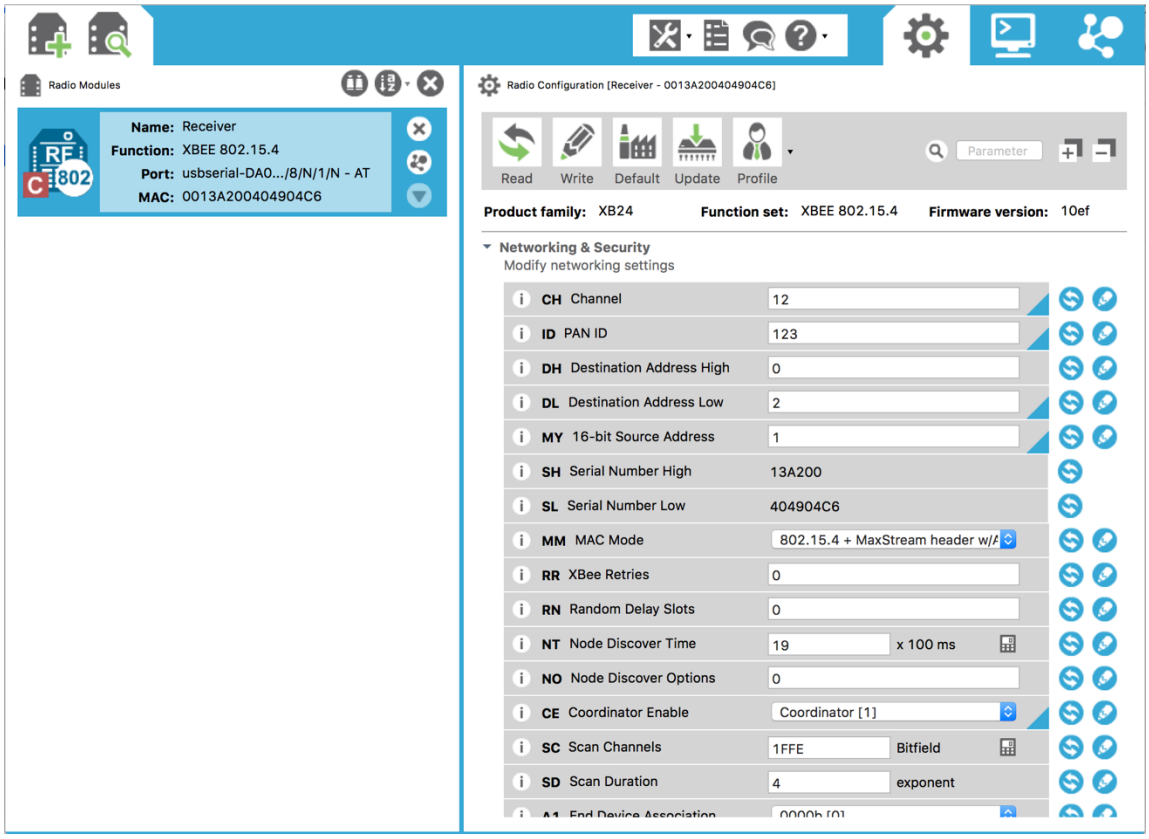

Figure 7: An example of the XCTU configuration interface

For most of the parameters, the default values could be used. Some parameters could be set to the same value for both XBee modules in the sensor node and the receiver node. These parameters are: Channel, PAN (Personal Area Network) ID, Interface Data Rate, and Packetization Timeout. They can be set to any number within its range respectively depending on personal needs. The only requirement for these parameters is to set them to the same for both XBee modules. Some parameters need to be set to different values depending on personal requirements. Every parameter's detailed description can

be found in the XCTU manual [25]. Some key parameters that were modified for this case study will be introduced.

The interface data rate, which is also referred to the baud rate, was set to “57600”. The higher the baud rate is, the faster the transmission speed will be. However, a higher baud rate requires a greater bandwidth for the signal channel. In other words, its tolerance of noisy signals will be reduced as the baud rate is set to higher values. There are eight options to set the baud rate to, which are “1200”, “2400”, “4800”, “9600”, “19200”, “38400”, “57600”, and “115200”. A faster speed of data transmission was preferable. However, the data was influenced too much by some noisy signals with “115200” baud rate during the tests. So, it was set to “57600” for reliability and stability.

The packetization timeout was set to “0”, whose default value is “3” and its range is from “0x0” to “0xFF”. This parameter was set to “0” to allow the XBee module to transmit characters as they arrive instead of buffering them into one RF packet. By performing some experiments with different settings, it was found that the receiver node can receive and process the data in MATLAB better with this specific setting.

The destination address low was set to “2” for the XBee module in the receiver node, while the destination address low for the XBee module in the sensor node was set to “1”. Its default value is “0” and its range is from “0x0” to “0xFFFFFFFF”. The 16-bit source address was set to “1” for the XBee module in the receiver node, while it was set to “2” for the XBee module in the sensor node. The default value of this parameter is “0” and its range is from “0x0” to “0xFFFF”. These two parameters were configured specifically for point to point wireless communication.

The XBee module in the receiver node is treated as a “coordinator” by setting the parameter of coordinator enable. This parameter for the XBee module in the sensor node was set to its default value – “end device”. The reason why I chose the XBee module in the receiver node as a “coordinator” is that the “coordinator” needs to start up before the “end device”. In this way, it can make sure the receiver node is always waiting for receiving data to avoid missing any data sent from the sensor node.

4.2 SENSOR NODE

A low-power and low-cost wearable prototype has been developed as the sensor node in the real-time biomechanical feedback system. By designing a customized PCB, its total expenditure (including the sensors, the XBee modules and the batteries) is roughly no more than CAD$1200 due to the high cost of the load cell (CAD$950). Without considering the sensors, the XBee modules and the batteries, the total expenditure of the board itself is less than CAD$100. Comparing to the VICON system (over US$300,000), the expenditure is dramatically reduced.

In this section, the sensor node will be elaborated in detail. First, how to design and develop the hardware will be introduced. Second, the calibration procedures for ensuring that the sensors work properly before installing them on the PCB will be discussed. Finally, the Arduino program for controlling all the sensors will be discussed as well.

4.2.1 HARDWARE

The proposed device is sealed in a customized box as illustrated in Figure 8 and Figure 9. The customized box and its lid were both designed with Autodesk Inventor 2014

[37]. A virtual model was drawn in Autodesk Inventor 2014 with its provided designing tools. I measured the actual size of every single element and considered every detail very carefully, such as the distance between the board and the slots, the height and the radius of a screw slot, and so on. Every parameter needed to be as small as possible to miniaturize the device. The virtual box and its lid were drawn separately. Then an "assembly" function in the software ensured that the two virtual parts can match well with each other before printing them out in reality.

Once the virtual model was created in the software, the model's two parts – the box and the lid were printed out respectively by using a 3D printer. The dimensions of the box are 8.6 centimeters (cm) in length * 7.8 cm in width * 5.3 cm in height. It is used to hold the board and the sensors for stability and reliability during field tests. The power switch can be installed on the top of the lid, as shown in Figure 8. The batteries' charge can be saved by turning off the switch when the device is on standby. There is a space (Figure 9) under the board at the bottom area of the box so that a belt can be put through the box and tied on the waist of an athlete.

Figure 8: One view of the customized box and its lid

Figure 9: Another view of the customized box and its lid

Figure 10 shows the customized PCB inside the 3D printed box. An Arduino Pro Mini 328 – 5V board [40] was used as the microcontroller. This Arduino board is tiny and inexpensive. It uses the ATmega328P [134] chip which is an 8-bit AVR microcontroller with high performance but low power consumption. It is the key to make the wearable device low-cost and low-power. This feature is also the heart of many devices that make up the Internet of Things (IoT) according to [135] posted on the official website of Avnet, one of the biggest distributors of electronic components and embedded solutions in the world.

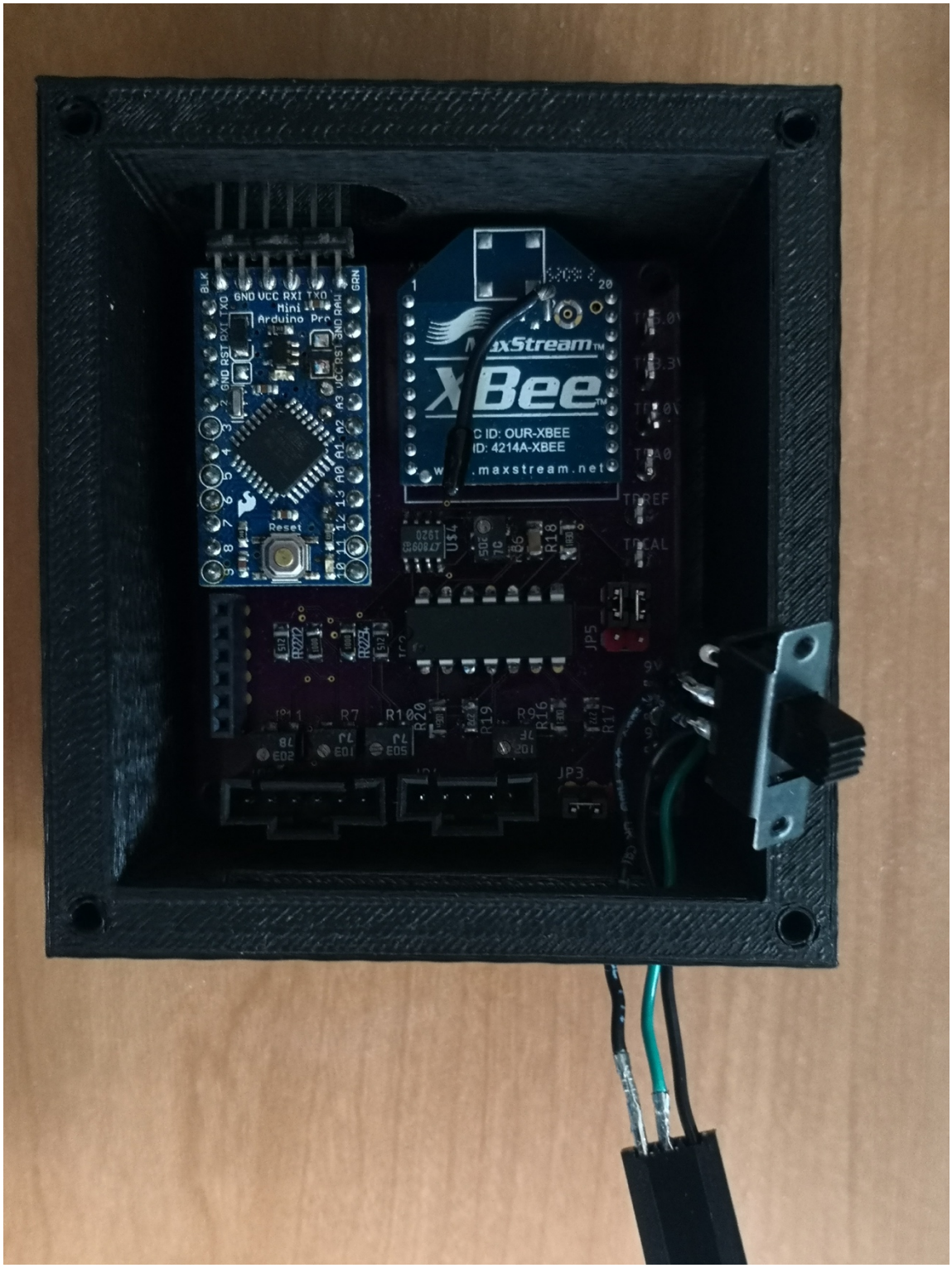

Figure 10: The board inside the 3D printed box

As shown in Figure 10, in the box, the Arduino Pro Mini board and an XBee module were all inserted into the PCB. The six pins of the right-angle male headers were soldered on the Arduino board for uploading programs. These pins can reach to the outside through a hole in one side of the box so that it would be easy and convenient to upload programs. Because more field tests need to be performed in the future, the only reason for opening the lid is to fix any circuit issue. For example, if there is any further improvement from the software perspective, it will not have to be opened for uploading a revised program. An FTDI basic breakout module [136] is used to upload programs to the Arduino Pro Mini board through a USB connection. It has 6-pin female header on the bottom that can match the soldered 6-pin right-angle male headers on the Arduino board. On the other side, a USB Mini-B cable can be used to connect it with a laptop.

The six pins of the FTDI basic breakout are: a DTR pin, an RXI pin, a TXO pin, a POWER pin, a CTS pin, and a GND pin [137]. The DTR pin allows the Arduino board to reset automatically when a new program is uploaded so that one does not have to hit the reset button by hand. The RXI and TXO pins are for transferring data. These two pins have similar functions of RX which is short for receiver or receive and TX which is short for transmission, but they have explicit directions for input and output. The RXI is the receiver input while the TXO is the transmitter output [138]. The POWER pin is for power supply and the default power of the breakout board is 5 volts (V). The CTS pin is an input pin as a handshaking [139] signal. The GND pin is for ground supply.

On the bottom of the PCB, there are three slots for connecting the sensors. One of them is for connecting the load cell which is an LCFD-1K [39] made by Omega to collect the raw tension data. The other two slots are for connecting the IMUs which are MinIMU-

9 v5 digital combo boards [38] made by Pololu to collect the raw data of the vertical displacements for the hip and wrist. As the IMUs can only provide the raw data of acceleration and rotation speed, it is required to apply an IMU data fusion algorithm [42] for calculating the displacements from the raw data, which will be introduced in the later sections in Chapter 4 and Chapter 5. A SparkFun 6 Degrees of Freedom (6DoF) IMU Digital Combo Board - ITG3200/ADXL345 [140] and a Teensy 3.2 USB Microcontroller Development Board [141] were used in the earlier development to measure distance (Figure 15). The calibration of IMU in the following sections were based on these configurations. Recently, another efficient and cost-effective 9DoF IMU – the Pololu MinIMU-9 v5 Gyro, Accelerometer, and Compass [38] was found. In addition, it is much easier to install two Pololu IMUs on the PCB because they have a "slave address" feature. The slave address pin is pulled high by default. So, simply alternating one IMU's slave address pin (SA0) from high to low would realize making two IMUs connected on the same I2C (inter-integrated circuit) bus without any conflict. In the final proposed wearable device, the Pololu MinIMU-9 v5, a compact (0.8″×0.5″) board that includes a LSM6DS33 (3-axis gyroscope and 3-axis accelerometer) and a LIS3MDL (3-axis magnetometer) [38] was used.

Now that all the plug-in components on the surface of the board have been introduced, it is time to look at the PCB design. Figure 11 displays the PCB designed to miniaturize the physical size of the wearable device for data collection. The designed PCB depicts the top copper surface in red, bottom copper in blue, and pads which are visible on either side of the board in green. A copper ground pour is placed on either side of the board but is not depicted here.

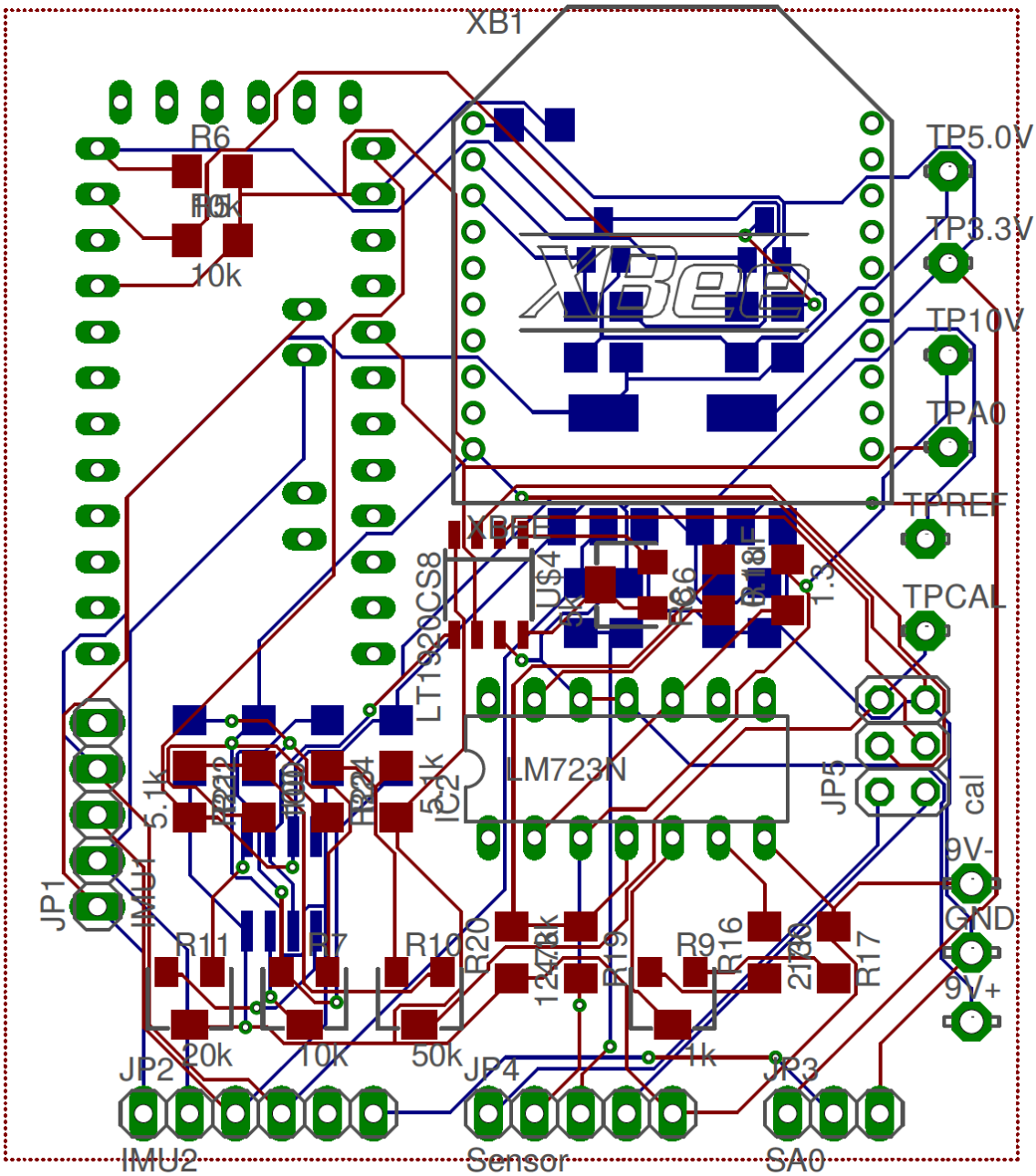

Figure 11: PCB design

The electronic components used in addition to the Arduino microcontroller and the XBee module are various resistors, capacitors, potentiometers, three voltage regulators, two MOSFETs (Metal-Oxide-Semiconductor Field-Effect Transistor), an operational

amplifier (OPAMP), and an instrumentation amplifier. Figure 12 shows the logic diagram of the major electronic components on the PCB.

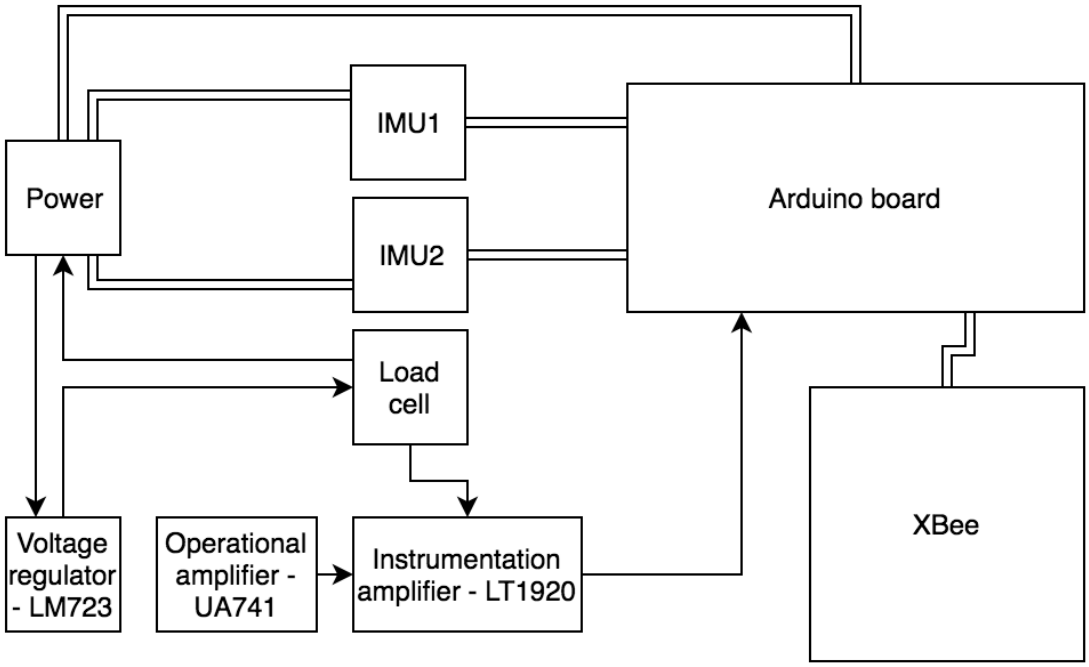

Figure 12: Logic diagram of the major electronic components on the PCB

The principle of the circuit design is straightforward. An 18V power supply (consisting of twelve 1.5V AA batteries) is divided into two, providing a +/-9V dual-rail supply. The two voltage regulators change it to 5V power for the Arduino and digital circuitry, and the XBee module receives 3.3V. Both of the IMUs also require 5V. The additional pin on the second IMU port is required to drive the slave address pin so that the two IMUs work on the same I2C bus. The voltage regulators are selected so that the required current for all components could be provided by a single 5V or 3.3V regulator.

The load-cell requires a constant and stable 10V supply because of power requirements for an excitation of greater than 25 pounds (lb) according to its datasheet

[39]. The linear voltage regulator – LM723 [142] is used to generate the required 10V supply. The voltage signal generated from the load cell is on a scale such that the analog to digital converter (ADC) on the Arduino is not sensitive enough to detect the signal during the calibration procedure. Thus, the instrumentation amplifier – LT1920 [143] is required to amplify the incoming signal. The OPAMP – UA741 [144], along with the accompanying resistors and potentiometers, can produce an offset voltage, allowing the signal to fall within the range of the Arduino's ADC.

JP5, shown in the middle right of Figure 11, allows the load cell of the circuit (pins 1 and 2) to be disconnected from the instrumentation amplifier (pins 3 and 4) and be connected to a calibration circuit instead (pins 5 and 6), depicted in Figure 13. Two jumpers, placed vertically, either connect pins 1&3 and 2&4 or pins 3&5 and 4&6. The calibration circuit, consisting of a voltage divider and a potentiometer, provides a range of voltages to the instrument amplifier and the Arduino ADC so that the gain and the offset can be adjusted to provide the best signal from the load cell.

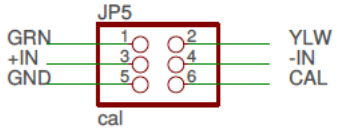

Figure 13: Calibration jumper pins

The calibration jumper pins allow for the disconnection of the load cell and the connection of a controlled voltage source such that the gain and the offset can be adjusted, which helps to avoid any unpredictable damage to the load cell. GRN (green) and YLW (yellow) pins relate to the colour of the wires that lead to the load cell. +/- INs refer to the

pins on the instrumentation amplifier. GND (ground) and CAL (calibration) refer to the ground level potential and the calibration voltage source.

Due to the small size of these surface-mount electronic components, careful attention must be taken while assembling the board. There were two issues when embedding the previous design [19] into the PCB. One issue was an inappropriate potentiometer used in the circuits for the load cell. It had to be a 500-ohm potentiometer, but a 5000-ohm one was used instead. The difference between the two potentiometers is the sensitivity. The proper potentiometer requires it to be turned many times, but for the 5000-ohm one, only a fraction of a turn was required to get the range of the required output signal. Because the potentiometer was too large, when tuning it, there would be a big chance of over adjusting that would lead to missing the desired value shown on the voltmeter. After replacing the potentiometer, it was discovered that two wires were mistakenly reversed; a correction of that restored the full function of the board.

4.2.2 CALIBRATIONS

There were two calibration procedures in the development of the wearable device. The calibration procedures are important to make sure each sensor can work properly before installing them into the device, i.e., the IMU and the load cell must be ensured to collect data accurately. The load cell had already been tested in the field [19]. As discussed in Section 3.2.1, after fixing the issues of the new circuit for the PCB, the load cell was effective in the new device. However, a new calibration procedure was still needed to make sure the correct tension data can be obtained.

Figure 14 shows the settings of the calibration for the load cell. The device was put on the table. The load cell, which is placed into the narrow end of the hammer-throw handle, was hanging freely in the air until it was still. A cable was tied on the load cell to hang different weights as a simulation of different wire-tension values. The initial weight was zero, i.e., no weight is hanging initially. The weights were added by 5 lb every time until 35 lb. For every 5 lb, I recorded the raw data displayed on the laptop. I obtained eight analog-to-digital values matching the real weights: 0 lb, 5 lb, 10 lb, 15 lb, 20 lb, 25 lb, 30 lb, 35 lb. First, the unit of the weight was converted from lb to kilogram (kg) as a convention. So, the array contained 0 kg, 2.27 kg, 4.54 kg, 6.8 kg, 9.07 kg, 11.34 kg, 13.61 kg, 15.88 kg.

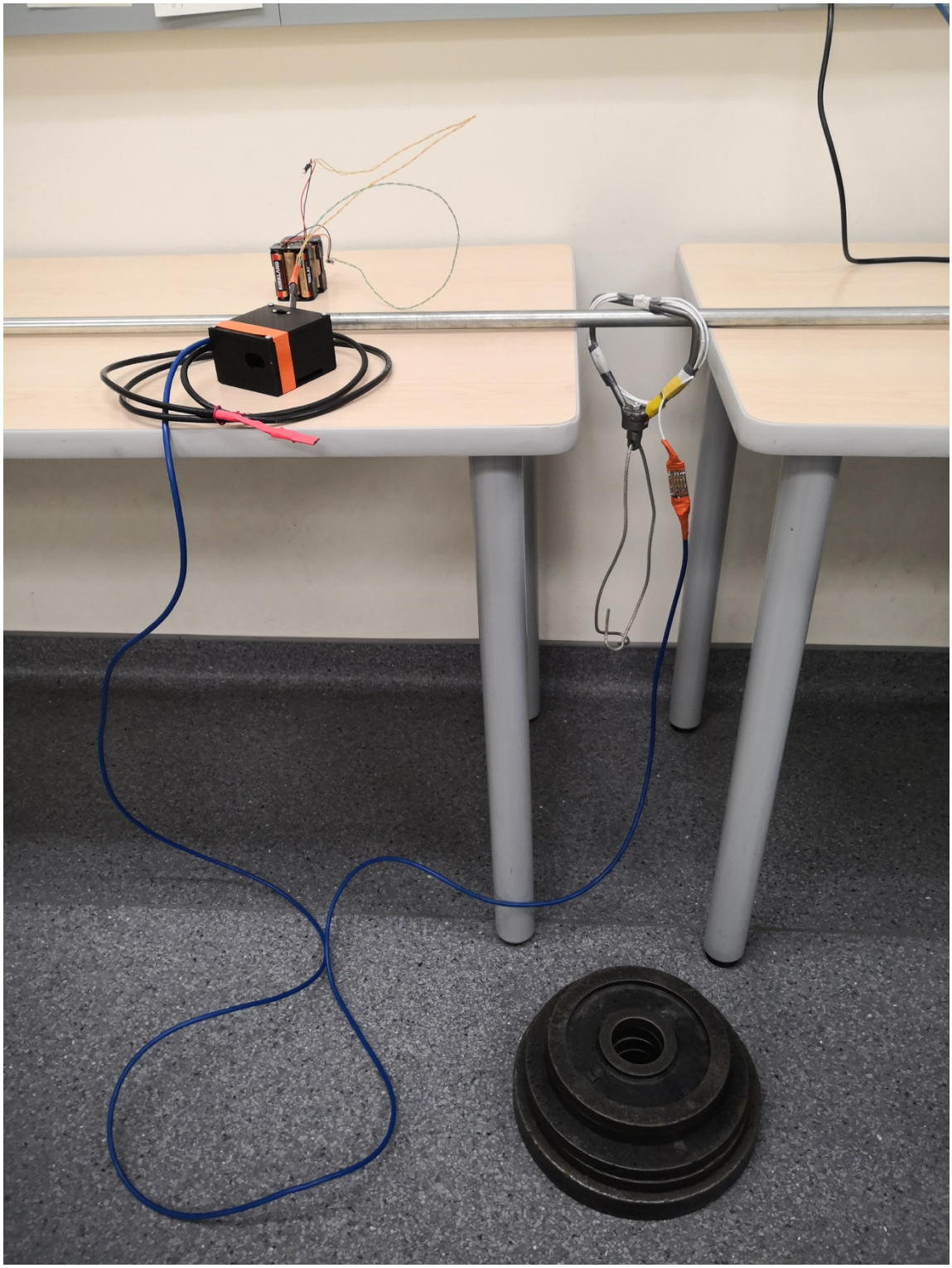

Figure 14: Calibration for the load cell

Then an online linear regression calculator [145] was used to get the calibration equation:

$$W = 0.51225 \times R - 3.03672, \quad (1)$$

where R is the raw data and W is the actual weight value whose unit is kg. This online calculator is quite straightforward. It calculates the slope and intercept of the regression line in the following steps:

(1) Suppose the analog-to-digital values are a vector named X while the actual weights are a vector named Y;

(2) Calculate $\sum X$ and $\sum Y$;

(3) Calculate $\bar{X}$ and $\bar{Y}$;

(4) Calculate $\sum_i^n (X_i - \bar{X})(Y_i - \bar{Y})$;

(5) Calculate $\sum_i^n (X_i - \bar{X})^2$;

(6) The slope is $\frac{\sum_i^n (X_i - \bar{X})(Y_i - \bar{Y})}{\sum_i^n (X_i - \bar{X})^2}$;

(7) The intercept is $\bar{Y} - slope \times \bar{X}$.

After getting the calibration equation, two tests were performed to examine its error with 45 lb (20.41 kg) and 55 lb (24.95 kg). The errors were 0.12 kg and -0.07 kg respectively, which are acceptable in the hammer-throw analysis. Therefore, by performing the calibration procedure, the meaningful data (weight) could be displayed on the laptop instead of a whole bunch of raw data (the analog-to-digital values). In other words, the calibration equation helps to convert to a unit that people can read. To get the tension value, I simply applied Newton's second law of motion:

$$T = W \times 9.81, \quad (2)$$

where W is the weight, T is the tension and 9.81 is the gravity of Earth.

The other calibration procedure was for the IMUs. An IMU testing device was used as shown in Figure 15 (a), that consists of a 6DoF IMU module [140], a teensy 3.2 board [141] and a breadboard. Because this IMU testing device was built in the early stage of the research, the new Pololu product [38] was not yet available at the time. The Pololu IMUs that were used in the final wearable device are 9DoF, but cheaper (about half price compared to the one in [140] which was used in the IMU testing device), and it could provide more accurate data.

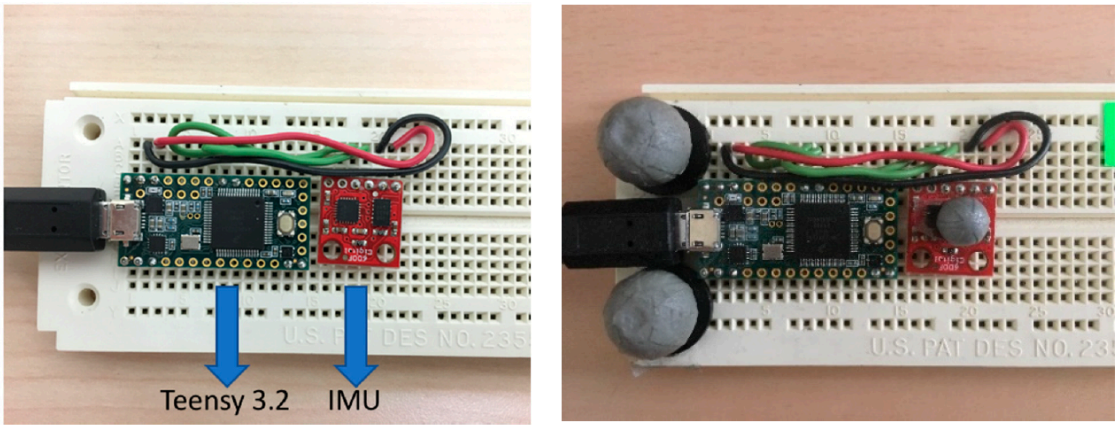

Figure 15: IMU testing device [24]

Returning to the IMU testing device, the 6DoF IMU is designed as a combo board, which has an accelerometer – ADXL345 and a gyroscope – ITG3200. 6DoF refers to the tri-axial accelerometer and the tri-axial gyroscope, which can return the acceleration and the angular speed, respectively, on the X, Y, and Z axes of a coordinate system. In other words, 6DoF can be described as the freedom of movement of a rigid body in a 3D space,

which refers to the following: Forward/back (on X axis), left/right (on Y axis), up/down (on Z axis), roll (around X axis), pitch (around Y axis), and yaw (around Z axis). A magnetometer would construct a so-called 9DoF IMU along with the accelerometer and the gyroscope. However, the 9DoF IMU would actually still describe the same freedom (i.e., 6DoF) of movement of a rigid body in a 3D space. The magnetometer just helps to calculate the yaw angle because the accelerometer can only calculate the roll and pitch angles. Although the accelerometer and the magnetometer can calculate the orientation of an object to some extent, it requires an ideally stationary condition to provide accurate results, i.e., only gravity would be applied on the object, which is inexistent in reality [146] – [148]. Furthermore, the accelerometer is quite sensitive to vibration. Especially, when the object is moving, there will be more force applied on it. This is why the gyroscope plays an important role in the orientation calculation. In this project, the result was acceptable with only the 6DoF data from the accelerometer and the gyroscope. Hence, the magnetometer was not used. Indeed, the drifting error cannot be eliminated thoroughly without the magnetometer. In other words, the error will grow as time goes on. However, the hammer-throw movement is an explosive motor skill, i.e., it is usually completed very quickly (within 20 seconds). The error within a short period would not cause too much trouble. For example, Barshan and Durrant-Whyte [149] successfully developed an inertial navigation system. In their application, they set the testing period to 25 seconds. The error could be reset to zero at the beginning of every short segment. In addition, there is a benefit without using the magnetometer. The wearable device can be used more easily and conveniently without the complicated calibration to the magnetometer before using it.

It effectively avoids any magnetic interference in the testing environment. For every test, one can just reset the drifting error to zero by initializing the system.

The Teensy 3.2 board is a breadboard-friendly microcontroller, which can be programmed in the Arduino IDE [41]. Compared to several Arduino boards, it is smaller than the Arduino UNO and Mega boards, and it has its own USB (Universal Serial Bus) port while the Arduino Mini board does not have one (i.e., Arduino Mini board needs soldering an FTDI basic breakout), which makes it more convenient as a testing device because a revised program can be uploaded anytime in an easier way and it is more portable. However, the Arduino Mini board was used in the final wearable device because the redesign of the PCB was based on the original circuits [19] using an Arduino Mega board.

In addition, as shown in Figure 15 (b), three motion capture markers (two are 9 mm in diameter and one is 5 mm in diameter) were glued on the IMU device for constructing a capture model for 3D motion capture using a 10-camera VICON MX40 motion capture system (VICON Motion Systems, Oxford Metrics Ltd., Oxford, England) [44]. The motion capture rate was set at 200 frames/s. Calibration residuals were determined in accordance with VICON's guidelines and yielded positional data accurate to within 1 mm. The VICON data was used to help in developing a motion tracking algorithm for the IMU in the vertical direction.

First, a configuration program needed to be uploaded to the Teensy 3.2 microcontroller, with the help of the Wire library [150], which allows communication with I2C (Inter-Integrated circuit) devices. Then, the accelerometer and the gyroscope

needed to be configured separately. I set the data format register of the accelerometer to 0x09, which can set the acceleration range from -4 g (1 g = 9.8 m/s^2) to +4 g. According to the datasheet of ADXL345 [151], it sets the device to a full resolution mode, where the output resolution increases with the g range set by the range bits to maintain a 3.9 mg/LSB scale factor (1 mg = 0.001 g and LSB is the least significant bit). So, the sensitivity of the output can be calculated as the following:

$$\frac{1}{3.9\ mg/LSB} = 0.256\ LSB/mg = 256\ LSB/g. \quad (3)$$

This value is useful for converting the unit of the accelerometer's raw data to g (the gravity of Earth). The raw data could be divided by 256 for unit conversion. The power control register was set to 0x08 to change the accelerometer to a measurement mode. Should one want to have minimum power consumption, this register could be set to 0x00 to change it to a standby mode.

Similarly, the ITG3200 gyroscope's settings needed to be configured as well following the instructions in its datasheet [152]. The range of rotation speed was set from -2000 degree/second (dps) to +2000 dps, which is a full-scale range. The sensitivity is 14.375 LSB/dps, which can also be used for converting the unit of the gyroscope's raw data to dps. The raw data could be divided by 14.375 for unit conversion. Various cut-off frequencies were tested and compared to the 3D motion capture data. The validations proved that the cut-off frequency of 98 hertz (Hz) could generate the highest accuracy. Therefore, the low pass filter bandwidth that determines the cut-off frequency was set to 98 Hz in the program.

4.2.3 ARDUINO PROGRAMMING

There are two programs coded in the Arduino IDE [41]. One is for the IMU testing device, and the other one is for the PCB. The program for the IMU testing device is quite straightforward. As discussed in Section 3.2.2, the accelerometer and the gyroscope needed to be configured following their datasheets. The baud rate was set to 115200. A loop function was used to display the data of acceleration and angular speed with converted units. One thing to note was displaying the negative values for the accelerometer and the gyroscope. It was noticed that negative values were not displayed during the calibration procedure. Without the proper calculation, only positive values could be printed. Therefore, to display negative values, the number – 65536 needs to be subtracted with the following two conditions: (1) for the accelerometer, if the analog-to-digital values are great than 1025; (2) for the gyroscope, if the analog-to-digital values are greater than 30000.

The program for the PCB is one of the core parts for the wearable device. It is used to configure and control all the sensors to collect the required data and send the data to the receiver node through an XBee module. I modified the program [153] provided by Pololu for their MinIMU-9 v5 product and added codes to control two IMUs and one load cell. The baud rate was changed to 57600 to match the baud rate of the XBee modules. It was the fastest transmitting speed that could be reached while still obtaining the stable and reliable data. If configured to the highest one baud rate – 115200, some unexpected values were received due to some noisy signals during the calibration. I also found that the load cell would always generate a very high voltage signal (over 1000 analog-to-digital value) when disconnecting the load cell (i.e., simulating the hammer would be thrown away by

an athlete). Therefore, the analog-to-digital value of 1000 was decided to be the ending threshold for determining when a hammer-throw movement is completed. The wearable device can automatically stop sending any garbage data as the threshold is detected. Similarly, when the analog-to-digital value of the load cell is less than 12, the pulling force is so tiny that it can be ignored (i.e., simulating no hammer is hanging on the load cell). Therefore, to avoid receiving lots of garbage data before an athlete is ready to start his/her movement, the starting threshold was set to 12 (analog-to-digital values).

4.3 RECEIVER NODE

As shown in Figure 16, the receiver node consists of an XBee module, an XBee explorer [154] and a laptop. The XBee module can communicate with the other XBee module used in the sensor node remotely by following IEEE 802.15.4 protocol [27]. It is very convenient for a research/lab-based environment.

Figure 16: Receiver node [19]

During the field tests, I carried the laptop to collect data in real-time as shown in Figure 17. A graphical user interface (GUI) was implemented in MATLAB R2017a to display the received data in real-time. Based on the technique data and user instruction supplied by Madgwick [42], [155], I have designed and developed a data collection program for obtaining the data of the tension sensor and the two IMUs simultaneously. In the following sections, the GUI will be introduced first. Then the applied algorithm for the IMUs will be presented in detail.

Figure 17: A field test [19]

4.3.1 GRAPHICAL USER INTERFACE

An updated GUI from the previous design [19] has been implemented in MATLAB (Figure 18). There are three buttons on the top. The left and the right buttons are used to generate an animation and a figure of the change of vertical hip displacements and the change of vertical wrist displacements respectively. The middle one is used to run the main program to collect, save and process all the raw data in real-time. It will keep drawing the curve of the change of the tension data in the figure below as the program is running. A filtered (Butterworth filter) curve will be generated immediately in the same figure once the program stops automatically from detecting that the hammer is released. As mentioned earlier in the sensor node section, there will be a super high analog-to-digital value when the easy-release connector for the load cell is interrupted (i.e., the hammer is thrown away).

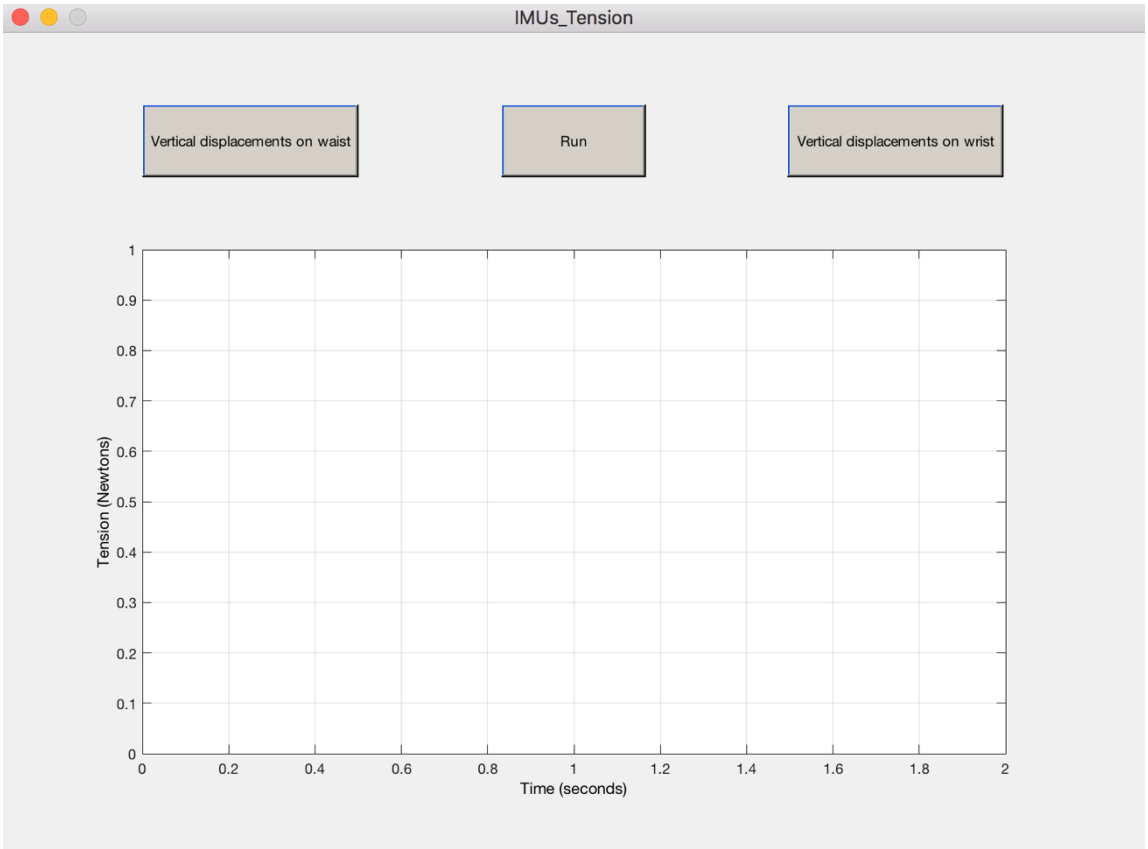

Figure 18: MATLAB GUI receiving, processing and displaying data

The GUI was designed as the following:

(1) Initializing the system environment, variables and hardware setting prepared for serial data transmission;

(2) Implementing the "Run" button, including receiving the serial input until no signal is transmitted from the sensor node, plotting the curve of the tension data in real-time and adding a filtered curve after receiving all the data, and saving all the data into .csv files;

(3) Implementing the "Vertical displacements on waist" button by calling "IMU1";

(4) Implementing the "Vertical displacements on wrist" button by calling "IMU2".

4.3.2 MADGWICK'S IMPLEMENTATION OF MAHONY'S AHRS ALGORITHM

Madgwick's implementation of MahonyAHRS algorithm [42], [155] is also known as the Madgwick's MARG (magnetic, angular rate, and gravity) filter or the AHRS (attitude and heading reference systems) algorithm. In short, it is a gradient-descent algorithm that uses several analytic formulas based on a quaternion representation to fuse IMU data. It enables the performance of low-power and low-cost IMUs at a low sampling rate. The quaternion representation is a four-dimensional complex number which stands for the orientation of a rigid body or coordinate frame in 3D space. For example, Q = [q_1 q_2 q_3 q_4] is a quaternion representation. The unit quaternion is represented as $a + bi + cj + dk$, where a, b, c, and d are real numbers, and i, j, and k are the fundamental units that have the imaginary numbers' property (i.e., $i^2 = j^2 = k^2 = -1$). It is also noticed that the unit quaternion has the property: $a^2 + b^2 + c^2 + d^2 = 1$.

To understand the algorithm better, there are some more preliminary mathematical equations to be introduced. For two quaternions A and B, their quaternion product (qProd) can be determined by the Hamilton rule:

$$A \otimes B = [a_1\ a_2\ a_3\ a_4] \otimes [b_1\ b_2\ b_3\ b_4] = \begin{bmatrix} a_1b_1 - a_2b_2 - a_3b_3 - a_4b_4 \\ a_1b_2 + a_2b_1 + a_3b_4 - a_4b_3 \\ a_1b_3 - a_2b_4 + a_3b_1 + a_4b_2 \\ a_1b_4 + a_2b_3 - a_3b_2 + a_4b_1 \end{bmatrix}^T \quad (4)$$

where T refers to the transpose of the matrix. A rotation matrix R representing the orientation is defined as the following:

$$R = \begin{bmatrix} 2q_1^2 - 1 + 2q_2^2 & 2(q_2q_3 + q_1q_4) & 2(q_2q_4 - q_1q_3) \\ 2(q_2q_3 - q_1q_4) & 2q_1^2 - 1 + 2q_3^2 & 2(q_1q_2 + q_3q_4) \\ 2(q_1q_3 + q_2q_4) & 2(q_3q_4 - q_1q_2) & 2q_1^2 - 1 + 2q_4^2 \end{bmatrix} \quad (5)$$

where q_1, q_2, q_3 and q_4 are the basic elements of a quaternion Q. By replacing 1 in the above equation (5) with the above unit quaternion's property, the rotation matrix R could be described as the following:

$$R = \begin{bmatrix} q_1^2 + q_2^2 - q_3^2 - q_4^2 & 2q_2q_3 + 2q_1q_4 & 2q_2q_4 - 2q_1q_3 \\ 2q_2q_3 - 2q_1q_4 & q_1^2 - q_2^2 + q_3^2 - q_4^2 & 2q_1q_2 + 2q_3q_4 \\ 2q_1q_3 + 2q_2q_4 & 2q_3q_4 - 2q_1q_2 & q_1^2 - q_2^2 - q_3^2 + q_4^2 \end{bmatrix} \quad (6)$$

Suppose that the direction of gravity defines the vertical Z axis, the estimated direction v could be calculated as the following:

$$v = R \times \begin{bmatrix} 0 \\ 0 \\ 1 \end{bmatrix} = \begin{bmatrix} 2q_2q_4 - 2q_1q_3 \\ 2q_1q_2 + 2q_3q_4 \\ q_1^2 - q_2^2 - q_3^2 + q_4^2 \end{bmatrix} \quad (7)$$

For two vectors A = [a_1 a_2 a_3] and B = [b_1 b_2 b_3], C = [c_1 c_2 c_3] is the cross product of A and B, which can be calculated as the following:

$$c_1 = a_2b_3 - a_3b_2, \quad c_2 = a_3b_1 - a_1b_3, \quad c_3 = a_1b_2 - a_2b_1 \quad (8)$$

Thus, Madgwick's implementation of MahonyAHRS algorithm can be described as the following:

(1) Setting the initial quaternion q to [1 0 0 0];

(2) Normalizing the acceleration data with Euclidean norm, i.e., $acc_{norm} = \sqrt{\sum_k acc_k^2}$ where acc_k refers to the acceleration data on the X, Y and Z axes, and

making the data in the range between -1 and +1 as $acc_k = \frac{acc_k}{acc_{norm}}$ where acc_{norm} cannot be 0;

(3) Calculating the estimated direction v based on the current quaternion by using the above equation (7);

(4) Calculating the error e, which is the cross product of the normalized acceleration data and v, by using the above equation (8);

(5) Calculating the integral error eInt, depending on the integral gain's value (i.e., if Ki > 0), as the following: eInt = eInt + e * samplePeriod, where eInt is 0 initially and samplePeriod is 0.02s, and eInt would remain 0 if Ki = 0;

(6) Optimizing the gyroscope data with a proportional integral (PI) controller, which is a variation of PID (proportional integral derivative) controller [156], as the following: gyr = gyr + Kp*e + Ki * eInt, where gyr is the gyroscope data, Kp is the proportional gain, and Ki is the integral gain;

(7) Calculating the rate of change of the quaternion q as the following: qDot = 0.5 * qProd (q, [0 gyr_x gyr_y gyr_z]) by using the above equation (4);

(8) Updating the quaternion q by integrating qDot as the following: q = q + qDot * samplePeriod;

(9) Normalizing the quaternion q with Euclidean norm to make it range between -1 and +1.

Finally, based on Madgwick's implementation, the IMU1 and IMU2 programs both run mainly as the following steps:

(1) Importing raw data from the accelerometer and the gyroscope: acc(i) = [acc_x, acc_y, acc_z], gyr(i) = [gyr_x, gyr_y, gyr_z], where i is from 1 to n (i.e., from the first group to the last group of data);

(2) Calculating the orientation: processing the raw data – acc(i) and gyr(i) through the MahonyAHRS algorithm as described above to get the quaternion, and using a quaternion-to-rotation-matrix function to get a 3*3 rotation matrix R(i), which describes the sensor relative to Earth (the unit of acceleration is "g" or "Gravity");

(3) Calculating the tilt-compensated acceleration data: from i = 1 to i = n, tcAcc(i) = R(i) * $acc(i)^T$, where $acc(i)^T$ is the transposed matrix;

(4) Calculating the linear acceleration in Earth frame by subtracting gravity (i.e., converting the unit from "g" to "m/s^2"): linAcc = (tcAcc – [0,0,1]) * 9.81;

(5) Calculating the linear velocity by integrating the acceleration data: from i = 2 to i = n, linVel(i) = linVel(i-1) + linAcc(i) * samplePeriod, where linVel(1) = 0 as the initial velocity;

(6) Applying a high-pass filter to linear velocity to remove a drifting error: linVelHP = Butterworth_filter(linVel);

(7) Calculating the linear position by integrating the velocity data: from i = 2 to i = n, linPos(i) = linPos(i-1) + linVelHP(i) * samplePeriod, where linPos(1) = 0 as the initial position;

(8) Applying a high-pass filter to linear position to remove a drifting error: linPosHP = Butterworth_filter(linPos);

(9) Drawing corresponding figures and playing an animation to show the move of the device.

4.4 DEEP LEARNING MODELS

By following an online tutorial [157] about a regression problem, two deep learning models have been built in Python with the help of TensorFlow [158] embedded in Anaconda [159], which is one of the most popular data science platforms in the world. The Sequential models from Keras API [43] imported from TensorFlow are used. Two densely connected hidden layers (i.e., dense layers) are set in the models. In each dense layer, a rectified linear unit (ReLU) [160] activation function is used for both models. The ReLU function refers to $f(x) = \max(0, x)$. For an input x coming from the previous layer, it will be calculated by the ReLU function in the current layer. Then its output will be the input of the next layer or the final output. ReLU has the advantage of increasing the sparsity of the neural network because some neuron's outputs can be zero. In other words, it can reduce the dependence of each parameter so that it can help to avoid overfitting. It is known as an efficient gradient descent algorithm using backpropagation. By simplifying the calculation, the calculation cost can be reduced. The two models use RMSprop [161] as the optimizer, which is similar to the gradient descent algorithm with momentum. The gradient descent algorithm is used to minimize some function by iteratively moving towards the steepest descent. So, there will be some oscillations during iterations. The RMSprop optimizer limits the oscillations in vertical direction. Mean squared error (MSE) was used as the loss function for both models. Mean absolute error (MAE) and MSE were used as the metrics in both models for measuring accuracy.

All the datasets were collected by using the VICON camera system [44] from a college-level hammer-throw athlete. It recorded the subject's trajectories (in millimeters) in a 3D coordinate system as a full-body model. All the VICON data are saved in .csv files and processed with Microsoft Excel. A sample of the raw data from the VICON system is shown in Figure 19.

A	B	C	D	E	F	G	H	I	J	K	L	M	N	O	P	Q
Trajectories																
200																
		SL:LFHD			SL:RFHD			SL:LBHD			SL:RBHD			SL:C7		
Frame	Sub Frame	X	Y	Z	X	Y	Z	X	Y	Z	X	Y	Z	X	Y	Z
		mm	mm	mm	mm	mm	mm	mm	mm	mm	mm	mm	mm	mm	mm	mm
373	0	-102.72	994.049	1614.62	70.3816	980.955	1611.89	-95.089	851.242	1621.43	42.1557	841.125	1623.55	0.3843	756.862	150
374	0	-103.599	994.904	1614.56	69.4316	981.703	1611.86	-96.0978	852.091	1621.11	41.1572	841.861	1623.27	-0.590265	757.89	150
375	0	-104.64	995.912	1614.48	68.3071	982.584	1611.82	-97.2913	853.091	1620.72	39.9792	842.727	1622.92	-1.74082	759.102	150
376	0	-105.841	997.071	1614.39	67.0084	983.598	1611.77	-98.6693	854.24	1620.28	38.6226	843.723	1622.53	-3.06661	760.497	150
377	0	-107.198	998.375	1614.29	65.5404	984.741	1611.72	-100.227	855.533	1619.77	37.0939	844.843	1622.08	-4.56192	762.069	
378	0	-108.704	999.813	1614.17	63.9127	986.004	1611.66	-101.953	856.96	1619.21	35.4038	846.08	1621.58	-6.21703	763.808	150
379	0	-110.348	1001.37	1614.05	62.1379	987.377	1611.59	-103.837	858.508	1618.58	33.566	847.422	1621.03	-8.01921	765.699	150
380	0	-112.117	1003.04	1613.91	60.2317	988.847	1611.52	-105.862	860.163	1617.91	31.5971	848.858	1620.44	-9.95357	767.726	150
381	0	-113.998	1004.8	1613.77	58.2111	990.4	1611.45	-108.011	861.909	1617.18	29.515	850.373	1619.82	-12.004	769.873	150
382	0	-115.975	1006.64	1613.61	56.0945	992.023	1611.38	-110.266	863.729	1616.41	27.3385	851.954	1619.15	-14.1536	772.12	150
383	0	-118.033	1008.53	1613.46	53.9007	993.702	1611.31	-112.608	865.607	1615.6	25.0864	853.587	1618.46	-16.3859	774.451	150
384	0	-120.159	1010.47	1613.3	51.648	995.421	1611.24	-115.019	867.526	1614.76	22.777	855.258	1617.75	-18.6845	776.846	150
385	0	-122.338	1012.43	1613.14	49.3542	997.168	1611.18	-117.481	869.471	1613.89	20.428	856.953	1617.01	-21.0343	779.291	150
386	0	-124.557	1014.4	1612.98	47.0357	998.929	1611.13	-119.977	871.426	1613	18.0555	858.662	1616.26	-23.421	781.768	150
387	0	-126.802	1016.36	1612.83	44.7076	1000.69	1611.1	-122.49	873.379	1612.1	15.6742	860.371	1615.5	-25.8317	784.264	150
388	0	-129.063	1018.31	1612.68	42.3831	1002.45	1611.07	-125.006	875.316	1611.17	13.297	862.072	1614.74	-28.2548	786.765	150
389	0	-131.329	1020.22	1612.53	40.074	1004.19	1611.07	-127.511	877.228	1610.25	10.9352	863.755	1613.97	-30.6798	789.259	150
390	0	-133.589	1022.1	1612.4	37.79	1005.9	1611.08	-129.993	879.103	1609.31	8.59837	865.412	1613.2	-33.0975	791.736	150
391	0	-135.836	1023.93	1612.28	35.5392	1007.57	1611.11	-132.443	880.933	1608.38	6.2944	867.037	1612.43	-35.4998	794.186	149
392	0	-138.061	1025.71	1612.17	33.3285	1009.21	1611.17	-134.85	882.712	1607.45	4.0297	868.622	1611.67	-37.8792	796.601	149
393	0	-140.256	1027.42	1612.07	31.1629	1010.79	1611.25	-137.207	884.433	1606.52	1.80937	870.163	1610.92	-40.2295	798.972	14
394	0	-142.416	1029.06	1611.99	29.0467	1012.33	1611.35	-139.508	886.091	1605.61	-0.362621	871.656	1610.17	-42.5447	801.293	149

Figure 19: A sample of the raw data from the VICON system

The data columns of the left wrist thumb side (LWRA) and the left wrist pinkie side (LWRB) are selected to calculate the vertical wrist displacements by using their average values. The data columns of the left anterior superior iliac spin (LASI) and the right anterior superior iliac spin (RASI) are selected to calculate the vertical hip displacements by using their average values. A sample of the processed data from the VICON system is shown in Figure 20.

A	B	C	D	E	F	G	H	I	J	K
Frame	Wrist_Pos	Wrist_Vel	Waist_Pos	Waist_Vel	LHipAngles	RHipAngles	LKneeAngles	RKneeAngles	LAnkleAngles	RAnkleAngles
	mm	mm/s	mm	mm/s	deg	deg	deg	deg	deg	deg
374	980.7645	91.2	990.9885	-51.6	33.4232	-7.22937	145.5412	174.55895	86.00014	116.5668
375	981.292	105.5	990.6805	-61.6	33.2451	-7.19166	145.7207	174.49319	86.34839	116.7008
376	981.888	119.2	990.3275	-70.6	33.0419	-7.1467	145.928	174.41704	86.74191	116.8539
377	982.5465	131.7	989.931	-79.3	32.8152	-7.09423	146.1619	174.3308	87.17673	117.0249
378	983.259	142.5	989.488	-88.6	32.5675	-7.03419	146.4204	174.23503	87.64771	117.2123
379	984.0155	151.3	989.0015	-97.3	32.3021	-6.96668	146.7006	174.13065	88.14887	117.4137
380	984.805	157.9	988.4795	-104.4	32.0225	-6.89196	146.9991	174.01881	88.67384	117.6266
381	985.6175	162.5	987.9205	-111.8	31.733	-6.8105	147.312	173.90098	89.216084	117.8481
382	986.441	164.7	987.334	-117.3	31.4376	-6.7229	147.6349	173.77873	89.769335	118.0751
383	987.265	164.8	986.7235	-122.1	31.1406	-6.62986	147.9632	173.65382	90.327717	118.3045
384	988.079	162.8	986.088	-127.1	30.8462	-6.53234	148.2927	173.52816	90.885876	118.5331
385	988.875	159.2	985.431	-131.4	30.5582	-6.4313	148.619	173.40367	91.43918	118.7579
386	989.6445	153.9	984.7605	-134.1	30.2799	-6.32782	148.9383	173.2823	91.98366	118.976
387	990.381	147.3	984.0805	-136	30.0145	-6.22309	149.2472	173.166	92.51607	119.1849
388	991.08	139.8	983.388	-138.5	29.7643	-6.11831	149.5427	173.05655	93.03388	119.3825
389	991.738	131.6	982.6885	-139.9	29.5311	-6.01464	149.8227	172.9556	93.53515	119.5673
390	992.3535	123.1	981.9835	-141	29.3164	-5.91331	150.0854	172.8647	94.01853	119.7381
391	992.9245	114.2	981.276	-141.5	29.1206	-5.81544	150.33	172.78504	94.48317	119.8944
392	993.45	105.1	980.5675	-141.7	28.944	-5.72213	150.556	172.71765	94.92873	120.0364
393	993.941	98.2	979.861	-141.3	28.7858	-5.6344	150.7637	172.66332	95.35522	120.1647
394	994.3945	90.7	979.158	-140.6	28.6452	-5.55313	150.9538	172.62255	95.76296	120.2803
395	994.813	83.7	978.463	-139	28.5205	-5.47915	151.1276	172.59561	96.15255	120.3851
396	995.209	79.2	977.777	-137.2	28.4098	-5.41311	151.2865	172.58252	96.52483	120.4809
397	995.5925	76.7	977.1035	-134.7	28.3106	-5.35561	151.4327	172.5831	96.88072	120.5699
398	995.967	74.9	976.4465	-131.4	28.2204	-5.30702	151.5681	172.59687	97.22132	120.6546
399	996.338	74.2	975.809	-127.5	28.1363	-5.26767	151.6952	172.62333	97.5477	120.7375
400	996.727	77.8	975.1945	-122.9	28.0554	-5.23773	151.8162	172.6617	97.86099	120.8211

Figure 20: A sample of the processed data from the VICON system

Therefore, the subject's timely change of the vertical wrist and hip displacements can be used as two input variables for the deep learning models. In addition to the displacements, the velocity values can also be calculated out from the trajectories so that two more input variables can be added to increase the data volume. Because of the known VICON system's sampling rate – 200 Hz, i.e., the timestamp between two adjacent datasets is 0.005 seconds, the velocity values could be calculated as the following:

$$vel_i = (pos_{i+1} - pos_i) \div 0.005, \tag{9}$$

where vel_i is the velocity at time i, pos_i is the position at time i, and pos_{i+1} is the position at the next timestamp. So, four groups of input variables can be used in the two models,

including Wrist_Pos (the wrist displacements), Wrist_Vel (the wrist velocities), Waist_Pos (the hip displacements), and Waist_Vel (the hip velocities).

In addition, the VICON system's data can also be used to generate the timely change of the subject's specific joints' angles by using some fundamental mathematical and physical formulas. For example, knowing the coordinates of the left hand, the left elbow and the left shoulder, one can calculate out the elbow's angle (i.e., calculating a joint angle from three points' coordinates). The calculation procedure by using Excel is a time-consuming course. Therefore, the data volume is quite limited in this research study. The main purpose of the research is not to obtain large amounts of data from the VICON system. The aim is to find the way to make use of a wearable system that can provide the biomechanical feedback, just like any 3D motion capture and analysis system can do. This is also the current AI modeling's role that can train the synchronized data from a 3D motion capture system and the proposed wearable system. So far, the models have not yet reached the highest reliable stage because the volume of the training datasets is limited. However, the deep learning models will become powerful and reliable in the future by using the wearable device developed in this research along with a 3D motion capture system to test hundreds of athletes to collect and use large amounts data. Once the deep learning model is quite reliable, then it can be embedded in the wearable system that will realize the ultimate goal of substituting any 3D motion capture system.

In this case study, the output variables were selected as the following: LHipAngle (the left hip angle), RHipAngle (the right hip angle), LKneeAngle (the left knee angle), RKneeAngle (the right knee angle), LAnkleAngle (the left ankle angle), RAnkleAngle (the right ankle angle), LShoulderAngle (the left shoulder angle), RShoulderAngle (the

right shoulder angle), LElbowAngle (the left elbow angle), RElbowAngle (the right elbow angle), LWristAngle (the left wrist angle), RWristAngle (the right wrist angle), and ThoraxAngle (the thorax angle). More angles can be calculated out from the VICON's data, but they are not used in this case.

The models require a normalized form of datasets. So, all the data was normalized before using it to train in the models, as the following:

$$x_{norm} = \frac{x-\bar{x}}{\sigma(x)}, \tag{10}$$

where x_{norm} is the normalized data, x is the original data, $\bar{x}$ is the mean of the original data, and $\sigma(x)$ is the standard deviation of the original data. All the data for the two models was randomly separated into two groups with a factor of 0.8. In other words, the two models randomly selected 80% of the data as their training datasets and selected the remaining 20% as their testing datasets. A sample of the training datasets for the simple model is shown in Figure 21, while a sample of the testing datasets for the same model is shown in Figure 22.

	Waist_Pos	Waist_Vel	LHipAngles	RHipAngles	LKneeAngles	RKneeAngles	LAnkleAngles	RAnkleAngles
7258	963.4565	391.4	-0.220173	-27.69450	172.86277	147.58120	-26.97600	110.61320
31	972.2055	-79.5	27.472900	-5.25355	152.54160	173.08935	99.51705	121.45390
7023	829.1920	-274.4	3.553450	38.78690	91.82700	122.72390	101.98460	99.66164
7735	1059.3600	-93.0	-7.011430	-17.44690	164.90060	144.34810	97.25510	81.07506
7039	797.5185	-98.4	14.885000	34.80690	87.28550	115.26530	111.90100	110.33480
...	...	...	...	...	...	...	...	...
8850	907.8695	31.3	17.044600	38.57080	129.36980	82.11680	99.39634	92.56149
110	1028.8700	-11.0	3.330200	-12.28360	166.20640	164.70200	102.61210	110.40700
1257	892.8200	-51.7	24.264300	46.36400	141.23110	80.98990	111.25300	95.23243
5201	1084.4695	-1894.7	-2.892440	34.28710	89.00350	118.03270	102.95590	108.10040
8539	985.8935	-417.1	-19.495300	14.24300	112.33310	149.95320	108.68740	123.05250

Figure 21: A sample of the training dataset for the simple model

	Waist_Pos	Waist_Vel	LHipAngles	RHipAngles	LKneeAngles	RKneeAngles	LAnkleAngles	RAnkleAngles
0	990.6805	-61.6	33.245100	-7.19166	145.7207	174.49319	86.348390	116.7008
19	979.1580	-140.6	28.645200	-5.55313	150.9538	172.62255	95.762960	120.2803
21	977.7770	-137.2	28.409800	-5.41311	151.2865	172.58252	96.524830	120.4809
25	975.1945	-122.9	28.055400	-5.23773	151.8162	172.66170	97.860990	120.8211
28	973.5295	-104.4	27.801300	-5.20462	152.1669	172.83945	98.732250	121.0984
...	...	...	...	...	...	...	...	...
9266	994.2865	-118.0	-1.240570	-25.18070	162.0255	143.16710	92.501010	108.2436
9267	993.8370	-89.9	-0.959358	-24.76470	162.5846	142.96410	91.914610	108.5626
9269	993.0690	-91.2	-0.309597	-23.80110	163.6495	141.64280	90.830872	109.6913
9279	992.1345	-16.2	1.735520	-22.61760	164.8589	130.05930	87.702840	111.8709
9292	988.0135	-134.1	4.133230	-26.28310	161.5464	133.97730	81.979700	107.4891

Figure 22: A sample of the testing dataset for the simple model

The first model was designed as a simple model in the biomechanical analysis. It focused on the athlete's legs' joints. This model was used to verify that the coordination of the lower limbs could be revealed by the data of vertical hip displacements. The model has two inputs that are Waist_Pos, and Waist_Vel. Because the position of the hip is very close to the position of the waist, the distance between these two points can be ignored in this case. It has six outputs: LHipAngle, RHipAngle, LKneeAngle, RKneeAngle, LAnkleAngle, and RAnkleAngle.

The second model was designed as a complicated model in the biomechanical analysis. It focused on the athlete's legs' joints, arms' joints and thorax. This model was used to verify that the coordination of both the upper and the lower limbs could be revealed by the change of the vertical hip and wrist displacements. The model has four inputs: Waist_Pos, Waist_Vel, Wrist_Pos, and Wrist_Vel. In addition to the above model's output variables, each dataset of the complicated model has seven more variables to

represent the upper body, including LShoulderAngle, RShoulderAngle, LElbowAngle, RElbowAngle, LWristAngle, RWristAngle, and ThoraxAngle.

4.5 SUMMARY

In this chapter, the proposed wearable system that can provide real-time biomechanical feedback in a hammer-throw case study has been introduced in detail. The current system has two elements – the sensor node (i.e., the wearable device) and the receiver node (i.e., software) that have been developed and realized their functions of providing three key parameters in real-time. However, the deep learning models are still not reliable enough due to the limited amount of data so that they are not worth being integrated into the system yet. The idea of making use of the wearable device combined with the AI modeling is quite clear. A lot of more data will be collected by using the wearable device, and those data will be trained in the deep learning models to improve their reliability. Eventually, the deep learning models will be integrated into the system to make the system smart.

Currently, the system uses XBee modules for wireless data transmission. How to configure the XBee modules in XCTU has been introduced. The wearable device was miniaturized with the help of PCB design. It consists of an Arduino Pro Mini board as the microcontroller, an XBee module for data transmission, a load cell for collecting the wire-tension measurements, two IMUs for collecting the vertical hip and wrist displacements. The hardware design and the calibrations for the sensors have been presented in detail. The programming in Arduino IDE for data collection has been introduced. For the receiver node, a GUI and an IMU data fusion algorithm have been described as well.

Last, the details about building two deep learning models in Python by using the Sequential models from Keras API have been provided. In the next chapter, the experiments and results of both the hardware and the deep learning models will be discussed.

CHAPTER 5: EXPERIMENTS AND RESULTS

The experiments can be described from a hardware perspective and a software perspective. The VICON motion capture system was used to examine all the experiments as a supervisor because it can provide quite reliable data. In terms of the hardware, a motion tracking algorithm was applied to both the IMU testing device and the PCB of the wearable device. In terms of the software, the deep learning models were used to verify the feature that the timely change of vertical wrist and hip displacements could reveal the upper and lower limbs' coordination by validating their predictions. In this chapter, the experiments and the results of both the hardware and the deep learning models will be discussed.

5.1 EXPERIMENTS AND RESULTS OF THE HARDWARE

After calibrating the IMU testing device by configuring its accelerometer and gyroscope, an algorithm was required for predicting its orientation. Kalman-based filters have been widely used in orientation estimation [162]. Initially, a complementary Kalman-based algorithm was tried. However, the result of the orientation estimation was unacceptable due to a drifting error that kept occurring when calculating the velocity.

Figure 23 displays the acceleration data obtained from the IMU sensor and the corresponding velocity data, which was calculated by the complementary Kalman-based filter. Figure 23 (a) shows the acceleration data obtained from the IMU testing device, and Figure 23 (b) shows the corresponding velocity data. As shown in the figures, the velocity data does not return to zero at the end of the test. This is known as a data drifting error. It is a typical issue during the integral calculation from acceleration to velocity. This issue will cause the error to be higher and higher (i.e., drifting up).

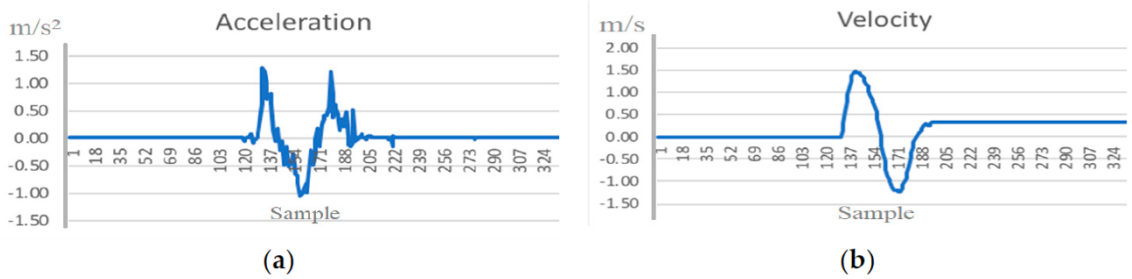

Figure 23: Drifting error [24]

To avoid the data drifting error, another algorithm was tried. As Hamel and Mahony claim in their paper [163], it has been proven that traditional linear Kalman based filters are difficult to be applied robustly to low quality sensor systems. The inherent non-linearity of a system and non-Gaussian noise that occurs in practice could lead to bad results from such filters. Hyyti and Visala also discuss that unlike high-quality and high-precision gyroscopes and accelerometers, low-cost IMUs provide more inaccurate measurements so that their calibration has become a challenging problem [148]. In addition, Madgwick mentions in his work [42], Kalman-based filters are difficult to implement because they may require sampling rates far exceeding the device's bandwidth. It is noticed that the sensor device used in the proposed wearable system has a fairly low sampling rate (only 50 Hz). This could be a major reason for the velocity drifting error that occurred in this application. As Madgwick claims in his study, his algorithm can be effective at even lower sampling rates, like 10 Hz. Also, Madgwick compares the performance of his algorithm with a complementary Kalman-based filter, and the results indicate his algorithm has a slightly better accuracy. Therefore, Madgwick's filter was applied in the final system that has already been introduced in Section 4.3.2.

During a test, I moved the device up and down three times. As displayed in Figure 24, relatively accurate feedback of the 3D positioning data could be obtained. Indeed, the Madgwick algorithm eliminated the drifting error from integrating the velocities. The three different curves stand for the changing distances over time on the X axis, Y axis, and Z axis in 3D space. The dynamic distance on the Z axis (blue lines) shows exactly three times up and down of the device. The range of vertical movements is ~0.33 m for the first vertical movement, ~29 cm for the second one, and ~32 cm for the last one. The next step was to validate the accuracy of the device.

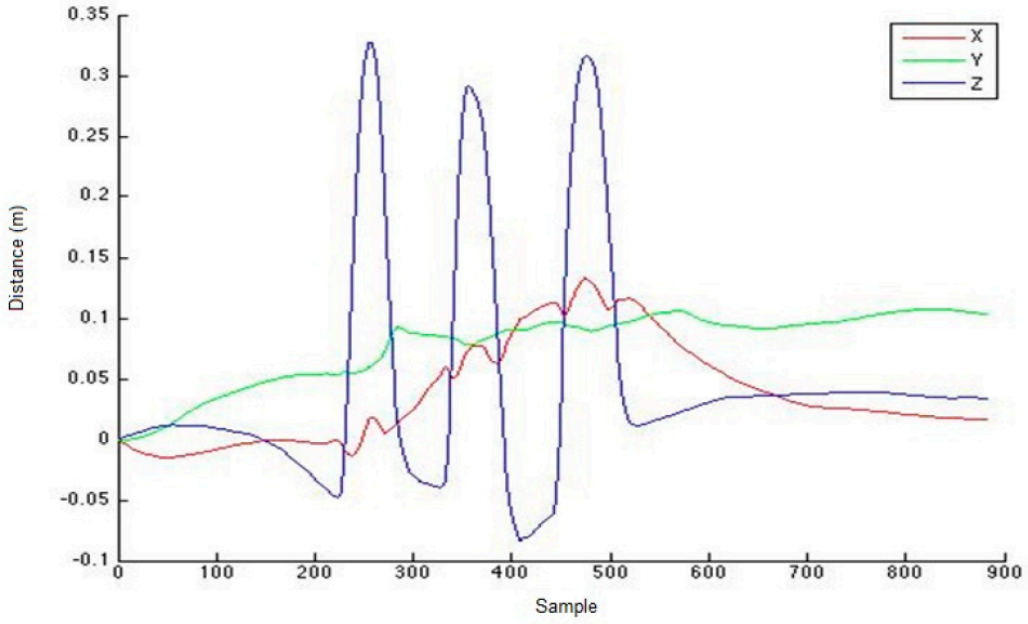

Figure 24: Three times of up-and-down movements by using the IMU testing device with Madgwick's filter [24]

3D motion capture technology provides an accurate and objective analysis of a variety of human motor skills [21], [55], [71], [104], [164]. Therefore, the synchronized data collection of the IMU and 3D motion capture was employed, such as in Figure 1 (b),

for validating and improving the accuracy of the IMU device. The VICON data was used to supervise the IMU testing device's data. In other words, the curves of the IMU testing device's vertical displacements generated from the MATLAB program were compared to the curves of the VICON's data that was processed in Microsoft Excel (i.e., selecting the column of the Z axis of the marker glued on the IMU sensor and then inserting a Line chart by using the Chart tool provided in Excel).

There were eight synchronized tests performed to obtain thousands of data for the validation. Since the aim was to gain the dynamic vertical distance, the validation of the Z axis was selected. Figure 25 shows a typical test's data. The synchronized data demonstrate a matching vertical excursion over time between the IMU data and the accurate 3D motion capture data. The results suggest that the testing device works principally by comparing the two curves in Figure 25. The accuracy needs to be improved.

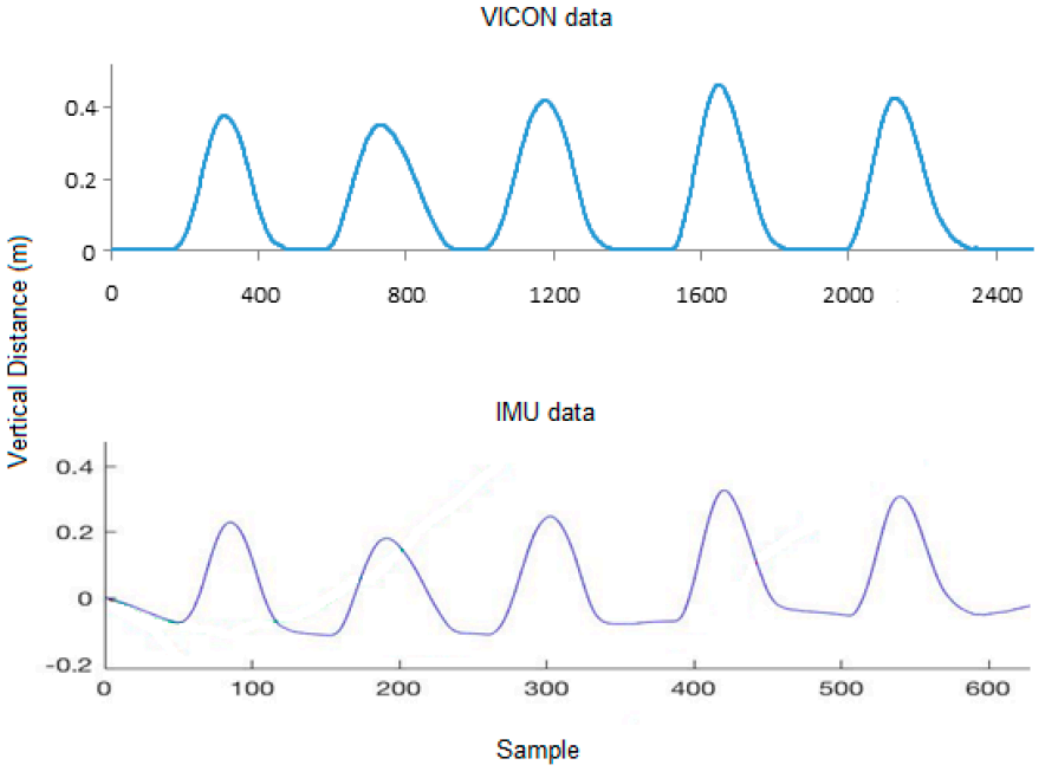

Figure 25: A synchronized test's data obtained from 3D motion capture (VICON data, top, sampling rate 200 Hz) and the IMU testing device without re-calibration (IMU data, bottom, sampling rate 50 Hz) [24]

A magnitude comparison shows that the excursion of the VICON data was larger than that of the IMU data as displayed in Figure 25. A timely comparison between the synchronized data of all trials revealed that the two excursions ran in a quasi-parallel way, which suggested that a factor for re-calibrating the IMU device could be applied to improve the accuracy of the IMU data. After the quantitative comparison between the two excursions of all trials, a re-calibration factor of 1.31 was determined. After the simple re-calibration, a renewed synchronized measurement was done, and the result is shown in Figure 26. This time, the average data error of the IMU data decreases to under 6%, which

is accurate enough for sport skills analysis using a biomechanical modeling method [69], [97], [98], [102], [111].

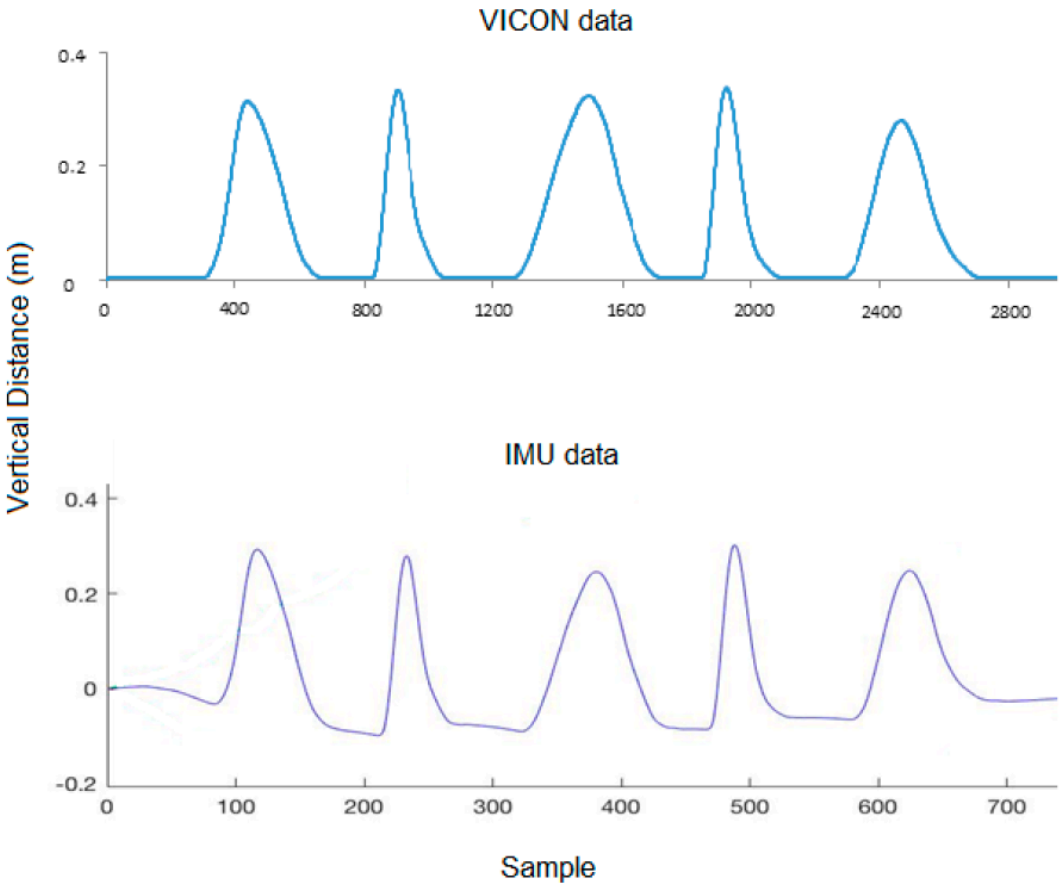

Figure 26: A renewed synchronized test's data obtained from 3D motion capture (VICON data, top, sampling rate 200 Hz) and the IMU testing device after calibration (IMU data, bottom, sampling rate 50 Hz) [24]

Finally, it should be noted that the device needs an initial value for its application. As shown in Figure 26, the device will start at zero regardless of its actual vertical position. Therefore, for its application in the hammer throw, an accurate feedback needs the initial heights of the hip and wrist (Hhip and Hwrist) as shown in Figure 27.

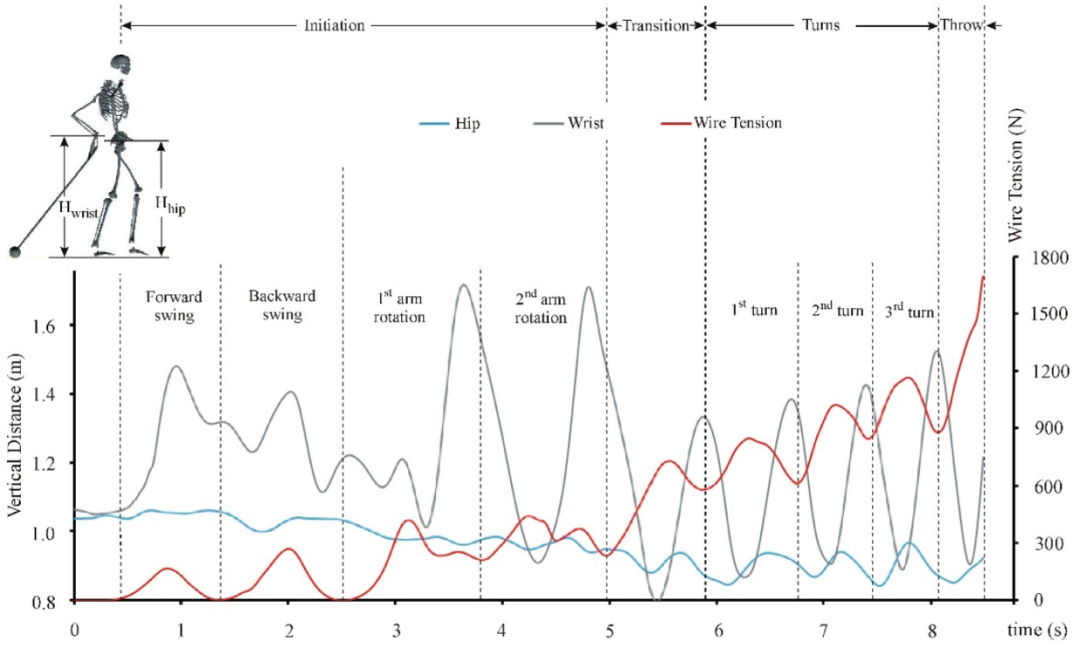

Figure 27: The upper and lower limbs' coordination (i.e., motor control pattern) revealed by the vertical distances of hip and wrist as well as the wire-tension during a hammer throw by a college-level athlete [24]

After testing the IMUs and the load cell on the PCB, everything was assembled together to build the wearable prototype, as shown in Figure 28, for the real-time biomechanical feedback training of the hammer throw. The new wearable device was tested in the field. A varsity-level athlete (male, 25 years, 81 kg, 1.75 m with seven years training experience) tried out the real-time biomechanical feedback device. The wearable device permitted considerable freedom of movement for the subject with negligible influence on his performance. Taking advantage of this, no restrictions were placed on the subject's movements during the in-field test to preserve his normal "control style". Four trials were done.

Figure 28: The wearable prototype

The in-field test on the college-level athlete using the wearable prototype confirms the potential of using wire-tension and IMUs in real-time feedback training, as shown in Figure 27. In practice, the motor control of the hammer throw can be divided into four phases: initiation, transition, turns, and throw. The goal of the initiation phase is to launch the hammer spinning around the body. It commonly consists of a forward and backward swing of the hammer (i.e., to set the hammer to motion) and two over-head arm rotations (i.e., to set the hammer into rotation). The transition phase aims to switch the body from standing posture to the first body rotation, building a rotating system of the body and the hammer. The phase of turns accelerates the rotating system of the body and the hammer to their highest circulation. The final phase is the throwing. The data has revealed the following motor control information: (1) During the transition phase, the upper and lower limbs' controls are transferring from an unclear coordination pattern to a quasi-out-of-phase coordination in the turning phase as displayed in Figure 27. (2) The transition phase helps the power generation (i.e., wire-tension) become in phase (quasi) with the hips' up-and-down movement, indicating the hammer's acceleration depends on the timely flexion/extension of lower limbs. (3) The characteristic of quasi-out-of-phase between the arm control and wire-tension finishes in the transition phase.

5.2 EXPERIMENTS AND RESULTS OF THE DEEP LEARNING MODELS

The two deep learning models were trained for different epochs (i.e., iterations), such as 1000, 10000, etc. The training and validation accuracy were recorded. There was nearly no difference from the results of training with different epochs over 1000. So, training the models with 1000 epochs was selected in this case. An example of training the deep learning models for 1000 epochs is shown in Figure 29. Different learning rates

were also tried. The learning rate of 0.001 for both models provided the best results. The losses for both models decreased dramatically after training them. The last five losses for the simple model were around 10, while the last five losses for the complicated model had an even better result (down to around 3).

```
Epoch: 0, loss:89.5481,  mae:7.0707,  mse:89.5480,
.....................................................................................
Epoch: 100, loss:72.4495,  mae:6.3683,  mse:72.4495,
.....................................................................................
Epoch: 200, loss:59.0162,  mae:5.7801,  mse:59.0162,
.....................................................................................
Epoch: 300, loss:47.8073,  mae:5.2167,  mse:47.8073,
.....................................................................................
Epoch: 400, loss:39.8328,  mae:4.7746,  mse:39.8328,
.....................................................................................
Epoch: 500, loss:33.2834,  mae:4.3853,  mse:33.2834,
.....................................................................................
Epoch: 600, loss:27.6411,  mae:4.0241,  mse:27.6411,
.....................................................................................
Epoch: 700, loss:23.1412,  mae:3.7062,  mse:23.1412,
.....................................................................................
Epoch: 800, loss:19.7878,  mae:3.4358,  mse:19.7879,
.....................................................................................
Epoch: 900, loss:17.5672,  mae:3.2372,  mse:17.5672,
.....................................................................................
```

Figure 29: An example of training the deep learning model for 1000 epochs

Finally, the two models were evaluated with the testing datasets. An example of the plot of the simple model's predictions for those specific joint angles is shown in Figure 30. Similarly, an example of the plot of the complicated model's predictions is shown in Figure 31. The joint angles' unit is in degree. The MAE for the simple model in a typical test, which only focuses on the lower limbs' angles, (i.e., LHipAngle, RHipAngle, LKneeAngle, RKneeAngle, LAnkleAngle, and RAnkleAngle) was 2.62 calculated out in Python. The MAE for the complicated model in a typical test was 1.42. However, the complicated model focuses on both the upper and lower limbs' angles (i.e., LHipAngle, RHipAngle, LKneeAngle, RKneeAngle, LAnkleAngle, RAnkleAngle, LShoulderAngle, RShoulderAngle, LElbowAngle, RElbowAngle, LWristAngle, and RWristAngle). If

comparing the two models, only the lower limbs' angles in the complicated model should be considered. Therefore, the MAE of the lower limbs' angles in the complicated model was calculated out in Python, that was 1.38.

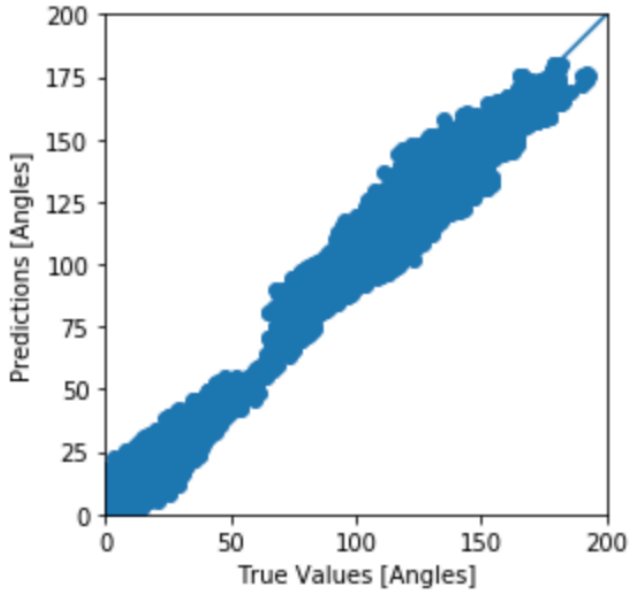

Figure 30: An example of the plot of the simple model's predictions

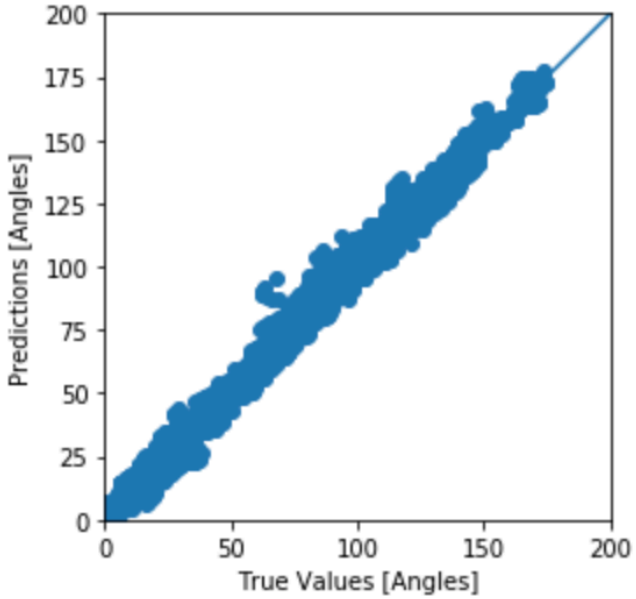

Figure 31: An example of the plot of the complicated model's predictions

In more detail, the results from one typical test were obtained as the following. For the simple model (i.e., only focusing on lower limbs), the MAE of the LHipAngle was 3.99, the MAE of the RHipAngle was 4.55, the MAE of the LKneeAngle was 0.71, the MAE of the RKneeAngle was 3.48, the MAE of the LAnkleAngle was 1.67, and the MAE of the RAnkleAngle was 1.33. So, the MAE of the simple model was calculated out from the average of the above MAEs, that was 2.62. For the complicated model (i.e., focusing on both lower and upper limbs), the MAE of the LHipAngle was 1.23, the MAE of the RHipAngle was 1.42, the MAE of the LKneeAngle was 1.23, the MAE of the RKneeAngle was 1.79, the MAE of the LAnkleAngle was 1.43, and the MAE of the RAnkleAngle was 1.19. So, the MAE of the lower limbs' angles for the complicated model was 1.38, which was calculated out from the average of its above MAEs as well.

It can be found that the complicated model looks better than the simple model from Figure 30 and Figure 31, because the points around the linear regression line are closer and more compact, which means the prediction values will be closer to the true values. As a result, the prediction errors from both models can be accepted. The complicated model has a slightly better result than the simple model, i.e., 1.38 degrees versus 2.62 degrees. However, their difference is only 1.24 degrees which can nearly be ignored in a biomechanical analysis. By comparing the results of these two models, it is still difficult to decide whether to use complicated models or simple models in a future biomechanical study. Although a complicated model may provide a bit more accurate result than a simple model, it is indeed more difficult to build because a complicated model requires to consider more details on 3D motion analysis and more IMUs are needed, which also might

cause movement constraints. Therefore, people may tend to build simple models instead of complicated models to analyze motor skills more specifically in the future.

5.3 SUMMARY

In this chapter, the experiments and the results of the IMU testing device and the final wearable device have been provided. The results have indicated that the obstacles of the hardware and software development of a wearable device have been overcome. The wearable device is ready to be combined with a 3D motion capture system such as the VICON system to collect lots of more data from hundreds of hammer-throw athletes.

In addition, the experiments and the results of the deep learning models have also been discussed. The models need large amounts of synchronized data collected by the wearable device and the VICON system simultaneously to improve their reliability. Furthermore, the results from the current stage of the deep learning models indicate that simple models might be preferred than complicated models in the future. The conclusions of this thesis will be made in the next chapter and the future work will be discussed as well.

CHAPTER 6: CONCLUSIONS AND FUTURE WORK

Dr. Yoshua Bengio, a Canadian computer scientist, who is famous for his work on artificial neural networks and deep learning, once answered a question on Quora:

> Science is NOT a battle; it is a collaboration. We all build on each other's ideas. Science is an act of love, not war. Love for the beauty in the world that surrounds us and love to share and build something together. That makes science a highly satisfying activity, emotionally speaking!

This thesis is based on a cross-disciplinary research study that collaborates with people from different areas, such as computer science, kinesiology, engineering, etc. It is a valuable experience of executing the spirit of science that mentioned by Dr. Bengio above.

6.1 CONCLUSIONS

The study on real-time biomechanical feedback consists of the development of both hardware and software and the AI modeling. If comparing the proposed wearable system to a simplified human system, its hardware are like body parts, including the brain (the Arduino microcontroller board), the skeletal or muscular system (the 3D printed box and its lid), the circulatory system (the power supply and the circuits), and different sensory organs (the sensors); while its software is like the neural control system that makes the whole system come alive.

To establish a user-friendly and practical tool, 3D motion capture technology has been applied to quantify the throw skill, as such dominant parameters of the skill can be identified. In other words, the 3D motion analysis helps to minimize wearable sensors required for hardware development. AI modeling is another technology applied in the study. It helps to create biomechanical feedback by interpreting data obtained from

wearable sensors. The training of the deep learning models has been done by both 3D data and wearable data.

The 3D data has shown that the dynamic data of the hip and wrist could be used for revealing the coordination between the upper and the lower limbs during a throw. To verify this, two deep learning models based on the related 3D motion captured data have been built and trained. It is validated by the results of the models that the timely change of the wrist and hip displacements could reveal the upper and lower limbs' coordination in a hammer-throw movement. It is worth noting that the complicated model has a slightly better result than the simple model. However, their difference is so tiny that can be ignored in a biomechanical analysis. A tentative suggestion on a future biomechanical analysis is to build as many simple models as possible to provide solutions separately rather than to build a complicated model as an integral solution, considering the movement limitation caused by too many IMUs, etc. In addition, hundreds of hammer-throw athletes need to perform lots of tests by using the wearable device along with a 3D motion capture system so that "big data" will be able to improve the deep learning models' reliability. Once the deep learning models can be proved to reach a high reliable stage, then the AI will play an important role of providing biomechanical feedback in real-time to help coaches in the hammer-throw training sessions to facilitate the motor skill learning and training.

A customized PCB has been designed based on the previous schematics of the wireless device [19]. By embedding two IMUs, one load cell (i.e., tension sensor), an XBee module, and an Arduino microcontroller along with other required electronic components, a wearable prototype has been developed. Therefore, by combining the wearable wire-tension measurement with the vertical hip and wrist displacements, various

motor control patterns employed for the hammer throw could be identified. In short, the study has justified that three wearable sensors (i.e., one tension sensor and two IMUs) could be sufficient for creating a real-time biomechanical feedback device.

In any elite sports training, people could use such a methodology developed and provided by this thesis. The general modus operandi for developing wearables of real-time biomechanical feedback is summarized as the following: (1) 3D motion analysis at the beginning; (2) the first translation – simplifying the 3D motion capture to a practical wearable system (i.e., practicality of the wearable system); (3) hardware design and development (including selections of wearable sensors and wireless communication methods); (4) software development (i.e., programming of data collection); (5) system calibration; and (6) the second translation – returning to biomechanical parameters by AI modeling. Such an approach has great potential to become a coach-friendly tool for effective learning and/or training in practice. It would help coaches and athletes to facilitate their motor learning and optimize their motor skills efficiently.

6.2 FUTURE WORK

In the future, the wearable device can be applied into more field tests to examine its practicality and stability. After all, this is still a prototype. So, there still exists a potential to improve its reliability from a prototype to a mature product. For example, the cables that are used to connect the tension sensor and the external IMU to the microcontroller might be able to be cut shorter depending on more practical measurements of more athletes' physical parameters, such as height, arm lengths, etc.

In addition, another IMU could be added into the system to be put on the back of an athlete so that an upper-body model could be analyzed as well. Then, by comparing the upper-body model, which can also be treated as a simple model, with the complicated model, a further validation can be made to determine whether a complicated model or a simple model should be used in future biomechanical study.

The tension sensor can probably be replaced by an IMU as well if the efficiency of the IMU data fusion algorithm can be improved, or a high quality IMU can be used, because the wire-tension has a very close correlation with the acceleration or rotation speed. Furthermore, a high accurate IMU can be used to obtain the trajectories of the hammer in the air that is another key parameter. The concern is that how to avoid destroying the IMU sensor attached on the hammer. As the hammer will fly with a very fast speed in the air, when it drops down to the ground randomly, there will be a high possibility of destroying the sensor.

The tension sensor and the external IMU can also be separated from the current wearable device. They can become two independent wearable devices with their own microcontrollers and wireless communication modules. If so, the wireless sensor network will be expanded rather than a point-to-point network. However, the concerns are the following: would the wireless data transmission still have high reliability when receiving data from several sensor nodes? Would the added weight of the wearable sensor from joining the microcontroller and the wireless communication module cause any movement constraint?

Moreover, a server could be built to make the wearable product as an IoT application. A mobile GUI platform could be developed based on the proposed four types of the sensor nodes so that the customers can reconfigure the system's communication method by their own requirements easily.

For some other areas that may need privacy, such as healthcare, a security algorithm can be easily applied into the wearable system. For example, the XBee modules can be configured with an encryption setting. Also, a security algorithm of AES (Advanced Encryption Standard) can be implemented with Arduino IDE.

Regarding the motor control information revealed by the data, there are still many questions. Would such characteristics appear at different levels of athletes? How can the real-time feedback (i.e., wearable devices) be helpful in the optimization of individual hammer-throw skills? Are there additional potentials of wearables in the learning and training of the hammer throw? Following the framework established in this study, future studies with more athletes at various levels would be able to answer the above questions.

REFERENCES

[1] H. Lee et al, "A Lightweight Lap Time Measurement System for Alpine Ski Sport Using a TDMA-Based Linear Wireless Sensor Network," International Journal of Distributed Sensor Networks, vol. 8, (2), pp. 674380, 2012.

[2] S. A. Haque, M. Rahman and S. M. Aziz, "Sensor anomaly detection in wireless sensor networks for healthcare," Sensors (Basel, Switzerland), vol. 15, (4), pp. 8764-8786, 2015.

[3] K. King et al, "Wireless MEMS inertial sensor system for golf swing dynamics," Sensors & Actuators: A. Physical, vol. 141, (2), pp. 619-630, 2008.

[4] R. Steele et al, "Elderly persons' perception and acceptance of using wireless sensor networks to assist healthcare," International Journal of Medical Informatics, vol. 78, (12), pp. 788-801, 2009.

[5] C. B. Medeiros and M. M. Wanderley, "A comprehensive review of sensors and instrumentation methods in devices for musical expression," Sensors (Basel, Switzerland), vol. 14, (8), pp. 13556-13591, 2014

[6] T. Michailidis et al, "Improvising through the senses: a performance approach with the indirect use of technology," Digital Creativity, vol. 29, (2-3), pp. 149-164, 2018.

[7] A. Londral, S. Pinto and M. de Carvalho, "Markers for upper limb dysfunction in Amyotrophic Lateral Sclerosis using analysis of typing activity," Clinical Neurophysiology, vol. 127, (1), pp. 925-931, 2016.

[8] R. A. Magill, Motor Learning: Concepts & Applications. (6th -- ed.) Boston, MA: McGraw-Hill, 2001.

[9] R. A. Schmidt and T. D. Lee, Motor learning and performance: from principles to application. (5th -- ed.) Champaign, IL: Human Kinetics, 2014.

[10] G. Shan and P. Westerhoff, "Full-body kinematic characteristics of the maximal instep soccer kick by male soccer players and parameters related to kick quality," Sports Biomechanics, vol. 4, (1), p. 59, 2005.

[11] X. Zhang and G. Shan, "Where do golf driver swings go wrong? Factors influencing driver swing consistency: Golf swing consistency," Scandinavian Journal of Medicine & Science in Sports, vol. 24, (5), pp. 749-757, 2014.

[12] D. Yu et al, "Biomechanical characteristics of the Axe Kick in Tae Kwon-Do," Archives of Budo, vol. 8, (4), pp. 213-218, 2012.

[13] G. Shan et al, “Bicycle kick in soccer: is the virtuosity systematically entrainable?” Science Bulletin, vol. 60, (8), pp. 819-821, 2015.

[14] World Athletics, Hammer Throw. Accessed on: Feb. 3, 2020. [Online]. Available: https://www.worldathletics.org/disciplines/throws/hammer-throw

[15] G. Shan and X. Zhang, “From 2D leg kinematics to 3D full-body biomechanics-the past, present and future of scientific analysis of maximal instep kick in soccer,” Sports Medicine, Arthroscopy, Rehabilitation, Therapy & Technology: SMARTT, vol. 3, (1), pp. 23-23, 2011.

[16] B. Wan and G. Shan, “Biomechanical modeling as a practical tool for predicting injury risk related to repetitive muscle lengthening during learning and training of human complex motor skills,” Springerplus, vol. 5, (1), p. 441, 2016.

[17] G. Shan et al, “Biomechanical analysis of maximal instep kick by female soccer players,” Journal of Human Movement Studies, vol. 49, (3), pp. 149-168, 2005.

[18] G. Shan, “Influence of gender and experience on the maximal instep soccer kick,” European Journal of Sport Science, vol. 9, (2), pp. 107-114, 2009.

[19] Y. Wang et al, “A wireless sensor system for a biofeedback training of hammer throwers,” Springerplus, vol. 5, (1), pp. 1-14, Aug. 2016.

[20] K. Aminian and B. Najafi, “Capturing human motion using body-fixed sensors: outdoor measurement and clinical applications,” Computer Animation and Virtual Worlds, vol. 15, (2), pp. 79-94, 2004.

[21] G. Shan et al, “Quantification of Golfer-club Interaction and Club-type's Affect on Dynamic Balance during a Golf Swing,” International Journal of Performance Analysis in Sport, vol. 11, (3), pp. 417-426, 2011.

[22] G. Shan et al, “Regression equations for estimating the quality of maximal instep kick by males and females in soccer,” Kinesiology, vol. 44, (2), p. 139, 2012.

[23] B. Wan et al, “Hammer Throw: a Pilot Study for a Novel Digital-Route for Diagnosing and Improving Its Throw Quality,” Applied Sciences, vol. 10, no. 6, p. 1922, Mar. 2020.

[24] Y. Wang et al, “Obtaining Vital Distances Using Wearable Inertial Measurement Unit for Real-Time, Biomechanical Feedback Training in Hammer-Throw,” Applied Sciences, vol. 8, no. 12, p. 2470, Dec. 2018.

[25] XCTU. Accessed on: Mar. 4, 2020. [Online]. Available: https://www.digi.com/products/embedded-systems/digi-xbee/digi-xbee-tools/xctu

[26] XBee. Accessed on: Mar. 4, 2020. [Online]. Available: https://www.sparkfun.com/datasheets/Wireless/Zigbee/XBee-Datasheet.pdf

[27] IEEE 802.15.4 standard, Dec. 2015. [Online]. Available: https://standards.ieee.org/content/ieee-standards/en/standard/802_15_4-2015.html

[28] I. Calvo et al, "Building Wireless Control Applications with XBee and LabVIEW," Applied Sciences-Basel, vol. 9, (11), p. 2379, 2019.

[29] J. Baca et al, "Configuration discovery of modular self-reconfigurable robots: Real-time, distributed, IR+XBee communication method," Robotics and Autonomous Systems, vol. 91, pp. 284-298, 2017.

[30] A. Cama-Pinto et al, "Received strength signal intensity performance analysis in wireless sensor network using Arduino platform and XBee wireless modules," International Journal of Distributed Sensor Networks, vol. 13, (7), pp. 1-9, 2017.

[31] B. Allen et al., "Evaluation of fall risk for post-stroke patients using bluetooth low-energy wireless sensor," 2013 IEEE Global Communications Conference (GLOBECOM), Atlanta, GA, 2013, pp. 2598-2603.

[32] E. Mackensen, M. Lai and T. M. Wendt, "Bluetooth Low Energy (BLE) based wireless sensors," SENSORS, 2012 IEEE, Taipei, 2012, pp. 1-4.

[33] C. Gomez, J. Oller and J. Paradells, "Overview and Evaluation of Bluetooth Low Energy: An Emerging Low-Power Wireless Technology," Sensors (Basel, Switzerland), vol. 12, (9), pp. 11734-11753, 2012.

[34] G. Cerruela García, I. Luque Ruiz and M. Gómez-Nieto, "State of the Art, Trends and Future of Bluetooth Low Energy, Near Field Communication and Visible Light Communication in the Development of Smart Cities," Sensors (Basel, Switzerland), vol. 16, (11), pp. 1968, 2016.

[35] IEEE 802.15.1 standard, Jun. 2005. [Online]. Available: https://standards.ieee.org/standard/802_15_1-2005.html

[36] IEEE 802.11 standards, Dec. 2016. [Online]. Available: https://standards.ieee.org/standard/802_11-2016.html

[37] Autodesk Inventor. Accessed on: Mar. 4, 2020. [Online]. Available: https://www.autodesk.com/products/inventor/overview

[38] MinIMU-9 v5. Accessed on: Mar. 4, 2020. [Online]. Available: https://www.pololu.com/product/2738

[39] Load cell. Accessed on: Mar. 4, 2020. [Online]. Available: https://assets.omega.com/pdf/test-and-measurement-equipment/load-and-force/load-cells/LCFD.pdf

[40] Arduino Pro Mini 328 – 5V board. Accessed on: Mar. 4, 2020. [Online]. Available: https://www.sparkfun.com/products/11113

[41] Arduino IDE. Accessed on: Mar. 4, 2020. [Online]. Available: https://www.arduino.cc/en/main/software

[42] S. Madgwick, "An efficient orientation filter for inertial and inertial/magnetic sensor arrays," x-io Technologies Limited, Bristol, UK, Internal Rep., Apr. 2010.

[43] Keras API. Accessed on: Aug. 18, 2020. [Online]. Available: https://www.tensorflow.org/api_docs/python/tf/keras

[44] VICON. Accessed on: Mar. 4, 2020. [Online]. Available: https://www.vicon.com/

[45] X. Zhang et al, "Wearables, Biomechanical Feedback, and Human Motor-Skills' Learning & Optimization," Applied Sciences, vol. 9, (2), p. 226, Jan. 2019.

[46] J. Lu, Y. T. Shams and K. Whitehouse, "Smart Blueprints: How Simple Sensors Can Collaboratively Map Out Their Own Locations in the Home," ACM Transactions on Sensor Networks (TOSN), vol. 11, (1), pp. 1-23, 2014.

[47] B. E. Bilgin and V. C. Gungor, "Performance evaluations of ZigBee in different smart grid environments," Computer Networks, vol. 56, (8), pp. 2196-2205, 2012.

[48] A. H. Kioumars and L. Tang, "Wireless network for health monitoring: Heart rate and temperature sensor," 2011 Fifth International Conference on Sensing Technology (ICST), pp. 362-369, Nov. 2011.

[49] H. Mansor et al, "Body temperature measurement for remote health monitoring system," 2013 IEEE International Conference on Smart Instrumentation, Measurement and Applications (ICSIMA), pp. 1-5, Nov. 2013.

[50] F. Dadashi et al, "Front-crawl instantaneous velocity estimation using a wearable inertial measurement unit," Sensors (Basel, Switzerland), vol. 12, (10), pp. 12927-12939, 2012.

[51] J. Y. Xu et al, "Integrated Inertial Sensors and Mobile Computing for Real-Time Cycling Performance Guidance via Pedaling Profile Classification," IEEE Journal of Biomedical and Health Informatics, vol. 19, (2), pp. 440-445, 2015.

[52] M. M. Najafabadi et al, "Deep learning applications and challenges in big data analytics," Journal of Big Data, vol. 2, (1), pp. 1-21, 2015.

[53] G. Shan et al, "Quantifying Compensation Strategies Between Gross and Fine Motor Control in Violin Performance," Arts BioMechanics, vol. 1, (2), pp. 143-163, 2012.

[54] J. K. Aggarwal and L. Xia, "Human activity recognition from 3D data: A review," Pattern Recognition Letters, vol. 48, pp. 70-80, 2014.

[55] G. Shan et al, "A Biomechanical Study for Developing Wearable-Sensor System to Prevent Hip Fractures among Seniors," Applied Sciences, vol. 7, (8), p. 771, 2017.

[56] A. A. Kumar Somappa, K. Øvsthus and L. M. Kristensen, "An Industrial Perspective on Wireless Sensor Networks - A Survey of Requirements, Protocols, and Challenges," IEEE Communications Surveys & Tutorials, vol. 16, (3), pp. 1391-1412, 2014.

[57] T. Seel, J. Raisch and T. Schauer, "IMU-Based Joint Angle Measurement for Gait Analysis," Sensors (Basel, Switzerland), vol. 14, (4), pp. 6891-6909, 2014.

[58] J. A. Hesch et al, "Camera-IMU-based localization: Observability analysis and consistency improvement," The International Journal of Robotics Research, vol. 33, (1), pp. 182-201, 2014.

[59] C. Eling, L. Klingbeil and H. Kuhlmann, "Real-time single-frequency GPS/MEMS-IMU attitude determination of lightweight UAVs," Sensors (Basel, Switzerland), vol. 15, (10), pp. 26212-26235, 2015.

[60] Shiverware. Accessed on: Mar. 5, 2020. [Online]. Available: https://shiverware.com/iot/iot-vs-wsn.html

[61] S. Seneviratne et al., "A Survey of Wearable Devices and Challenges," in IEEE Communications Surveys & Tutorials, vol. 19, no. 4, pp. 2573-2620, Fourthquarter 2017.

[62] A. Nag, S. C. Mukhopadhyay and J. Kosel, "Wearable Flexible Sensors: A Review," in IEEE Sensors Journal, vol. 17, no. 13, pp. 3949-3960, 1 July1, 2017.

[63] D. R. Seshadri et al, "Wearable Devices for Sports: New Integrated Technologies Allow Coaches, Physicians, and Trainers to Better Understand the Physical Demands of Athletes in Real time," IEEE Pulse, vol. 8, (1), pp. 38-43, 2017.

[64] R. Neal, "Smart Soccer: MLS, Chelsea FC Using Adidas Wearable Technology to Improve Training." IBT.com. https://www.ibtimes.com/smart-soccer-mls-chelsea-

fc-using-adidas-wearable-technology-improve-training-1360145 (accessed Mar. 5, 2020)

[65] J. Mischke, “Wearable Technology: The Latest trend in Professional Sports.” WT.com. https://www.wearable-technologies.com/2018/05/wearable-technology-the-latest-trend-in-professional-sports/ (accessed Mar. 5, 2020)

[66] R. Chambers et al, “The Use of Wearable Microsensors to Quantify Sport-Specific Movements,” Sports Medicine, vol. 45, (7), pp. 1065-1081, 2015.

[67] A. Chen and C. D. Ennis, “Goals, Interests, and Learning in Physical Education,” The Journal of Educational Research, vol. 97, (6), pp. 329-339, 2004.

[68] P. Visentin, G. Shan and E. B. Wasiak, "Informing music teaching and learning using movement analysis technology," International Journal of Music Education, vol. 26, (1), pp. 73-87, 2008.

[69] G. Shan et al, “How Can Dynamic Rigid-body Modeling Be Helpful in Motor Learning? – Learning performance using dynamic modeling,” Kinesiology, vol. 36, (2), pp. 182-191, 2004.

[70] G. Shan, P. Visentin and A. Schultz, “Multidimensional signal analysis as a means of better understanding factors associated with repetitive use in violin performance,” Medical Problems of Performing Artists, vol. 19, (3), p. 129, 2004.

[71] G. Shan and P. Visentin, “A quantitative three-dimensional analysis of arm kinematics in violin performance,” Medical Problems of Performing Artists, vol. 18, (1), p. 3, 2003.

[72] R. A. Schmidt, Motor control and learning: a behavioural emphasis. (2nd -- ed.) Champagne, IL: Human Kinetics, 1988.

[73] S. Markovska-Simoska, N. Pop-Jordanova and D. Georgiev, “Simultaneous EEG and EMG biofeedback for peak performance in musicians,” Prilozi, vol. 29, (1), p. 239, 2008.

[74] T. Egner and J. H. Gruzelier, “Ecological validity of neurofeedback: modulation of slow wave EEG enhances musical performance,” Neuroreport, vol. 14, (9), pp. 1221-1224, 2003.

[75] J. Raymond et al, “Biofeedback and Dance Performance: A Preliminary Investigation,” Applied Psychophysiology and Biofeedback, vol. 30, (1), pp. 65-73, 2005.

[76] R. M. Smith and C. Loschner, “Biomechanics feedback for rowing,” Journal of Sports Sciences, vol. 20, (10), pp. 783-791, 2002.

[77] P. N. Page and D. A. Hawkins, “A real-time biomechanical feedback system for training rowers,” Sports Engineering, vol. 6, (2), pp. 67-79, 2003.

[78] D. M. Landers, “Effect of learning on electroencephalographic and electrocardiographic patterns in novice archers,” International Journal of Sport Psychology, vol. 22, (3), pp. 313-330, 1994.

[79] J. Jonsdottir et al, “Concepts of Motor Learning Applied to a Rehabilitation Protocol Using Biofeedback to Improve Gait in a Chronic Stroke Patient: An A-B System Study with Multiple Gait Analyses,” Neurorehabilitation and Neural Repair, vol. 21, (2), pp. 190-194, 2007.

[80] Mayo Clinic. Accessed on: Mar. 5, 2020. [Online]. Available: https://www.mayoclinic.org/tests-procedures/biofeedback/about/pac-20384664

[81] J. J. Tate and C. E. Milner, “Real-Time Kinematic, Temporospatial, and Kinetic Biofeedback During Gait Retraining in Patients: A Systematic Review,” Physical Therapy, vol. 90, (8), pp. 1123-1134, 2010.

[82] A. J. Bandodkar and J. Wang, "Non-invasive wearable electrochemical sensors: a review," Trends in Biotechnology, vol. 32, (7), pp. 363-371, 2014.

[83] J. V. Basmajian, Biofeedback: principles and practice for clinicians. (3rd -- ed.) Baltimore, MD: Williams & Wilkins, 1989.

[84] R. J. Marzano, T. Frontier, and D. Livingston, Effective supervision: supporting the art and science of teaching. Alexandria, Egypt: Ascd, 2011.

[85] D. A. Sleight, “A developmental history of training in the United States and Europe”, unpublished, 1993.

[86] S. C. Mukhopadhyay, “Wearable Sensors for Human Activity Monitoring: A Review,” IEEE Sensors Journal, vol. 15, (3), pp. 1321-1330, 2015.

[87] A. Baca, “Feedback systems,” WIT Transactions on State of the Art in Science and Engineering, vol. 32, pp. 43-67, 2008.

[88] D. R. Seshadri et al, “A review of wearable technology: Moving beyond the hype: From need through sensor implementation,” 2016 8th Cairo International Biomedical Engineering Conference (CIBEC), Cairo, 2016, pp. 52-55.

[89] S. Patel et al, "A review of wearable sensors and systems with application in rehabilitation," Journal of Neuroengineering and Rehabilitation, vol. 9, (1), pp. 21-21, 2012.

[90] A. Zijlstra et al, "Biofeedback for training balance and mobility tasks in older populations: a systematic review," Journal of Neuroengineering and Rehabilitation, vol. 7, (1), pp. 58-58, 2010.

[91] O. M. Giggins, U. M. Persson and B. Caulfield, "Biofeedback in rehabilitation," Journal of Neuroengineering and Rehabilitation, vol. 10, (1), pp. 60-60, 2013.

[92] M. Schwenk et al, "Interactive balance training integrating sensor-based visual feedback of movement performance: a pilot study in older adults," Journal of Neuroengineering and Rehabilitation, vol. 11, (1), p. 164, 2014.

[93] F. Attal et al, "Physical Human Activity Recognition Using Wearable Sensors," Sensors (Basel, Switzerland), vol. 15, (12), pp. 31314-31338, 2015.

[94] J. Heikenfeld, "Bioanalytical devices: Technological leap for sweat sensing," Nature, vol. 529, (7587), p. 475, 2016.

[95] Z. Sonner et al, "The microfluidics of the eccrine sweat gland, including biomarker partitioning, transport, and biosensing implications," Biomicrofluidics, vol. 9, (3), May 2015, Art. no. 031301.

[96] E. L. Radin, "Role of muscles in protecting athletes from injury," Acta Medica Scandinavica. Supplementum, vol. 711, p. 143, 1986.

[97] G. Shan et al, "How Can Dynamic Rigid-body Modeling Be Helpful in Motor Learning? – Diagnosing Performance Using Dynamic Modeling," Kinesiology, vol. 36, (1), pp. 5-14, 2004.

[98] G. Shan and C. Bohn, "Anthropometrical data and coefficients of regression related to gender and race," Applied Ergonomics, vol. 34, (4), pp. 327-337, 2003.

[99] G. Shan and P. Visentin, Arts Biomechanics – an Infant Science: Its Challenges and Future. New York, NY: Nova Science Publishers, 2010.

[100] S. J. Petruzzello, D. M. Landers and W. Salazar, "Biofeedback and sport/exercise performance: Applications and limitations," Behaviour Therapy, vol. 22, (3), pp. 379-392, 1991.

[101] D. J. Vernon, "Can Neurofeedback Training Enhance Performance? An Evaluation of the Evidence with Implications for Future Research," Applied Psychophysiology and Biofeedback, vol. 30, (4), pp. 347-364, 2005.

[102] R. Ballreich, W. Baumann, Grundlagen der Biomechanik des Sports. Stuttgart, Germany: Enke Verlag (in German), 1996.

[103] S. J. Hall, Basic Biomechanics. (8th -- ed.) Boston, MA: McGraw-Hill, 2018.

[104] P. Visentin et al, "Unraveling mysteries of personal performance style; biomechanics of left-hand position changes (shifting) in violin performance," Peerj, vol. 3, e1299, 2015.

[105] G. R. Colborne, S. J. Olney and M. P. Griffin, "Feedback of ankle joint angle and soleus electromyography in the rehabilitation of hemiplegic gait," Archives of Physical Medicine and Rehabilitation, vol. 74, (10), pp. 1100-1106, 1993.

[106] E. Ceceli, E. Dursun, and A. Cacki, "Comparison of joint-position biofeedback and conventional therapy methods in Genu recurvatum after stroke - 6 months' follow-up," European Journal of Physical Medicine & Rehabilitation, vol. 6, (5), pp. 141 – 144, 1996.

[107] E. Isakov, "Gait rehabilitation: a new biofeedback device for monitoring and enhancing weight-bearing over the affected lower limb," Europa Medicophysica, vol. 43, (1), p. 21, 2007.

[108] S. C. White and R. M. Lifeso, "Altering Asymmetric Limb Loading After Hip Arthroplasty Using Real-Time Dynamic Feedback When Walking," Archives of Physical Medicine and Rehabilitation, vol. 86, (10), pp. 1958-1963, 2005.

[109] S. Li et al, "The relevance of body positioning and its training effect on badminton smash," Journal of Sports Sciences, vol. 35, (4), pp. 310-316, 2017.

[110] Z. Zhang et al, "The Influence of X-Factor (Trunk Rotation) and Experience on the Quality of the Badminton Forehand Smash," Journal of Human Kinetics, vol. 53, (1), pp. 9-22, 2016.

[111] G. Shan et al, "Biomechanics of coaching maximal instep soccer kick for practitioners," Interdisciplinary Science Reviews, vol. 44, (1), pp. 12-20, 2019.

[112] D. A. Winter, *Biomechanics and Motor Control of Human Movement*. (4th -- ed.) Hoboken, NJ: John Wiley & Sons, 1990.

[113] G. Shan et al, "A Frequency-Based Characterization of Spiccato Bowing in Violin Performance," Perceptual and Motor Skills, vol. 105, (3_suppl), pp. 1027-1051, 2007.

[114] M. A. O'Reilly et al, "A Wearable Sensor-Based Exercise Biofeedback System: Mixed Methods Evaluation of Formulift," JMIR mHealth and uHealth, vol. 6, (1), e33, 2018.

[115] O. Y. Al-Jarrah et al, "Efficient Machine Learning for Big Data: A Review," Big Data Research, vol. 2, (3), pp. 87-93, 2015.

[116] O. Faust et al, "Deep learning for healthcare applications based on physiological signals: A review," Computer Methods and Programs in Biomedicine, vol. 161, pp. 1-13, 2018.

[117] Z. Zhang and G. Shan, "Developing Novel Devices to Predict and Prevent Age-Related Falls," in Proc. Int. Conf. on Energy, Environment and Materials Engineering (EEME 2014), Shenzhen, China, 2014, pp. 1077 – 1081.

[118] J. Shan et al, "A Novel Measurement System for Quantitative Assessment of Age-Related Sensori-motor Degradation," Biomedical Engineering: Applications, Basis and Communications, vol. 21, (1), pp. 17-28, 2009.

[119] G. Shan, D. Daniels and R. Gu, "Artificial neural networks and center-of-pressure modeling: a practical method for sensorimotor-degradation assessment," Journal of Aging and Physical Activity, vol. 12, (1), pp. 75-89, 2004.

[120] G. Shan, G. Wu and L. Haugh, "A method to determine the interdependent relationships between biomechanical variables in artificial neural network models: the case of lower extremity muscle activity and body sway," Neurocomputing, vol. 61, pp. 241-258, 2004.

[121] H. Brock and Y. Ohgi, "Assessing Motion Style Errors in Ski Jumping Using Inertial Sensor Devices," IEEE Sensors Journal, vol. 17, (12), pp. 3794-3804, 2017.

[122] N. K. Chauhan and K. Singh, "A Review on Conventional Machine Learning vs Deep Learning," 2018 International Conference on Computing, Power and Communication Technologies (GUCON), Greater Noida, Uttar Pradesh, India, 2018, pp. 347-352.

[123] M. Längkvist et al, "A review of unsupervised feature learning and deep learning for time-series modeling," Pattern Recognition Letters, vol. 42, (1), pp. 11-24, 2014.

[124] Y. Bengio and O. Delalleau, "On the expressive power of deep architectures," in Proc. 22nd Int. Conf. on Algorithmic Learning Theory (ALT 2011), Espoo, Finland, 2011, pp. 18-36.

[125] Y. LeCun, Y. Bengio and G. Hinton, "Deep learning," Nature, vol. 521, (7553), pp. 436-444, 2015.

[126] Hidden Layer. Accessed on: Aug. 21, 2020. [Online]. Available: https://deepai.org/machine-learning-glossary-and-terms/hidden-layer-machine-learning#:~:text=In%20neural%20networks%2C%20a%20hidden,inputs%20entered%20into%20the%20network.

[127] S. Kumar, "Deep Learning Made Easy: Part 3: Activation Functions, Parameters and Hyperparameters and Weight Initialization," Towards Data Science, Apr. 2019. [Online]. Available: https://towardsdatascience.com/deep-learning-made-easy-activation-functions-parameters-and-hyperparameters-and-weight-c7bcfeb9af24#:~:text=Activation%20functions%20determine%20the%20output,a%20large%20scale%20neural%20network.&text=Activation%20functions%20also%20help%20normalize,or%20between%20%2D1%20and%201.

[128] R. Grandhi, "A Look at Gradient Descent and RMSprop Optimizers," Towards Data Science, Jun. 19, 2018. [Online]. Available: https://towardsdatascience.com/a-look-at-gradient-descent-and-rmsprop-optimizers-f77d483ef08b

[129] H. Brock, "Deep learning – Accelerating Next Generation Performance Analysis Systems?" Proceedings, vol. 2, (6), p. 303, 2018.

[130] J. Yang et al, "Deep Convolutional Neural Networks on Multichannel Time Series for Human Activity Recognition," in Proc. 24th Int. Conf. on Artificial Intelligence (IJCAI'15), 2015, pp. 3995-4001.

[131] K. Wei and K. P. Kording, "Behavioural tracking gets real," Nature Neuroscience, vol. 21, (9), pp. 1146-1147, 2018.

[132] F. Ofli et al, "Berkeley MHAD: A comprehensive Multimodal Human Action Database," 2013 IEEE Workshop on Applications of Computer Vision (WACV), Tampa, FL, 2013, pp. 53-60.

[133] S. M. Brice et al, "Development and validation of a method to directly measure the cable force during the hammer throw," Sports Biomechanics, vol. 7, (2), pp. 274-287, 2008.

[134] ATmega328P. Accessed on: Mar. 4, 2020. [Online]. Available: https://www.microchip.com/wwwproducts/en/ATmega328p

[135] Avnet. "Internet of Things: low power, low cost, connected devices fuel demand for microco." https://www.avnet.com/wps/portal/us/resources/technical-articles/article/iot/internet-of-things-low-power-low-cost-connected-devices-fuel-demand-for-microco/ (accessed Apr. 2, 2020).

[136] FTDI basic breakout. Accessed on: Mar. 4, 2020. [Online]. Available: https://www.sparkfun.com/products/9716

[137] FT232R USB UART IC Datasheet. Accessed on: Mar. 4, 2020. [Online]. Available: https://www.ftdichip.com/Support/Documents/DataSheets/ICs/DS_FT232R.pdf

[138] Serial Communication Tutorial. Accessed on: Mar. 4, 2020. [Online]. Available: https://learn.sparkfun.com/tutorials/serial-communication/all

[139] Handshake. Accessed on: Apr. 2, 2020. [Online]. Available: https://en.wikipedia.org/wiki/Handshaking

[140] 6DoF IMU Digital Combo Board – ITG3200/ADXL345. Accessed on: Apr. 3, 2020. [Online]. Available: https://www.sparkfun.com/products/retired/10121

[141] Teensy 3.2 board. Accessed on: Apr. 3, 2020. [Online]. Available: https://www.sparkfun.com/products/13736

[142] LM723. Accessed on: Apr. 2, 2020. [Online]. Available: https://media.digikey.com/pdf/Data%210Sheets/Texas%20Instruments%20PDFs/LM723(C).pdf

[143] LT1920. Accessed on: Apr. 2, 2020. [Online]. Available: https://www.analog.com/media/en/technical-documentation/data-sheets/1920f.pdf

[144] UA741. Accessed on: Apr. 2, 2020. [Online]. Available: https://www.st.com/content/ccc/resource/technical/document/datasheet/group1/d6/9e/4e/8a/fa/65/4c/d0/CD00001252/files/CD00001252.pdf/jcr:content/translations/en.CD00001252.pdf

[145] A Linear Regression Calculator. Accessed on: Apr. 14, 2020. [Online]. Available: https://www.socscistatistics.com/tests/regression/default.aspx

[146] M. B. Del Rosario, N. H. Lovell and S. J. Redmond, "Quaternion-Based Complementary Filter for Attitude Determination of a Smartphone," IEEE Sensors Journal, vol. 16, (15), pp. 6008-6017, 2016.

[147] Starlino, "A Guide to Using IMU (Accelerometer and Gyroscope Devices) in Embedded Applications," Starlino Electronics, Dec. 29, 2009. [Online]. Available: http://www.starlino.com/imu_guide.html

[148] H. Hyyti and A. Visala, "A DCM Based Attitude Estimation Algorithm for Low-Cost MEMS IMUs," International Journal of Navigation and Observation, vol. 2015, pp. 1-18, 2015.

[149] B. Barshan and H. F. Durrant-Whyte, “Inertial navigation systems for mobile robots,” IEEE Transactions on Robotics and Automation, vol. 11, (3), pp. 328-342, 1995.

[150] Arduino Wire Library. Accessed on: Apr. 3, 2020. [Online]. Available: https://www.arduino.cc/en/Reference/Wire

[151] ADXL345. Accessed on: Apr. 3, 2020. [Online]. Available: https://www.sparkfun.com/datasheets/Sensors/Accelerometer/ADXL345.pdf

[152] ITG3200. Accessed on: Apr. 3, 2020. [Online]. Available: https://www.sparkfun.com/datasheets/Sensors/Gyro/PS-ITG-3200-00-01.4.pdf

[153] MinIMU9AHRS Library. Accessed on Apr. 5, 2020. [Online]. Available: https://github.com/pololu/minimu-9-ahrs-arduino

[154] XBee Explorer. Accessed on: Apr. 4, 2020. [Online]. Available: https://www.sparkfun.com/products/11812

[155] S. O. H. Madgwick, A. J. L. Harrison and R. Vaidyanathan, “Estimation of IMU and MARG orientation using a gradient descent algorithm,” 2011 IEEE International Conference on Rehabilitation Robotics, Zurich, 2011, pp. 1-7.

[156] M. A. Johnson, M. H. Moradi, and J. Crowe, “PID Control Technology,” in *PID Control: New Identification and Design Methods.* 2005. [Online]. Available: https://ebookcentral-proquest-com.ezproxy.uleth.ca/lib/uleth/reader.action?docID=303713

[157] A Regression Tutorial. Accessed on: Apr. 4, 2020. [Online]. Available: https://www.tensorflow.org/tutorials/keras/regression#conclusion

[158] TensorFlow. Accessed on: Apr. 6, 2020. [Online]. Available: https://www.tensorflow.org/

[159] Anaconda. Accessed on: Apr. 6, 2020. [Online]. Available: https://www.anaconda.com/

[160] ReLU. Accessed on: Aug 21, 2020. [Online]. Available: https://machinelearningmastery.com/rectified-linear-activation-function-for-deep-learning-neural-networks/

[161] RMSprop. Accessed on: Aug. 21, 2020. [Online]. Available: https://keras.io/api/optimizers/rmsprop/

[162] S. Won, W. Melek and F. Golnaraghi, “Position and orientation estimation using Kalman filtering and particle diltering with one IMU and one position sensor,” in

Proc. 34th Annu. Conf. of IEEE Industrial Electronics, Orlando, FL, 2008, pp. 3006-3010.

[163] T. Hamel and R. Mahony, "Attitude estimation on SO[3] based on direct inertial measurements," in Proc. 2006 IEEE Int. Conf. on Robotics and Automation (ICRA 2006), Orlando, FL, 2006, pp. 2170-2175.

[164] G. Shan, "Biomechanical Know-how of Fascinating Soccer-kicking Skills—3D, Full-body Demystification of Maximal Instep Kick, Bicycle kick & Side Volley," In Proc. 8th Int. Scientific Conf. on Kinesiology, Zagreb, Opatija, Croatia, 2017, pp. 133–135.

APPENDIX 1: RESEARCH CONSENT FORM

Development of new biomechanical feedback tools for improving human motor skill learning and training

Hammer Throw Project

Biomechanics Laboratory

University of Lethbridge

We invite you to participate in a study that aims to develop new tools for understanding of fundamental processes in humans and modulating various human movements, ranging from daily activities to specialized sport and music skills. Learning how to move is a challenging task. Even the most basic skill of walking requires years to develop and can quickly deteriorate with age and sedentary lifestyles. Age-related falls are the cause of 70% of accidental deaths in people 75 years and older and is the leading (74%) cause of hospitalization for seniors. More specialized skills such as violin playing, and soccer kicking require "talent" and years of extensive practice to fully master. These practices can easily cause career-ending vocational diseases if conducted improperly. Our research group uses the science of biomechanics and state-of-the-art motion analysis technologies to determine which muscle movements are critical for successful skill development and which expose us to vocational disease development. In this fashion, we are able to unlock some of the secrets of talented musicians and athletes and scientifically

inform music pedagogy and sports coaching, while preventing the occupational disease to occur, i.e. biofeedback learning and training.

Biomechanical feedback can be broadly divided into two categories: real-time and post-measurement. Real-time feedback is more useful for practitioners and thus our ultimate goal, but its successful development hinges on robust post-measurement feedback. Therefore, your participation in the project will be the post-measurement one.

Hammer throw has a long-standing history in track and field, but unlike other events, hammer throw has not seen a new world record since 1986. One reason for this stagnation could be the lack of scientific bio-feedback training. This study aims to develop a biofeedback analyser that can 1) measure real-time wire tension and vertical hip displacement, 2) establish how to reach desirable tension and displacement, and ultimately 3) provide biomechanical-guided training plans customized to each athlete's anthropometric data.

The experiment takes about 60 minutes. The test will be in the hammer training area located in UofL gym (the training area is protected by a surrounding net). You will be asked to wear a black garment made of stretchable material, which covers the upper and lower body. Affixed to the garment will be 42 reflective markers (reusable), each with a diameter of 9mm. The garment will be washed between each participant use. Before the test, you will be allowed to perform a sufficient number of warm-up exercises to get used to the test environment. After warm-up you will be asked to perform 6 throws using a real hammer (like throws in your training). During each throw, the kinematic (3D motion) and wire tension data will be captured simultaneously. The kinematic data will be collected by a twelve-camera Vicon system. Wire tension will be measured by a tension

sensor system developed at Biomechanics Lab. The tension sensor is installed between the Hammer grip and wire. There are no anticipated risks from participating in this study. Nothing is intrusive into the body. The tests are natural and do not use any sort of medication.

The information gathered from you during this study is considered confidential. To maximize your anonymity, you will be assigned a code, and this code will be used instead of your name at all times. Research assistants will also be required to sign a confidentiality agreement. All personal information (body weight, body height, age, and training hours per week) will remain locked in a file cabinet that can only be accessed by researchers involved in this study and will not be disclosed without your permission. We may, however, wish to use your data measurements for a research presentation or education purposes in the future. Your identity will be kept confidential. It should be mentioned that the twelve-camera system will not in any way videotape participants' faces, so that participants truly do remain anonymous.

Your participation in this study is entirely voluntary and you may withdraw from participating at any time. Should you decide not to participate in this study, your relationship with the Biomechanics Lab or any other department of the University of Lethbridge will not be affected in any way. If you choose to withdraw, any information collected from you up to the point of withdrawal will be deleted or destroyed. If you wish to see your performance analysis, we will supply you a CD containing your 3D dynamic analysis data. If you have any further questions about this research, please feel free to contact Dr. Gongbing Shan, at (403) 329-2683 or g.shan@uleth.ca. If you have any further

questions regarding your rights as a participant, please contact the University of Lethbridge Office of Research Ethics at (403) 329-2747 or research.services@uleth.ca.

Your signature below indicates that you have read and understood the information provided above, and that any and all questions you might ask to have been answered to your satisfaction. Your signature also indicates that you willingly agree to participate in this study, and that you understand you may withdraw from this experiment at any time.

I have read the attached Informed Consent form and I consent to participate in the "development of new biomechanical feedback tools for improving human motor skill learning and training" research study.

Printed Name:_____ Date:_____

Signature:_____

Witnessed by:_____ Date:_____